

Pannexin 1 and Adipose Tissue

Samantha Elizabeth Adamson

Fort Seybert, WV

BA, Princeton University, 2006

MS, University of Virginia, 2013

A Dissertation presented to the Graduate Faculty  
of the University of Virginia in Candidacy for the Degree of Doctor of Philosophy

Department of Pharmacology

University of Virginia

August, 2015

Norbert Leitinger, Ph.D. (Advisor)

Doug Bayliss, Ph.D.

Thurl Harris, Ph.D.

Coleen McNamara, MD

Bimal Desai, Ph.D.

Copyright Page

## ABSTRACT

Defective glucose uptake in adipocytes leads to impaired metabolic homeostasis and insulin resistance, hallmarks of type 2 diabetes. Extracellular ATP-derived nucleotides and nucleosides are important regulators of adipocyte function, but the pathway for controlled ATP release from adipocytes is unknown. Here, we investigated whether Pannexin 1 (Panx1) channels control ATP release from adipocytes and contribute to metabolic homeostasis. Our studies show that adipocytes express functional Pannexin 1 (Panx1) channels that can be activated to release ATP by known mechanisms including alpha adrenergic stimulation and caspase-mediated C-terminal cleavage during apoptosis. Further, we identify insulin as a novel activator of Panx1 channels. Pharmacologic inhibition or selective genetic deletion of Panx1 from adipocytes decreased insulin-induced glucose uptake *in vitro* and *in vivo* and exacerbated diet-induced insulin resistance in mice. In obese humans, Panx1 expression in adipose tissue is increased and correlates with the degree of insulin resistance. Although in other systems extracellular ATP has been shown to be chemotactic for immune cells such as macrophages, we observed no difference in the level of macrophage infiltration or inflammation in adipose tissue of diet-induced obese, insulin resistant AdipPanx1 KO mice, (mice in which Panx1 was selectively deleted in adipocytes). We also observed that deficiency of the ATP receptor P2Y2 on myeloid cells in mice did not affect glucose intolerance in a model of diet-induced obesity and insulin resistance. However, mice which lack P2Y2 receptors in myeloid cells show decreased crown-like structure formation in perigonadal adipose tissue although the amount of macrophages within the tissue are not different from WT mice. In conclusion, Panx1 channel activity controls metabolic homeostasis in adipocytes, namely through the regulation of insulin-stimulated glucose uptake.

## ACKNOWLEDGMENTS

“Who is wise and understanding among you? The wisdom from above is first pure, then peaceable, gentle, open to reason, full of mercy and good fruits, impartial and sincere.”

James 3:13, 17 (ESV)

I am immensely grateful for my advisor, Dr. Norbert Leitinger. His enthusiasm for science is contagious. I am thankful that he took a chance on a graduate student with zero experience in biology. He allowed me the utmost freedom to pursue questions and perform experiments which was an invaluable learning experience. My ideas and suggestions were rarely met with a “No” and I was able to gain experience in many different techniques. I am very thankful to have been given opportunities to travel to many conferences and to be involved in writing review articles and helping with grant submissions. There were times when my faith in projects flagged, but Norbert’s optimism never wavered that our studies would advance and be published. We had our share of obstacles and miscommunications along the way, but I am very proud of the work that we accomplished, and I have the highest regard for Dr. Leitinger. One of the greatest lessons I learned in the lab was to believe in my data and its importance.

Many thanks to Rachael Griffiths and Poonam Sharma for teaching me everything from qPCR to mouse handling. Thank you for your expertise and your friendship. You turned a chemist into a biologist! I am grateful to Akshaya Meher for excellent initial work on the Panx1 project and continuing to be a valuable colleague. Kathryn, thank you for your eternal cheer and countless hours of image analysis! You are a true blessing. Thanks to other wonderful undergraduate students including Garren and Nathaniel. It has been a pleasure getting to know the newest members of the Leitinger Lab: Subbu and Gael. Subbu, thanks for many great science conversations, and I look forward to exciting Dab2 publications for years to come. Vlad, thank

you for taking over many of the lab management tasks when I felt like I just couldn't order one more primer! I look forward to attending your PhD defense very soon, and I hope you take me up on my offer for any help I can give you!

It has been an honor to be part of the Pharmacology Department at UVA. I have benefitted greatly from the wonderful spirit of collaboration in our department. I especially want to thank those involved in the Metabolic Interest Group, Pannexin Interest Group, and Cardiovascular Research Center Training Grant for giving great feedback through the years and presenting excellent research to ponder. I could not have gotten where I am without the help of Dr. Thurl Harris, Dr. Ira Schulman, and Dr. Bimal Desai. Thank you for always having an open door for experiment advice and life advice! I am also indebted to Dr. Susanna Keller for help in performing metabolic studies with the assistance of her technicians Natalie and Stefan. I am very thankful to our other collaborators for the Pannexin study including Dr. Douglas Bayliss, Joanna Sandilos, and Dr. Eva Chiu for electrophysiology studies, Dr. Coleen McNamara for human samples and also for being a great physician scientist role model for me, Dr. Brant Isakson and lab members, Dr. Shayn Peirce-Cottler and Scott Seaman for confocal microscopy. It was a pleasure to work with you! I would also like to thank Dr. Paula Barrett and Dr. Dean Kedes for advice along the way and for indefatigable support.

I am so happy to have made many great friends during my time at UVA who have been a wonderful support. Many great happy hours and coffee walks! Monica, Janelle, Julia, Laura, Tash, you are the best! Dr. Michael Digruccio, thanks for hanging around UVA long enough to be introduced to me and for everything you do! Last but not least, I want to thank my dear family. One of the best things about coming to UVA was coming back close to home and wild, wonderful West Virginia and all of you. All my love!

**TABLE OF CONTENTS**

ABSTRACT.....	3
ACKNOWLEDGMENTS.....	4
TABLE OF CONTENTS.....	6
LIST OF FIGURES.....	9
ABBREVIATIONS .....	11
Chapter 1 : INTRODUCTION .....	15
1.1 ADIPOSE TISSUE: OBESITY AND DIABETES .....	15
1.2 PURINERGIC SIGNALING IN ADIPOSE TISSUE .....	21
1.3 PANNEXIN 1 CHANNELS .....	22
Chapter 2 : EXPERIMENTAL METHODS .....	23
2.1 MATERIALS .....	23
2.2 CELL CULTURE .....	23
2.3 ISOLATION OF PRIMARY ADIPOCYTES .....	24
2.4 ADIPOCYTE GLUCOSE UPTAKE .....	25
2.5 ATP RELEASE FROM ISOLATED ADIPOCYTES.....	26
2.6 WESTERN BLOT, COIMMUNOPRECIPITATION, MEMBRANE ENRICHMENT AND FRACTIONATION .....	27
2.7 ELECTROPHYSIOLOGY .....	29
2.8 RNA ISOLATION AND qRT-PCR.....	30
2.9 ANIMAL CARE.....	30
2.10 MOUSE GENOTYPING .....	31
2.11 DIET-INDUCED OBESITY MODEL .....	31
2.12 BONE MARROW TRANSPLANTATION .....	32
2.13 ENDOTOXEMIA MODEL .....	33
2.14 ADIPOSE TISSUE FLOW CYTOMETRY.....	33
2.15 INDIRECT CALORIMETRY .....	34
2.16 CONFOCAL MICROSCOPY.....	34
2.17 MASS SPECTROSCOPY OF LIPIDS.....	35

2.18 BIOSORTER ANALYSIS OF ISOLATED ADIPOCYTES .....	35
2.19 STATISTICAL ANALYSIS .....	36
2.20 PRIMER SEQUENCES .....	36
Chapter 3 : Pannexin 1 is expressed and functional on adipocytes .....	37
3.1 ABSTRACT.....	37
3.2 INTRODUCTION.....	37
3.3 RESULTS .....	38
3.3.1 Expression of Panx1 .....	38
3.3.2 PE stimulation of adipocyte Pannexin 1 .....	42
3.3.3 Caspase-mediated Panx1 activation in apoptotic 3T3-L1 adipocytes .....	45
3.3.4 Insulin-mediated opening of Panx1 channels.....	51
3.3.5 Panx1 expression during adipocyte differentiation.....	54
3.4 DISCUSSION.....	57
Chapter 4 Pannexin 1-P2Y2 receptor inflammatory signaling in obese adipose tissue .....	60
4.1 ABSTRACT.....	60
4.2 INTRODUCTION.....	60
4.3 RESULTS .....	62
4.3.1 Adipocyte Panx1 function <i>in vitro</i> drives macrophage migration .....	62
4.3.1 Generation of AdipPanx1 Mouse and BMT P2Y2 .....	65
4.3.2 Characterization of high fat diet- and chow-fed AdipPanx1 KO and P2Y2 <sup>-/-</sup> -tp mice. ..	75
4.3.3 Analysis of adipose tissue inflammation and macrophage infiltration in obese AdipPanx1KO mice and P2Y2 <sup>-/-</sup> -tp mice.....	82
4.3.4 Pannexin 1 expression in human adipose tissue correlates with obesity and insulin resistance .....	88
4.4 DISCUSSION.....	91
Chapter 5 Pannexin 1 and Adipocyte Metabolic Function .....	94
5.1 ABSTRACT.....	94
5.2 INTRODUCTION.....	94
5.3 RESULTS .....	95
5.3.1 Glucose uptake in WT and Panx1 KO adipocytes .....	95
5.3.2 Lipid genes and Lipidomics .....	99

5.4 DISCUSSION.....	111
Chapter 6 DISCUSSION.....	112
6.1 SUMMARY OF FINDINGS.....	112
6.2 SIGNIFICANCE AND FUTURE DIRECTIONS.....	113
REFERENCES.....	122
PUBLICATIONS RESULTING FROM THIS WORK.....	136

## LIST OF FIGURES

Figure 1-1 Metabolic homeostasis of adipose tissue <sup>17</sup> .....	17
Figure 1-2 Adipose tissue dysfunction and metabolic syndrome <sup>17</sup> .....	19
Figure 3-1 Panx1 is expressed in murine adipocytes .....	40
Figure 3-2 Pannexin 1 channel function in adipocytes is regulated by alpha-adrenergic stimulation .....	43
Figure 3-3 Pannexin 1 channel function in adipocytes is regulated by caspase-mediated C-terminal cleavage .....	46
Figure 3-4 UV irradiation of 3T3-L1 adipocytes causes apoptosis and the opening of Panx1 channels .....	49
Figure 3-5 Insulin induces Panx1 channel activation and ATP release .....	52
Figure 3-6 Panx1 expression during 3T3-L1 differentiation may be downregulated via PPAR $\gamma$ ...	55
Figure 4-1 Adipocyte Panx1 function <i>in vitro</i> drives macrophage migration .....	63
Figure 4-2 Generation of adipocyte specific Pannexin 1 KO mouse .....	67
Figure 4-3 Generation of myeloid specific P2Y2 receptor KO mouse (P2Y2 <sup>-/-</sup> -tp) by bone marrow transplantation .....	70
Figure 4-4 P2Y2 <sup>-/-</sup> -tp mice challenged acutely with LPS are protected from inflammation. ....	73
Figure 4-5 Weight gain, energy expenditure, serum free fatty acids and insulin are not different between high fat fed WT and <i>AdipPanx1KO</i> mice .....	76
Figure 4-6 High fat fed P2Y2 <sup>-/-</sup> -tp mice show weight gain, adiposity, and glucose intolerance similar to high fat fed WT-tp .....	80
Figure 4-7 Adipose tissue inflammation is not different between high fat fed WT and <i>AdipPanx1KO</i> mice .....	83

Figure 4-8 High fat fed P2Y <sub>2</sub> <sup>-/-</sup> mice have decreased formation of crown-like structures in adipose tissue. ....	86
Figure 4-9 Pannexin 1 expression in human adipose tissue is associated with obesity and insulin resistance. ....	89
Figure 5-1 Full activation of insulin-stimulated glucose uptake in adipocytes requires ATP release by Panx1 channels. ....	97
Figure 5-2 Expression of metabolism genes in adipocytes from WT and AdipPanx1 KO mice. ...	100
Figure 5-3 Phosphatidylcholine and phosphatidylethanolamine content in adipose tissue from chow and high fat diet-fed WT and AdipPanx1 KO mice. ....	103
Figure 5-4 Phosphatidylserine and diacylglycerol content in adipose tissue from chow and high fat diet-fed WT and AdipPanx1 KO mice. ....	106
Figure 5-5 Phosphatidic acid content in adipose tissue from chow and high fat diet-fed WT and AdipPanx1 KO mice. ....	109
Figure 6-1 Adipocyte Panx1 is required for full activation of insulin-stimulated glucose uptake	120

**ABBREVIATIONS**

- Acsl1. Acyl-CoA Synthetase Long-Chain Family Member 1
- AdipPanx1 KO. Adipocyte-specific Pannexin 1 knockout mice
- Akt. Protein kinase B
- ANOVA. Analysis of variance
- ap2. Adipocyte protein 2/ Adipocyte Fatty Acid Binding Protein 4
- ATP. Adenosine triphosphate
- AUC. Area under the curve
- BAC. Bacterial artificial chromosome
- BAT. Brown adipose tissue
- BCA. Bicinchoninic acid
- BMDM. Bone marrow-derived macrophage
- BMI. Body-mass index
- BMT. Bone marrow transplant
- CASP3. Caspase 3
- CBX. Carbenoxolone
- CCL2. Chemokine (C-C motif) ligand 2
- CLS. Crown-like structure
- CREB. cAMP response element-binding protein
- DAG. Diacylglycerol
- DAPI. 4',6-diamidino-2-phenylindole
- Dgat1. Diacylglycerol O-Acyltransferase 1
- DM1. Differentiation media 1

DM2. Differentiation media 2

DMEM. Dulbecco's Modified Eagle Medium

DNA. Deoxyribonucleic acid

EGFP. Enhanced green fluorescent protein

ER. Endoplasmic reticulum

ETV4. Ets Variant 4

FACS. Flow cytometry/ Fluorescence Activated Cell Sorting

FATP1. Fatty acid transport protein 1

FFA. Free fatty acid

FOCA. Fluidic and optical core assembly

Glut4. Glucose transporter type 4

HDM. High density microsomes

HEPES. 4-(2-hydroxyethyl)-1-piperazineethanesulfonic acid

HOMA-IR. homeostatic model assessment-insulin resistance

IBMX. 3-Isobutyl-1-methylxanthine

IL1 $\beta$ . Interleukin 1 beta

IL6. Interleukin 6

Irs1. Insulin receptor substrate 1

kDa. Kilodalton

KRH-BSA. Kreb's Ringer HEPES Buffer with Bovine Serum Antigen

LDM. Low density microsomes

LPA. Lysophosphatidic acid

LPS. Lipopolysaccharide

LY. Lymphocyte

MO. Monocyte

Mogat1. Monoacylglycerol O-Acyltransferase 1

mRNA. Messenger ribonucleic acid

mTOR. Mammalian target of rapamycin

NCBI. National Center for Biotechnology Information

NE. Neutrophil

NT5E. 5'-Nucleotidase, Ecto (CD73)

Panx1. Pannexin 1

PBS. Phosphate-buffered Saline

PC. Phosphatidylcholine

PCR. Polymerase chain reaction

PE. Phosphatidylethanolamine or Phenylephrine

PGC1 $\alpha$ . Peroxisome proliferator-activated receptor gamma coactivator 1-alpha

PI. Propidium iodide

Ppar $\gamma$ . Peroxisome Proliferator-Activated Receptor Gamma

Pref1. Preadipocyte factor 1

PS. Phosphatidylserine

RIPA. Radioimmunoprecipitation assay buffer

s.d.. Standard deviation

s.e.m.. Standard error of the mean

SDS. Sodium dodecyl sulfate

SVF. Stromal vascular fraction

TBS. Tris-buffered saline

TES. Tris-EDTA-sucrose

TEV. Tobacco etch virus

TG. Triglyceride

TNF $\alpha$ . Tumor necrosis factor alpha

TOF. Time of flight

UCP1, Uncoupling protein 1

UTP. Uridine triphosphate

UV. Ultraviolet

WAT. White adipose tissue

## Chapter 1 : INTRODUCTION

### 1.1 ADIPOSE TISSUE: OBESITY AND DIABETES

Obesity and diabetes have reached epidemic proportions in the United States, with medical costs reaching over \$250 billion dollars.<sup>1,2</sup> Obesity is defined as having a body-mass index (BMI) of greater than or equal to 30<sup>3</sup> and characterized by excess adipose tissue. Obesity is associated with all-cause mortality; however, being overweight is less clearly associated with mortality and indeed in some studies was shown to protect against mortality.<sup>4,5</sup> Specifically, obesity increases the risk of mortality due to ischemic heart disease (Hazard Ratio: HR 1.39), stroke (HR 1.39), diabetes (HR 2.16), chronic kidney disease (HR 1.59), cancer (HR 1.10), and respiratory diseases (HR 1.20).<sup>6</sup> For heart disease, stroke, and diabetes, clinical evidence suggests that the distribution of body fat is also an important predictor of risk.<sup>7-10</sup> Excess visceral adipose tissue (as opposed to excess subcutaneous adipose tissue) contributes to risk and can be quantified using the waist-to-hip ratio measurement.

Adipose tissue is made up of adipocytes as well as connective tissue, networks of blood vessels and neurons, and self-renewing progenitor cells. Recently, it was discovered that adipose tissue also contains immune cells including macrophages, T-cells, and eosinophils.<sup>11</sup> The human body contains various types of adipose tissue including white adipose tissue, which is subdivided into subcutaneous and visceral adipose tissue and brown adipose tissue. The classical function of white adipose tissue is lipid storage, meaning that excess nutrition which is converted to lipid is stored within lipid droplets of adipocytes. The adipocyte lipid droplet can expand to accommodate more lipid or contract when energy sources are needed and lipid is metabolized in times of starvation (Fig 1-1). In contrast, the main function of brown adipose tissue is thermogenesis.<sup>12</sup> In addition to functioning as a lipid storage depot, white adipose

tissue is also a key endocrine organ.<sup>13</sup> Adipocytes secrete molecules termed adipokines such as leptin, adiponectin, visfatin, and others that are carried through the blood to different areas of the body such as the brain where signaling cascades occur to trigger homeostatic mechanisms.<sup>14</sup>

Nearly all cells in the body require glucose as a metabolic substrate; thus, maintaining glucose homeostasis is essential. Dysfunctional glucose homeostasis results in hypoglycemia (low blood sugar levels) which can result in seizures and death, or hyperglycemia (elevated blood sugar levels) which is a defining characteristic of diabetes mellitus. Although muscle and liver tissue contribute greatly to glucose homeostasis, adipose tissue is also highly insulin sensitive, and metabolic dysfunction of adipocytes exacerbates insulin resistance.<sup>13</sup> In healthy adipose tissue, insulin stimulates glucose uptake and lipogenesis while inhibiting lipolysis, but these effects are blunted during insulin resistance.<sup>13</sup> Furthermore, glucose uptake in adipocytes is a major contributor to whole body insulin sensitivity.<sup>15</sup> Metabolic syndrome is defined as a cluster of risk factors that increase a person's risk for heart disease, diabetes, and stroke. These risk factors include high waist circumference due to excess abdominal fat, high triglycerides, low HDL-cholesterol, high blood pressure, and high fasting blood glucose suggestive of insulin resistance.<sup>16</sup> Adipose tissue dysfunction such as decreased insulin sensitivity and increased inflammation contributes to the pathology of metabolic syndrome (Fig 1-2).

**METABOLIC HOMEOSTASIS**

nature  
medicine

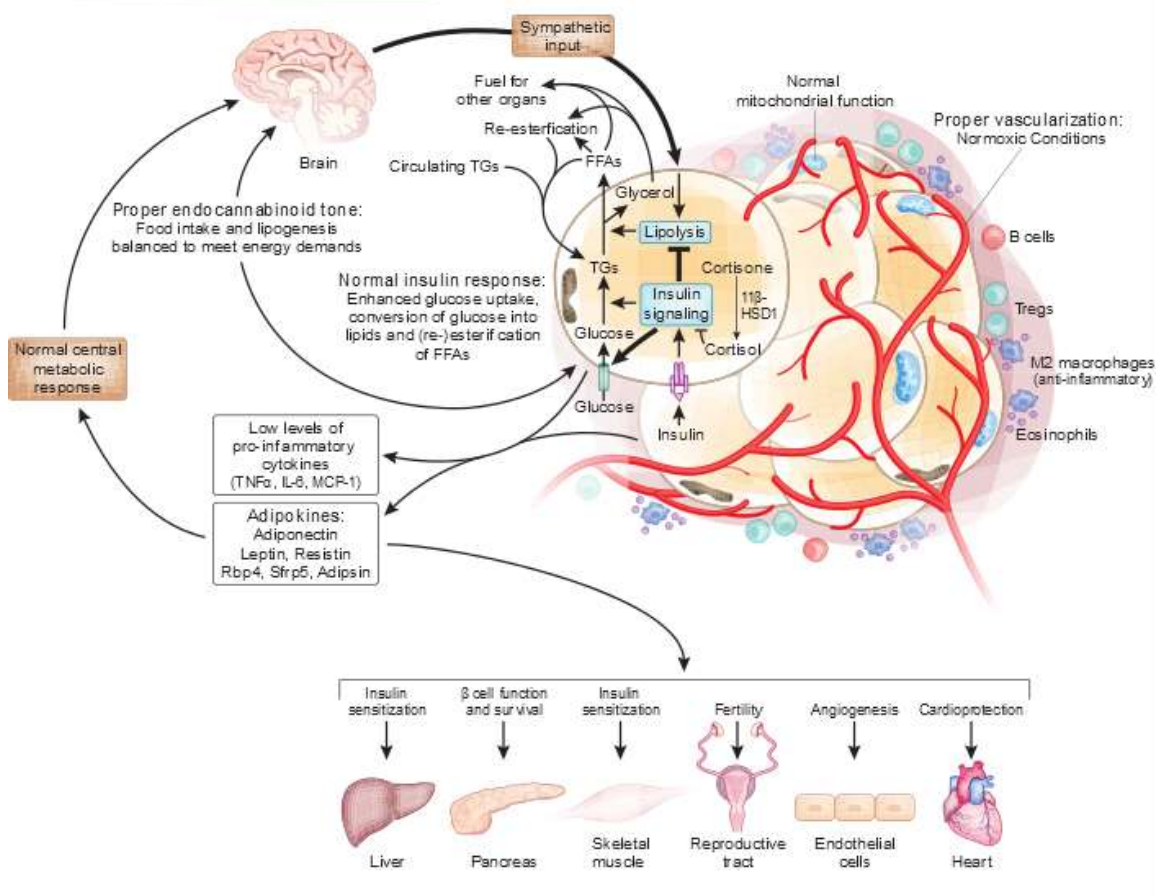


Figure 1-1 Metabolic homeostasis of adipose tissue<sup>17</sup>

**Figure 1-1. Metabolic Homeostasis of Adipose Tissue**

In addition to functioning as a lipid storage depot, white adipose tissue is also a key endocrine organ that secretes adipokines and other factors which ensure proper metabolic responses for key target tissues, such as the liver and muscle, the  $\beta$  cells in the pancreas and cardiac myocytes, and the endothelium. In healthy adipose tissue, there is a higher frequency of macrophages that fall into the general category of alternatively activated, anti-inflammatory “M2-type” macrophages, as well as regulatory T cells (Tregs). Eosinophils are present and help sustain the macrophages in an alternatively activated state. Mitochondrial function is preserved, and there is an adequate supply of oxygen and nutrients for the fat cells due to proper vascularization. Insulin sensitivity is fully preserved, and as a result, insulin potently stimulates glucose uptake through translocation of the GLUT4 transporter to the plasma membrane. Furthermore, insulin effectively stimulates esterification of FFAs to triglycerides (TGs). On the other hand, responsiveness to sympathetic input is highly preserved, reflecting the high degree of metabolic flexibility that the adipocytes display to adapt to environmental cues. Activation of the  $\beta$ 3 adrenergic receptors (not diagrammed) stimulates lipolysis. The FFAs and glycerol released under those conditions can serve as a fuel source for other tissues. However, there is also a relatively high degree of immediate re-esterification of these FFAs and glycerol back into TGs. Abbreviations used: TNF $\alpha$ : tumor necrosis factor alpha; IL-6: interleukin 6; MCP-1: monocyte chemoattractant protein-1; Rbp4: retinol binding protein 4; Sfrp5: secreted frizzled-related protein 5; 11 $\beta$  HSD1: 11 $\beta$ -hydroxysteroid dehydrogenase type 1. (Adapted from Nature Medicine Metabolic Syndrome ePoster, Adipose Tissue Section<sup>17</sup>)

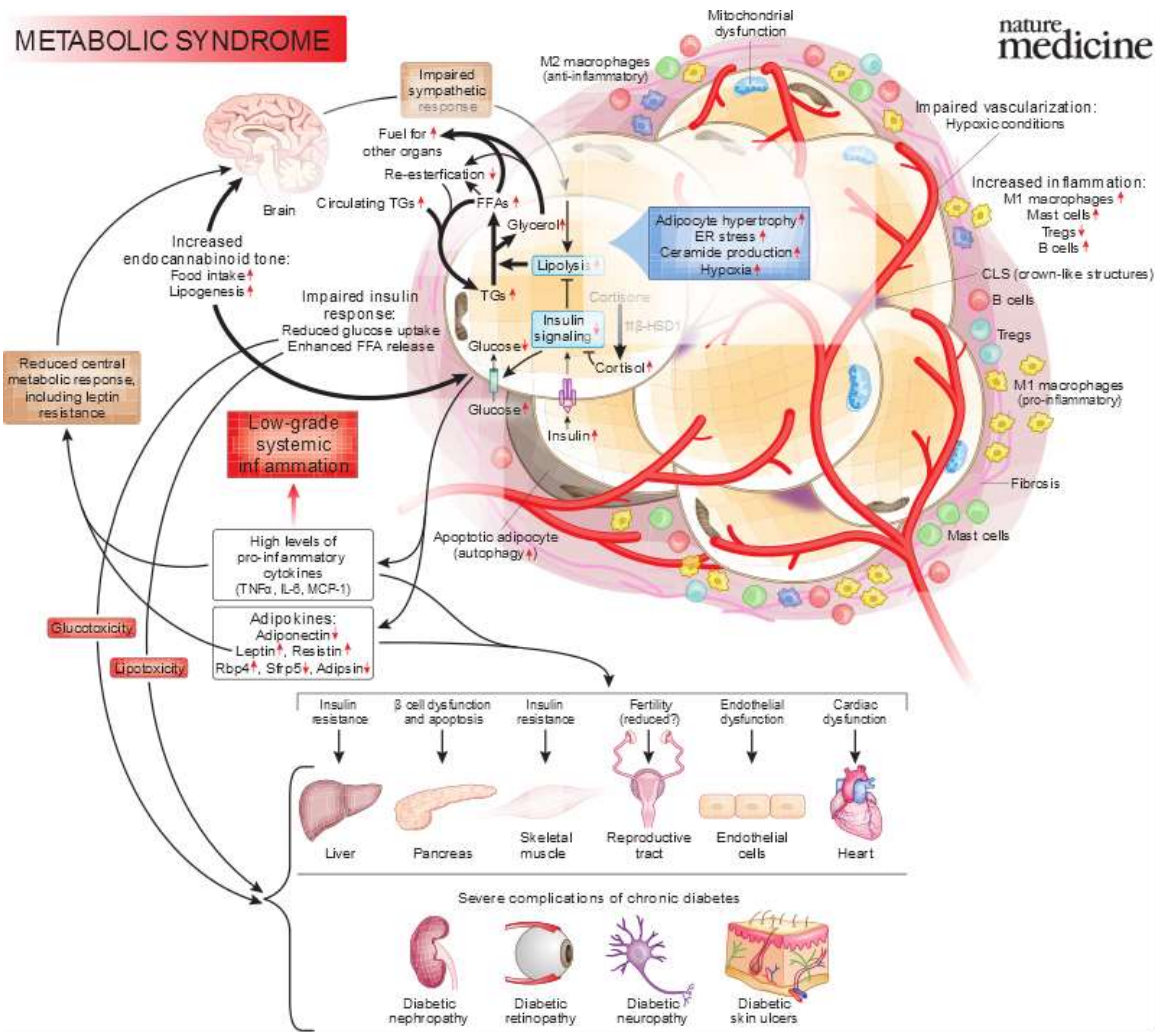


Figure 1-2 Adipose tissue dysfunction and metabolic syndrome<sup>17</sup>

**Figure 1-2 . Adipose tissue dysfunction and metabolic syndrome.**

In the presence of excess energy supply adipose tissue expands as a result of cellular hypertrophy and hyperplasia. Dead adipocytes attract immune cells including macrophages that are conventionally skewed towards an “M1-like” pro-inflammatory profile, resulting in increased inflammation. The vascular infrastructure generally does not keep pace with the rapid tissue expansion during obesity, leading to local hypoxia and further death of adipocytes which are surrounded by macrophages in what are termed crown like structures (CLS). Inflammation, endoplasmic reticulum stress, and increased levels of free fatty acids (FFAs) exacerbate insulin resistance and cause a decrease in insulin-mediated glucose uptake. The  $\beta$  adrenergic response downstream of sympathetic nerve activity is also impaired which leads to reduced metabolic flexibility. These adipocyte metabolic dysfunctions result in lipotoxic and glucotoxic effects that impact other tissues such as liver, pancreatic  $\beta$  cells, muscle cells, endothelial cells, and neurons that culminate in pathophysiological changes associated with diabetes, such as diabetic nephropathy, neuropathy, retinopathy and skin ulcer formation.

Abbreviations used: TNF $\alpha$ : tumor necrosis factor alpha; IL-6: interleukin 6; MCP-1: monocyte chemoattractant protein-1; Rbp4: retinol binding protein 4; Sfrp5: secreted frizzled-related protein 5; TGs: triglycerides; 11 $\beta$  HSD1: 11 $\beta$ -hydroxysteroid dehydrogenase type 1. (Adapted from Nature Medicine Metabolic Syndrome ePoster, Adipose Tissue Section<sup>17</sup>)

## 1.2 PURINERGIC SIGNALING IN ADIPOSE TISSUE

The purine nucleoside adenosine accumulates extracellularly in isolated adipocyte suspensions<sup>18-20</sup> and is thought to be derived from degradation of extracellular ATP. Adenosine can impact adipocyte metabolic function by inhibiting lipolysis<sup>21</sup>, increasing glucose uptake<sup>22,23</sup>, enhancing insulin action to stimulate glucose oxidation<sup>24</sup>, and by regulating adipose tissue blood flow<sup>25</sup>. In addition to adenosine, extracellular nucleotides such as ATP or UTP have autocrine effects on adipocytes. They signal through the purinergic P2 receptor family, which includes ATP-gated cation channels P2X1-7 and G-protein-coupled P2Y1,2,4,6,11-14 receptors.<sup>26</sup> In brown adipose tissue, extracellular ATP caused mobilization of intracellular calcium stores, consistent with nucleotide signaling through purinergic P2 receptors.<sup>27</sup> Extracellular ATP also led to increased cell membrane capacitance in adipocytes<sup>28,29</sup> and it was suggested that ATP activates exocytosis.<sup>30</sup> In white adipocytes, micromolar concentrations of ATP inhibit glucose oxidation<sup>31</sup>, but increase glycogen synthesis<sup>32</sup> and lipogenesis<sup>33</sup>. However, the effect of exogenous ATP on basal and insulin-induced glucose uptake in adipocytes is still a matter of controversy: ATP was shown in some studies to be inhibitory at millimolar concentrations<sup>34,35</sup> while in other work no effect of ATP was observed<sup>33</sup>.

Purinergic signaling in endocrine organs has been a major research focus [reviewed by<sup>36</sup>] and novel therapies based on purinergic receptors as potential drug targets for type II diabetes have been suggested<sup>37-39</sup>. However, there are many purinergic receptors and modulating ATP release could represent an alternative therapeutic strategy. In this respect, it remains an open question as to how nucleosides and nucleotides are released from adipocytes in a controlled manner. Pannexin 1 channels can release ATP from cells in a controlled manner and are the focus of this work.

### 1.3 PANNEXIN 1 CHANNELS

The three members of the pannexin family, Panx1, 2, and 3, are hexameric membrane channels, structurally similar to connexins but not gap-junction-forming.<sup>40</sup> Panx1 and 3 are present in many tissues while Panx2 is mainly expressed in the brain.<sup>41</sup> The function of Panx2 and Panx3 channels is reviewed elsewhere.<sup>41</sup> Panx1 channels located on the plasma membrane release ATP, other nucleotides, and molecules up to 1 kD, into the extracellular space, when activated.<sup>41</sup> Panx1 channels have also been observed to be present on the endoplasmic reticulum, functioning as intracellular calcium-leak channels.<sup>42</sup> Pannexin channels are post-translationally modified by N-glycosylation<sup>43</sup> and they can also be S-nitrosylated<sup>44</sup>, which has important functional consequences. Regulation of Panx1 expression remains to be fully studied, but it has been reported that treatment with IL1 $\beta$  upregulates Panx1 expression.<sup>45</sup> Known inhibitors of Panx1 include carbenoxolone (CBX), probenecid, mefloquine, which have other targets in addition to Panx1, and the food dye FD&C Blue No. 1 which has specificity for Panx1.<sup>46,47</sup> The antibiotic trovafloxacin was recently discovered to be a potent inhibitor of Panx1.<sup>48</sup> Activation of Panx1 can proceed by various mechanisms including mechano-stretch<sup>49</sup>,  $\alpha$ 1-adrenergic<sup>50</sup> or histamine stimulation<sup>51</sup>, and caspase-mediated cleavage of the C-terminal portion of Panx1, an irreversible process.<sup>52</sup> It is important to note that caspase-mediated cleavage and activation of Panx1 results in irreversible channel opening and perhaps higher amounts of extracellular ATP being released. Panx1 activation can be coupled to purinergic receptor activation as in the case of inflammasome activation, during which P2X7 receptor and Panx1 are associated. It has also been reported that activation of P2Y6 receptors in bladder urothelium mediates Panx1-dependent ATP release.<sup>53</sup>

## **Chapter 2 : EXPERIMENTAL METHODS**

### **2.1 MATERIALS**

Anti-Pannexin 1 antibody directed against the C-terminal region was a kind gift of Silvia Penuela as well as produced by the UVA Hybridoma Core. Anti-Pannexin 1 antibody directed to the extracellular loop region was a kind gift of Silvia Penuela. Anti-Panx1 antibody directed to the N-terminal region was from Invitrogen. Antibodies used for flow cytometry were from Biolegend or eBiosciences as indicated. Solid laboratory chemicals were from Sigma unless otherwise indicated. Cytokine ELISA kits were from Biolegend. Insulin ELISA kit was from Crystal Chem. [U-<sup>14</sup>C]-D-glucose was from ICN. [<sup>3</sup>H]-2-deoxy-D-Glucose was from Perkin Elmer.

### **2.2 CELL CULTURE**

3T3-L1 fibroblasts (ATCC) were cultured in high glucose DMEM supplemented with 10% newborn calf serum (Gibco) at 37°C, 95% relative humidity and 5% CO<sub>2</sub>. For differentiation into adipocytes, cells were grown to confluence and treated for three days with differentiation media I: DMEM high glucose, 10% fetal bovine serum, 1% anti-anti, 0.25 U/mL insulin (Humulin), 0.5mM IBMX (Sigma), 0.025 mM dexamethasone (Sigma), followed by treatment for three days with differentiation media II: DMEM high glucose, 10% FBS, 0.25 U/mL insulin and then adipocytes were maintained in DMEM high glucose with 10% FBS. When propagating 3T3-L1 fibroblasts, media should be refreshed every 2 days and cells must not reach confluency, otherwise differentiation into adipocytes will not occur. Fibroblasts grown in a 100 cm plate can be split 1:5 every two days, plating into two 24 well plates.

### 2.3 ISOLATION OF PRIMARY ADIPOCYTES

Low Phosphate Buffer (also called Krebs-ringer-HEPES (KRH) buffer):

Component:	Final Concentration:	Working Stock:	Grams per 100mL H <sub>2</sub> O for working stock:	mL working stock per 100mL final buffer:
NaCl	145 mM	2M	11.688	7.25
KCl	5.4 mM	100mM	0.7455	5.4
CaCl <sub>2</sub>	1.4 mM	50mM	0.7351 (FW 147.02)	2.8
MgSO <sub>4</sub>	1.4 mM	50mM	1.2324 (FW 246.48)	2.8
NaPO <sub>4</sub>	0.2 mM	10mM	0.1420	2
HEPES	10 mM	1M		1
BSA (insulin free)	0.1% w/v			
Glucose*	5mM			0.0903 g

\*Glucose uptake assays with isolated adipocytes must be performed in glucose-free KRH buffer

Digestion Buffer:

Low Phosphate Buffer with glucose containing Type I Collagenase (Worthington) at a 1 mg/mL concentration.

Buffer should be prepared fresh on the day of isolation; typically 400 mL of buffer is sufficient for most applications. Bring buffer to 37°C in water bath, pH to 7.4 with 1 M NaOH, sterile filter through 0.2 µm filter setup. Assays will not work properly if buffer is not pH 7.4 at 37°C. Remove perigonadal fat pads from mice, carefully avoiding gonadal tissue and place into preweighed glass vial containing 1 mL digestion buffer. Calculate weight of isolated adipose tissue and add additional collagenase-KRH-BSA buffer such that there are 2 mL of digestion buffer for every 1 g of adipose tissue. Mince tissue with 2 pairs of small, sharp scissors for 2 min or until well-minced (applesauce consistency). Place in reciprocating 37°C water bath shaking at 100 rpm for 1 hr. Pass digested tissue over nylon mesh into 50 mL conical tube, using 10 mL

syringe plunger to press through. Wide-bore 1 mL pipette tips are ideal because adipocytes will not be sheared. Adding extra buffer is very helpful in passing cell suspension through mesh. Allow adipocytes to float and withdraw infranatant with 20 gauge, long, blunted needle and 10 mL syringe. Infranant contains stromal vascular cells. Wash with at least 10 mL buffer. Typically for every 1 g of adipose tissue digested, 1 mL volume of packed adipocytes should be obtained. Cells should be washed with at least a 10X volume of buffer. Add first 2 washes to conical containing SVF. SVF cells are pelleted by centrifuging at 1500 rpm at 4 °C for 5min and then resuspended in 5 mL 0.83% ammonium chloride at room temperature for 10 min to lyse red blood cells and then repelleted and resuspended in buffer of choice.

For adipocytes, after 3 washes, calculate volume of packed cells. Centrifugation at room temperature for 200 g for 2 min will condense adipocyte packed cell layer, but may destroy some cells. Adipocytes are then placed in a 5X volume of buffer for downstream applications.

For RNA isolation, add 1 mL trizol to 0.5 mL packed cells, vortex well, and store in -80 °C freezer until further use.

For protein isolation, wash adipocytes in PBS pH 7.4 twice to remove BSA and then add appropriate lysis buffer. (See Western Blotting for more details)

#### **2.4 ADIPOCYTE GLUCOSE UPTAKE**

Glucose uptake was measured in isolated adipocytes as described.<sup>54</sup> Briefly, adipocytes were isolated from murine perigonadal adipose tissue by mincing and collagenase digestion followed by washing in Krebs-Ringer-HEPES-BSA buffer and then diluted 10-fold in KRH-BSA to give an approximate 5% (vol/vol) cell suspension. Aliquots of the cell suspension (100 µL) were added to 350 µL of KRH-BSA (0.5% BSA) containing insulin or ATP as indicated and incubated in a 37 °C shaking water bath (100 rpm) for 30 min. To each tube, 50 µL of 100 µM [U-14C]-D-glucose in

KRH-BSA (1.25  $\mu$ Ci/aliquot) was added, and the incubation continued for another 20 min.

Glucose uptake was terminated by separating the medium from the cells in a 200  $\mu$ L aliquot from each assay tube by centrifugation through 150  $\mu$ L of dinonyl phthalate.

Glucose uptake measurements in 3T3-L1 adipocytes were performed in a similar fashion using [3H]-2-deoxy-D-glucose. Cells were differentiated in 24-well plates. On the day of the assay, each well was washed with glucose free KRH buffer and a final volume of 500  $\mu$ L of glucose free KRH buffer was added per well. Cells were pretreated with Panx1 inhibitors in 500  $\mu$ L glucose-free KRH buffer for 20 min followed by addition of 5  $\mu$ L insulin (1 U/mL humulin) in KRH buffer for 10 min followed by addition of 5  $\mu$ L 20 mM 2-deoxy-D-glucose with 0.2  $\mu$ C [3H]-2-deoxy-D-glucose for 10 min. The reaction is terminated by 3 washes with cold PBS pH 7.4 followed by addition of 500  $\mu$ L 0.1 % SDS in PBS to lyse cells. 250  $\mu$ L of homogenate is added to 4 mL of scintillation fluid and vortexed well. Radioactivity is determined by scintillation counting for 3H. Nonspecific association of radioactive glucose with cells was assessed by performing the assay in the presence of cytochalasin B (20  $\mu$ M).

## **2.5 ATP RELEASE FROM ISOLATED ADIPOCYTES**

Adipocytes were isolated from murine perigonadal adipose tissue as above and washed with fresh Krebs-Ringer-HEPES-BSA buffer prior to each experiment and diluted 2.5-fold in KRH-BSA. 400 or 200  $\mu$ L of cell suspensions are used per replicate and added to tubes containing phenylephrine or media and incubated for indicated time. Alternatively, adipocytes are pretreated with Panx1 inhibitor probenecid for 30 min followed by addition of 50  $\mu$ L concentrated insulin and incubated for indicated time. Infranatant is collected with a blunted needle, carefully avoiding floating adipocyte and treated with Cell-titer glo reagent (Promega). Luminescence was read on a Tecan Infinite M200 plate reader.

## **2.6 WESTERN BLOT, COIMMUNOPRECIPITATION, MEMBRANE ENRICHMENT AND FRACTIONATION**

Cultured cells were lysed in RIPA buffer (Millipore) supplemented with protease inhibitor cocktail (Roche) and phosphatase inhibitors (Sigma). Snap frozen tissue pieces were lysed in RIPA buffer using a TissueLyser II (Qiagen) stainless steel bead homogenizer for up to 3 min at 30 Hz. Lysates were cleared by centrifugation at 12,000 g for 10 min at 4°C then subjected to BCA protein assay (Pierce). Samples were subjected to Laemmli buffer with beta-mercaptoethanol and 5-10 min denaturing at 95°C and then electrophoresed on 10% SDS-PAGE gel using Biorad Mini-Protean System (typically run at 60 mV for 2.5 hr). Proteins were transferred to nitrocellulose membrane (BioRad) using Biorad Mini-Protean System, typically run at 100 mV for 70 min in ice bath. Membranes were blocked for 30 min at room temperature in 1:1 Odyssey Licor blocking buffer: TBS. Blots were incubated in primary antibody diluted in 1:1 Odyssey Licor blocking buffer: TBS overnight at 4°C followed by three, 5 min washes in 1:1 Odyssey Licor blocking buffer: TBST at room temperature. Blots were incubated with appropriate secondary Licor IRDye antibodies at 1:10,000 dilution in 1:1 Odyssey Licor blocking buffer: TBS for 2 hours at room temperature followed by three, 5 min washes. Blots were scanned on Odyssey Licor Imager. Blots were occasionally stained with Ponceau stain to observed total protein. Actin (42 kDa), tubulin (50 kDa), or vinculin (130 kDa) were used as loading controls.

For coimmunoprecipitation, samples in RIPA buffer were incubated overnight at 4°C with 20 µL protein A/G beads (Santa Cruz) with antibody of interest. Samples were washed 3 times by centrifugation and removal of supernatant and then subjected to Laemmli buffer with beta-mercaptoethanol and 5-10 min denaturing at 95°C prior to electrophoresis. Controls

containing no antibody of interest were performed to determine non-specific binding, and samples were occasionally incubated overnight at 4 °C with 20 µL protein A/G beads alone and then supernatants were carried on to steps described above in order to decrease nonspecific bands on western blot. Licor IRDye® 680RD was added 1:1000 with primary antibody incubation for coimmunoprecipitation blots because it does not bind denatured heavy and light chain.

For crude membrane enrichment, isolated adipocytes were washed in Tris-EDTA-sucrose (TES) buffer (20 mM Tris, 1 mM EDTA, 250 mM sucrose, pH 7.4 at 4 °C), followed by lysis by forcing cells through a 21 g needle 5 times. Lysate was centrifuged in Eppendorf tube for 10 min at 800 g to pellet nuclei. Supernatant was transferred to a thick-walled polycarbonate tube and centrifuged for 30 min at 4 °C at 175,000 g (38,000 rpm) in a fixed-angle Ti90 rotor. Pellet contains enriched membranes and is resuspended by brief sonication in Laemmli buffer to load onto gel for Western blot. An alternative method for crude membrane enrichment is to sonicate isolated adipocytes in TES buffer containing phosphatase and protease inhibitors followed by centrifugation at 30,000 g for 30 min at 4 °C in a fixed-angle Ti90 rotor. Pellet contains membrane enriched fraction and is resuspended in RIPA buffer and solubilized by forcing through 21 g needle.

For isolation of plasma membranes<sup>55</sup>, lysates in TES buffer are centrifuged at 500 g for 3 min. Supernatant and pellet underneath fat layer are collected and centrifuged at 16,000 g for 30 min at 4 °C. Pellet contains plasma membranes and is resuspended in 1 mL TES buffer and placed on top of 11.25 mL of a 1.12 M sucrose cushion (20 mM Tris, 1 mM EDTA, 1.12 M sucrose, pH 7.4 at 4 °C) in thinwalled polypropylene tubes and centrifuged at 100,000 g for 60 min at 4 °C in a swinging bucket SW41 Ti rotor with acceleration and deceleration set to low. Plasma membranes are a fuzzy white band at the interface near the top of the tube and are

collected and resuspended in 5-6 mL TES buffer and centrifuged at 48,000 g for 30 min at 4 °C to obtain pellet with plasma membranes that can be resuspended in 100 µL of buffer to take forward for Western blotting. High density microsomes (HDM) and low density microsomes (LDM) can be isolated by processing the supernatant from the initial 16,000 g centrifugation for 30 min at 4°C. Centrifuge supernatant for 30 min at 4°C at 48,000 g. Pellet from this step contains HDM, and supernatant contains LDM which can be pelleted by centrifugation for 30 min at 250,000 g at 4°C in a fixed-angle 70.1 Ti rotor. This plasma membrane isolation protocol can be used to determine GLUT4 translocation to the plasma membrane in perigonadal adipose tissue isolated from mice injected with either saline or 0.75 U/kg insulin for 30 min. Two mice are used per condition, and perigonadal fat pads are combined and processed as one sample in order to yield enough protein for Western blotting. Whole fat pads are homogenized in TES buffer by 10 strokes at 1250 rpm with Teflon pestle and lysates are processed as described above, saving 100 µL of whole lysate to run on Western as a control for total Glut4 content in adipose tissue.

## **2.7 ELECTROPHYSIOLOGY**

Patch clamping of 3T3-adipocytes with active caspase 3 was performed as described previously<sup>52</sup>. Whole-cell recordings were made at room temperature using Axopatch 200B amplifier (Molecular Devices) with a bath solution composed of 140 mM NaCl, 3 mM KCl, 2 mM MgCl<sub>2</sub>, 2 mM CaCl<sub>2</sub>, 10 mM HEPES and 10 mM glucose (pH 7.3). Borosilicate glass patch pipettes (3-5 MΩ) were filled with an internal solution containing 30 mM tetraethylammonium chloride, 100 mM CsMeSO<sub>4</sub>, 4 mM NaCl, 1 mM MgCl<sub>2</sub>, 0.5 mM CaCl<sub>2</sub>, 10 mM HEPES, 10 mM EGTA, 3 mM ATP-Mg, and 0.3 mM GTP-Tris (pH 7.3). Ramp voltage commands were applied by using pCLAMP software and Digidata1322A digitizer (Molecular Devices). HEK293T cells were

transiently transfected using Lipofectamine2000 (Invitrogen), and underwent serum depletion for 2-4 hours before patch recording in order to reduce basal insulin receptor signaling. Basal Panx1 current was recorded, and then insulin (180 nM) was applied to the bath solution, followed by CBX (50  $\mu$ M). Note that no CBX-sensitive current was observed in HEK293T cells without heterologously expressing Panx1.<sup>52</sup> Constructs used in HEK293T heterologous system include mouse Panx1 wildtype construct<sup>44,56</sup>, human Panx1(TEV) construct<sup>52</sup>, and an EGFP-tagged human insulin receptor construct (Addgene).<sup>57</sup>

## **2.8 RNA ISOLATION AND qRT-PCR**

RNA isolation was performed using either extraction with trizol (Invitrogen) or RLT buffer (Qiagen) and then purified using RNeasy columns (Qiagen), followed by quantification and purification analysis with nanodrop (Thermo). cDNA was synthesized from 250 $\mu$ g total RNA with an iScript cDNA synthesis kit (Bio-rad) according to manufacturer's instructions. For real-time PCR from murine samples, synthesized cDNA forward and reverse primers along with SensiFast Sybr (Bioline) master mix were run on the CFX Connect Real-Time System.  $\beta$ -2-microglobin was used as an internal loading control and the Pfaffl method<sup>58</sup> of analysis was used.

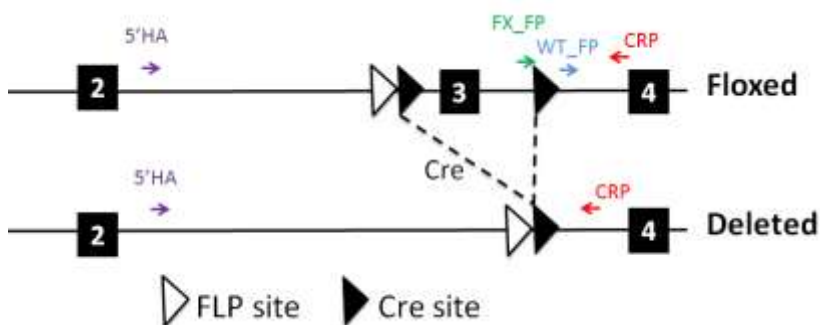
Because detection of Panx1 mRNA with standard primers was difficult, taqman probes were used: mm0045091\_m1 mpanx1, mm01545399\_m1 HPRT, Hs00209790\_m1 Panx1, and Hs99999901\_s1 18S. iTaq Universal Probes Supermix (Bio-rad) was used.

## **2.9 ANIMAL CARE**

All animal studies were approved by the Animal Care and Use Committee at the University of Virginia.

## 2.10 MOUSE GENOTYPING

Panx1<sup>fl/fl</sup>Adipoq<sup>Cre</sup> mice were generated through appropriate breeding between the Adipoq<sup>Cre</sup> mice<sup>59</sup> with Panx1<sup>fl/fl</sup> mice<sup>48</sup>. Littermate controls were used for all experiments. Genomic DNA was isolated from tail clips by Proteinase K digestion in DirectPCR reagent (Viagen). Genomic DNA was subjected to PCR using the Apex Taq Master Mix (Genesee Scientific) and specific primers. PCR products were resolved by electrophoresis in 2% agarose gel with ethidium bromide. Bands were recognized as wild type 331 bp, floxed 379 bp and null allele at 510 bp. A cre-specific band was detected at 100 bp using Cre-specific primers.



Px1 5'HA	AGGAACCATTCTGCAGGACAGGAA
Px1_WT_FP	CCGTAGCTTGCTTGCTTTGATCT
Px1_FX_FP	AGATGGCGCAACGCAATTAATGA
Px1_CRP	TGGCTCTCATAATTCTTGCCCTGG
ap2cre F	ATGTCCAATTTACTGACCG
ap2cre R	CGCCGCATAACCAGTGAAC

## 2.11 DIET-INDUCED OBESITY MODEL

Mice were fed a high fat diet containing 60% cal from fat and 0.2% cholesterol (Bioserv) or normal chow (Teklad). Fat and lean masses were measured by EchoMRI™-100H Body Composition Analyzer. Glucose and insulin tolerance tests were performed in accordance with recommendations published by Ayala et. al.<sup>60</sup>. For glucose tolerance test, mice were fasted for 6

hr and then injected with 1 g/kg glucose i.p. and blood glucose levels were measured from tail blood by glucometer (OneTouch Ultra) over 2 hr. For insulin tolerance test, mice were fasted 6 hr and then injected with 0.75 U/kg insulin i.p. and blood glucose levels were measured from tail blood by glucometer (OneTouch Ultra) over 1 hr.

In vivo glucose uptake studies were performed as described<sup>55</sup>. In brief, mice were fasted 6 hr followed by intraperitoneal injection of 2 g/kg glucose containing 10  $\mu$ Ci [3H] 2-deoxy-D-glucose. Gastrocnemius muscle and perigonadal adipose tissues were collected 2 hr post injection and snap frozen. 2-deoxyglucose uptake in tissues was determined by passing tissue homogenates over poly-prep chromatography columns with AG1-X8 resin (Bio-rad) and then calculating the difference in radioactive counts between total homogenate and column eluent, normalizing to specific activity of glucose as determined by serum samples processed with perchloric acid.

## **2.12 BONE MARROW TRANSPLANTATION**

For bone marrow transplantation, 4 wk old recipient C57Bl/6 mice received 80 mg/ml sulfmethoxazole and 0.37 mM trimethoprim in autoclaved water six days prior to receiving 2 doses of 600 RAD each, 4 hours apart (Shepard Mark irradiator). Bone marrow was harvested from tibias and femurs of donor WT (C57Bl/6) and global P2Y2<sup>-/-</sup> mice (kindly provided by Dr. Kodi Ravichandran, UVA), and 2 million bone marrow cells were given to each recipient mouse by tail vein injection. Recipient mice were maintained on antibiotics (80 mg/ml sulfmethoxazole and 0.37 mM trimethoprim in autoclaved water) for four weeks to protect them from infection. Further experiments described below were begun a total of 6 weeks post irradiation and transplantation to give sufficient time for reconstitution.

### **2.13 ENDOTOXEMIA MODEL**

Endotoxemia was induced by i.p. injection of 2 mg/kg lipopolysaccharide (LPS E. coli 0111:B4); for 24 hr. Blood was taken by tail bleed at indicated time points and spun down for serum cytokine analysis by ELISA (Biolegend). Peripheral whole blood was taken from the tails of mice and analyzed by Hemavet (Drew Scientific).

### **2.14 ADIPOSE TISSUE FLOW CYTOMETRY**

Stromal vascular cells were isolated from perigonadal adipose tissue as described above and resuspended in FACS buffer (2% FBS in PBS) following RBC lysis. Samples were distributed to wells in a clear plastic, round bottom 96-well plate and centrifuged at 1500 rpm at 4°C for 5 min to pellet. Supernatants were discarded by “flicking” the plate in a quick motion so as to not disturb the pellets. 10 µL of blocking solution (1:10 diluted TruStain FcX anti-mouse CD16/32 Biolegend in FACS buffer) was added to each well and cells were resuspended with a multi-channel pipette. Surface staining with conjugated monoclonal antibodies was performed by addition of 50 µL of antibody solution in FACS buffer to each well on ice in the dark for 25 min. 150 µL of FACS buffer was added to each well using multichannel pipette followed by centrifugation at 1500 rpm at 4°C for 5 min to wash. Cells were permeabilized with 100 µL BD Cytofix/Cytoperm Plus (BD Biosciences-554715) on ice for 20 min followed by washing with Cytoperm Buffer. Intracellular staining was performed by addition of 50 µL of antibody solution in Cytoperm Buffer on ice for 25 min followed by washing with Cytoperm Buffer and then washing with FACS buffer. Samples were resuspended in 200 µL of FACS buffer and transferred to collection microtubes (Qiagen) which fit inside a regular FACS tube to run samples. Addition of 20 µL counting beads (Spherotech) to each sample was done if required. Flow cytometry was performed on FACScalibur (BD Bioscience). Compensation beads (BD Biosciences, cat. 552845)

were used. Data were analyzed using FlowJo (Tree Star, Inc). Antibodies used for staining: CD45-APC-Cy7, CD11b-FITC, CD206-PE and CD11c-AF647 antibodies. In the future, it is advisable to use F4/80 antibody instead of or in addition to CD11b to properly gate on macrophages as CD11b is also expressed on neutrophils, some T cells, and other immune cells.

### **2.15 INDIRECT CALORIMETRY**

Oxygen consumption rate (VO<sub>2</sub>) and respiratory control ratio (RCR) were measured under consistent environmental temperature (20–22 °C) using an indirect calorimetry system (Oxymax series, Columbus Instruments, Columbus, OH), as described<sup>61</sup>. Studies were commenced after acclimation to the metabolic chamber with airflow of 0.5 L/min. Gas samples were measured at 16-min intervals over a 24 h period with food and water provided ad libitum unless indicated otherwise.

### **2.16 CONFOCAL MICROSCOPY**

Immunocytochemistry was performed on perigonadal adipose tissue sections as described using an anti-Panx1-CT Antibody<sup>50,56</sup>. For whole mount staining of adipose tissue, perigonadal fat pad samples were harvested and permeabilized by submersion in 0.2% saponin/PBS solution overnight at 4°C. Samples were submerged in a 5 µg/mL solution of BODIPY 493/503 for 15 minutes at 37°C in the dark. Following washing, samples were blocked in 0.2% saponin/PBS/5% goat serum. The samples were then incubated overnight in the dark in 0.2% saponin/PBS/5% goat serum containing antiPanx1CT primary antibody (1:300) and pre-conjugated Alexa Fluor 647 CD68 (1:300). Tissue samples were washed 3 times for 5 minutes in 0.2% saponin/PBS. Alexa Fluor 568 goat anti-rabbit (1:300) in 0.2% saponin/PBS was applied for 2 hours at room temperature followed by six 5 minute washes. Samples were mounted on gelatin coated microscope slides using 50:50 PBS/glycerol solution. Using a Nikon TE 2002-E2 microscope, a

Melles Griot Argon Ion Laser System, and a confocal attachment, digital confocal images of the stained samples were acquired for later analysis.

### **2.17 MASS SPECTROSCOPY OF LIPIDS**

Lipids were isolated from homogenized frozen adipose tissue (PBS-triton) by chloroform extraction. Dried lipids were redissolved in methanol:chloroform and analyzed by a Liquid Chromatography- Mass Spectrometry system. Phosphatidic acid, diacylglycerol, phosphatidylserine, phosphatidylcholine, and phosphatidylethanolamine content was analyzed using a Waters system consisting of a triple quadrupole mass spectrometer (Xevo TQ-S) and a solvent pump (Acquity UPLC). A binary solvent gradient with a flow rate of 0.8 mL/min was used to separate glycerolipids by reverse phase chromatography using an Phenomenex Kinetex C18 column (75 mm × 4.6 mm, 2.6 µm bead size). Mobile phases consisted of 6:4 acetonitrile:water (mobile phase A) and 9:1 isopropanol:acetonitrile (mobile phase B). Both phases were supplemented with 0.1% formic acid and 5 mM ammonium formate. Chromatographic runs started with 100% A for 1 minute. Solvent B was then increased linearly to 100% B in 7 minutes and held at 100% for 2 minutes. The column was finally re-equilibrated to 100% A for 2 minutes. Quantification was carried out by measuring peak areas using a commercially available software (Target Lynx, Waters Corp.) and data was normalized to a C17 standard.

### **2.18 BIOSORTER ANALYSIS OF ISOLATED ADIPOCYTES**

Suspensions of isolated adipocytes from perigonadal adipose tissue from *WT* and *AdipPanx1KO* mice were analyzed on a Biosorter (Union Biometrica) equipped with a 500 µm metal-free FOCA (fluidic and optical core assembly) and rotating sample cup with PBS plus 0.1% BSA pH 7.4 as sheath fluid. Similar to a flow cytometer, objects are passed axially, one by one, through the focus of a laser beam. Relative cell size is determined by time of flight (TOF) measurement and

optical density is determined by the extinction measurement. Sample cup rotation was set to rotate 180 degrees every 1.5 seconds in order that adipocyte suspension was well mixed. The sample cup was pressurized to 1.6 psi. Adipocytes were stained with Dye-cycle violet (Invitrogen) according to instructions.

## 2.19 STATISTICAL ANALYSIS

Statistical analyses were performed with Graph Pad Prism (GraphPad, San Diego, CA). Student's t-test or ANOVA with post hoc comparison tests were used as appropriate. F test was performed in Prism to determine if variances were similar among groups.

## 2.20 PRIMER SEQUENCES

Gene Name	Forward Primer Sequence	Reverse Primer Sequence
<i>Tnfa</i>	GAACTGGCAGAAGAGGCACT	AGGGTCTGGGCCATAGAACT
<i>IL18</i>	TACCAGTTGGGGAACCTCTGC	CAAATACCTGTGGCCTTGG
<i>β2M</i>	GCTATCCAGAAAACCCCTCAAATTCA	GCAGGCGTATGTATCAGTCTCAGTG
<i>IL10</i>	CCAAGGTGTCTACAAGGC	TAGAATGGGAACTGAGGTATC
<i>Arg1</i>	AAGACAGCAGAGGAGGTGAAGAG	TGGGAGGAGAAGGCGTTTGC
<i>Mgl1</i>	CTGGATCCTGGTGTCTTGGT	AGGTGGGTCCAAGAGAGGAT
<i>Ym1</i>	CTCCACACAGGAGCAGGAATC	GCTCCATGGTCCTTCCAGTA
<i>Mcp1/Ccl2</i>	CTTCTGGGCCTGCTGTTCA	AGCCTACTCATTGGGATCA
<i>Emr1</i>	GACAATTGGGATCTGCCCTA	GGCCCTCCTCCACTAGATTC
<i>IL18</i>	CAGTGAACCCCAGACCAAGAC	TCAGGTGGATCCATTTCTC
<i>Ifny</i>	TTGATGATGACCCTGTGCCTTGG	GATTCTGAAGTGCTGCGTTGATGG
<i>IL4</i>	TGTCATCCTGCTCTTCTTCTC	TCTGTGGTGTCTTCGTTGC

## **Chapter 3 : Pannexin 1 is expressed and functional on adipocytes**

### **3.1 ABSTRACT**

Extracellular ATP-derived nucleotides and nucleosides are important regulators of adipocyte function, but the pathway for controlled ATP release from adipocytes is unknown. Here, we investigated whether Pannexin 1 (Panx1) channels control ATP release from adipocytes. We assessed Panx1 functionality in cultured 3T3-L1 adipocytes and in adipocytes isolated from murine white adipose tissue by measuring YO-PRO dye uptake, ATP release, and electrophysiologic channel characteristics in response to known activators of Panx1 channels. Our data show that adipocytes express functional Pannexin 1 (Panx1) channels that can be activated to release ATP by known mechanisms including  $\alpha$ -adrenergic receptor stimulation and caspase-mediated channel cleavage. Further, we identify insulin as a novel activator of Panx1 channels. Regulation of Panx1 expression is just beginning to be understood, and we found that Panx1 expression is altered during adipogenesis and may be negatively regulated by PPAR $\gamma$ .

### **3.2 INTRODUCTION**

Pannexins (Panx1, 2, and 3) are hexameric, glycosylated membrane channels that are structurally similar to connexins but do not form gap-junctions<sup>41</sup>. Panx1 and 3 are present in many tissues while Panx2 is mainly expressed in the brain.<sup>41</sup> Pannexin 1 (Panx1) channels control the release of ATP and other nucleotides from many cell types.<sup>52</sup> For example, activation of Panx1 channels initiates paracrine signaling that controls blood vessel constriction<sup>50,62</sup> and clearance of dying cells<sup>63</sup>. Activation of Panx1 can proceed by various mechanisms including  $\alpha$ 1-adrenergic stimulation<sup>50</sup>, mechano-stretch<sup>49</sup>, and caspase-mediated cleavage of the C-terminal portion of Panx1, an irreversible process<sup>52</sup>. Various other Gq-coupled G-protein receptors have been shown to cause Panx1 channel activation, including histamine<sup>51</sup> but the exact mechanism

is not known. Some studies have reported co-immunoprecipitation of Panx1 and activating GPCRs<sup>50</sup>, and conclude that physical interaction between Panx1 and the activating GPCR is required for activation. However, the mechanism of GPCR-mediated Panx1 activation may involve signals downstream of G-protein dissociation from the GPCR. Posttranslational modification including phosphorylation and S-nitrosylation were suggested to regulate Panx1 channel function.<sup>44</sup> Known pharmacological inhibitors of Panx1 include carbenoxolone, probenecid, mefloquine, the food dye FD&C Blue No. 1, and trovafloxacin<sup>46,47,64,65</sup>. Activation of Panx1 channels result in uptake of various dyes including Yo-Pro and To-Pro, although these dyes are not specific for Panx1.

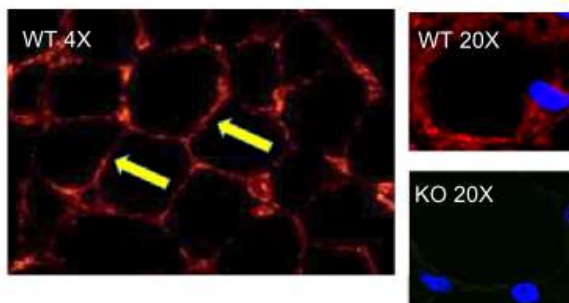
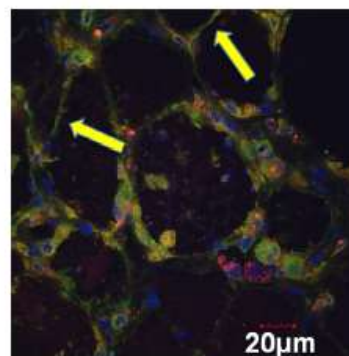
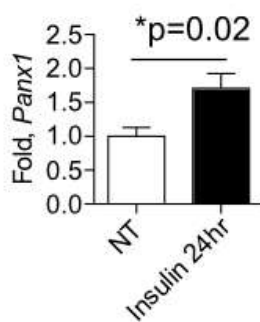
The following studies sought to determine whether adipocytes express functional Panx1 channels. The purine nucleoside adenosine accumulates extracellularly in isolated adipocyte suspensions<sup>18-20</sup> and is thought to be derived from degradation of extracellular ATP, although the mechanism of controlled ATP release from adipocytes was not known. Here we show that adipocytes express Panx1 channels that release ATP in a controlled manner.

### **3.3 RESULTS**

#### **3.3.1 Expression of Panx1**

The functional role of Pannexin 1 (Panx1) in adipose tissue has not been reported. To examine whether adipocytes express Panx1, we used immunohistochemistry. Panx1 protein expression was clearly observed on membranes of adipocytes (Fig 3.1A and B, arrows) in adipose tissue from wild-type C57Bl6 mice, while the staining was absent in adipose tissue from Panx1 knockout (KO) mice (Fig 3.1A). Panx1 protein was also present in adipose tissue from high fat-fed mice (Fig 3.1B). We found that Panx1 expression in 3T3-L1 adipocytes is induced by insulin

(Fig 3.1C), which is in line with reports that cAMP response elements play a role in transcriptional regulation of Panx1<sup>66</sup>.

**A** Murine Perivascular Adipose Tissue  
(Chow Diet)**B** Murine Perigonadal Adipose Tissue  
(High Fat Diet)**C** 3T3-L1 Adipocyte

**Figure 3-1** Panx1 is expressed in murine adipocytes.

**Figure 3.1 Panx1 is expressed in murine adipocytes.**

(A) Confocal microscopy of perivascular adipose tissue shows that Panx1 (red, anti-Panx1, recognizing the C-terminus) is present on adipocytes in chow-fed WT mice but not in Panx1 KO mice. Left image is at 4X magnification to show several adipocytes while right images are at 20X to show a single adipocyte in the field. Arrows indicate examples of positive Panx1 staining on adipocyte membranes. Panx1 staining is also present on stromal vascular cells in the tissue such as macrophages. Nuclei (blue) are stained with DAPI.

(B) Confocal microscopy of perigonadal adipose tissue from a WT mouse fed a high fat diet for 12 weeks shows that Panx1 (green, anti-Panx1 recognizing the C-terminus) is present on adipocyte membranes (arrows). Panx1 is also present on stromal vascular cells, particularly macrophages (red, anti-Mac2). Nuclei (blue) are stained with DAPI.

(C) Differentiated 3T3-L1 adipocytes were treated with insulin (0.25 U/mL) for 24 hr. Panx1 mRNA levels were detected via Taqman probes (mm0045091\_m1\_Panx1). Data was normalized to hypoxanthine-guanine phosphoribosyltransferase (HPRT) (mm01545399\_m1\_HPRT) mRNA and expressed as mean +/- s.e.m. \*p=0.02 by Student's t-test.

To explore the functionality of Panx1 channels in adipocytes we performed experiments with cultured 3T3-L1 adipocytes and primary adipocytes isolated from wild-type or Panx1 KO mice, using known activators of Panx1 channel function<sup>50,52,63</sup>.

### **3.3.2 PE stimulation of adipocyte Pannexin 1**

First indications for a functional role of Panx1 in adipocytes came from experiments where treatment of 3T3-L1 adipocytes with the  $\alpha$ -adrenergic receptor agonist phenylephrine (PE) caused a dose-dependent increase in the uptake of YO-PRO<sup>®</sup>, a green-fluorescent dye that can enter cells via open Panx1 channels<sup>63,67</sup> (Fig 3.2A). Furthermore, PE treatment induced the release of ATP from 3T3-L1 adipocytes into the media (Fig 3.2B). PE-induced ATP release was abrogated by a Panx1 intracellular loop peptide (IL2) corresponding to a region of the intracellular loop portion of the Panx1 channel (K191-K200) (Fig 3.2B inset) that disrupts  $\alpha$ -adrenergic-dependent activation of Panx1 channels<sup>68</sup>. In contrast, a C-terminal peptide (CT2) corresponding to the C-terminal region of Panx1 had no effect (Fig 3.2B). IL2 and CT2 peptides were kindly provided by Dr. Brant Isakson. To further examine whether PE-induced ATP release from adipocytes was dependent on Panx1 channel function, we treated adipocytes isolated from wildtype or global Panx1 knockout mice with PE, which resulted in significant ATP release into the media only when Panx1 was present (Fig 3.2C). These results show that Panx1 is not only present on adipocytes but also that channel function can be activated to release ATP through the known mechanism of alpha-adrenergic stimulation.

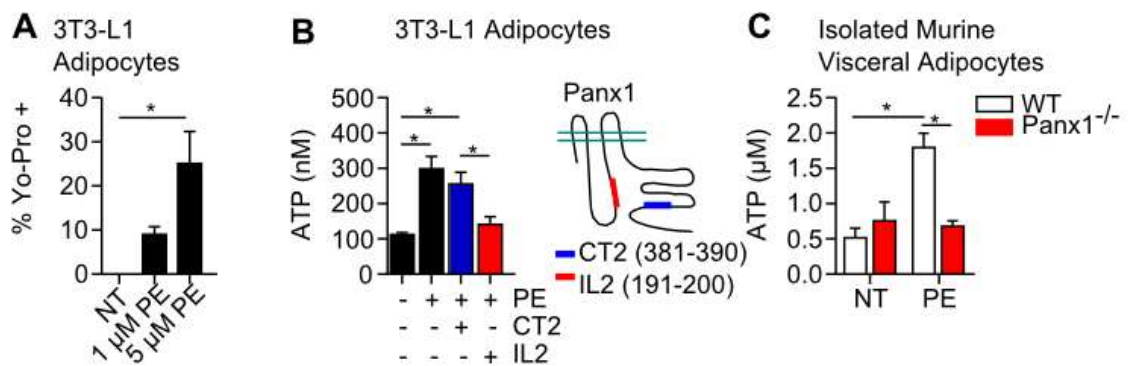


**Figure 3-2 Pannexin 1 channel function in adipocytes is regulated by alpha-adrenergic stimulation.**

**Figure 3-2 Pannexin 1 channel function in adipocytes is regulated by alpha-adrenergic stimulation**

(A) 3T3-L1 adipocytes were treated with indicated concentrations of phenylephrine (PE) for 30 min, and then stained with 1 $\mu$ M YO-PRO<sup>®</sup> and 1 $\mu$ g/mL Hoechst for 10 min. Experiment was performed in triplicate. Total cells were quantitated by counting Hoechst-positive cells. Cells positive for YO-PRO<sup>®</sup> indicate cells in which Panx1 channels have been activated and opened, allowing dye to enter. Data are expressed as mean  $\pm$  s.e.m. \*p=0.0087 by Student's t-test.

(B) 3T3-L1 adipocytes were treated with 5 $\mu$ M PE with or without pretreatment with a Panx1 intracellular loop peptide (IL2) or a C-terminal peptide (CT2). The IL2 peptide corresponds to a region of the Panx1 intracellular loop (aa 191-200) while the CT2 peptide is from a region of the C-terminal tail corresponding to aa 381-390 (inset) 39. ATP release into the media was measured using cell-titer glo assay (Promega). Experiment was performed in triplicate. Data are expressed as mean  $\pm$  s.e.m. \*p<0.05 by Student's t-test.

(C) Adipocytes were isolated from perigonadal adipose tissue of WT or Panx1 KO mice and ATP release was measured upon stimulation with phenylephrine (PE, 5  $\mu$ M, 15 min) or no treatment (NT). Experiment was performed in triplicate. Data are expressed as mean  $\pm$  s.e.m. \*p<0.04 by 2-way ANOVA with Sidak's multiple comparison test.

### **3.3.3 Caspase-mediated Panx1 activation in apoptotic 3T3-L1 adipocytes**

Another important mechanism of Panx1 channel opening is cleavage of the C-terminal tail of the channel by activated caspase-3 (CASP3), particularly relevant for Panx1-dependent ATP release from apoptotic cells<sup>52,63</sup>. To test if this mechanism can induce Panx1 opening in adipocytes, we applied activated CASP3 to cultured 3T3-L1 adipocytes through the patch pipette, which induced a current with Panx1-like voltage-dependent properties that was blocked by the Panx1 inhibitor carbenoxolone (CBX)<sup>52</sup> (Fig 3.3). These results suggested that Panx1 channels may be activated during apoptosis of adipocytes.

## 3T3-L1 Adipocytes

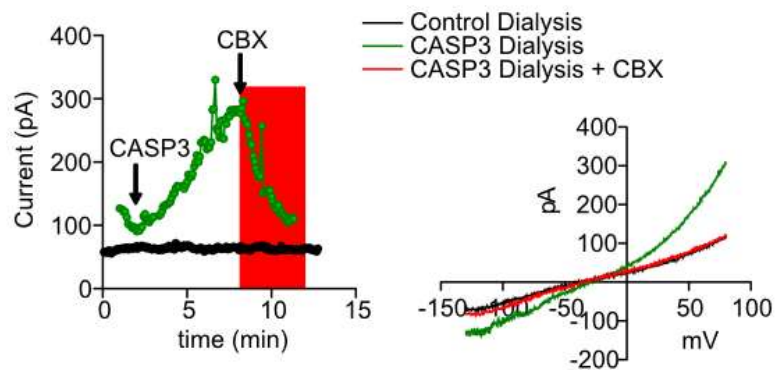


**Figure 3-3 Pannexin 1 channel function in adipocytes is regulated by caspase-mediated C-terminal cleavage**

**Figure 3-3. Pannexin 1 channel function in adipocytes is regulated by caspase-mediated C-terminal cleavage**

Whole cell patch clamping of 3T3-L1 adipocytes reveals a carbenoxolone-sensitive current when active caspase-3 is present in the pipette indicating that adipocyte Panx1 is activated by the caspase-cleavage mechanism. Arrows indicate time at which active caspase 3 (CASP3) or carbenoxolone (CBX) was added. Control dialysis shown in black. Current-voltage relationship (IV) curves are shown at right. Recordings performed by Joanna Sandilos.

To further investigate caspase-dependent activation of adipocyte Panx1 during apoptosis we exposed 3T3-L1 adipocytes to UV irradiation. Induction of apoptosis was confirmed by the formation of apoptotic bodies (Fig 3.4A) and by radiation dose-dependent uptake of YO-PRO® and propidium iodide, dyes known to enter cells via Panx1 47 (Fig 3.4B and C). Further support for caspase-dependent opening of Panx1 channels induced by UV irradiation of adipocytes was demonstrated by a significant increase in ATP release into the supernatant that was blocked by treatment with the Panx1 inhibitor carbenoxolone (CBX) (Fig 3.4D and E) and the pan-caspase inhibitor zVAD (Fig 3.4E). Together, these results show that opening of Panx1 channels can be induced in adipocytes either by  $\alpha$ -adrenergic stimulation or via caspase-mediated C-terminal cleavage during apoptosis.

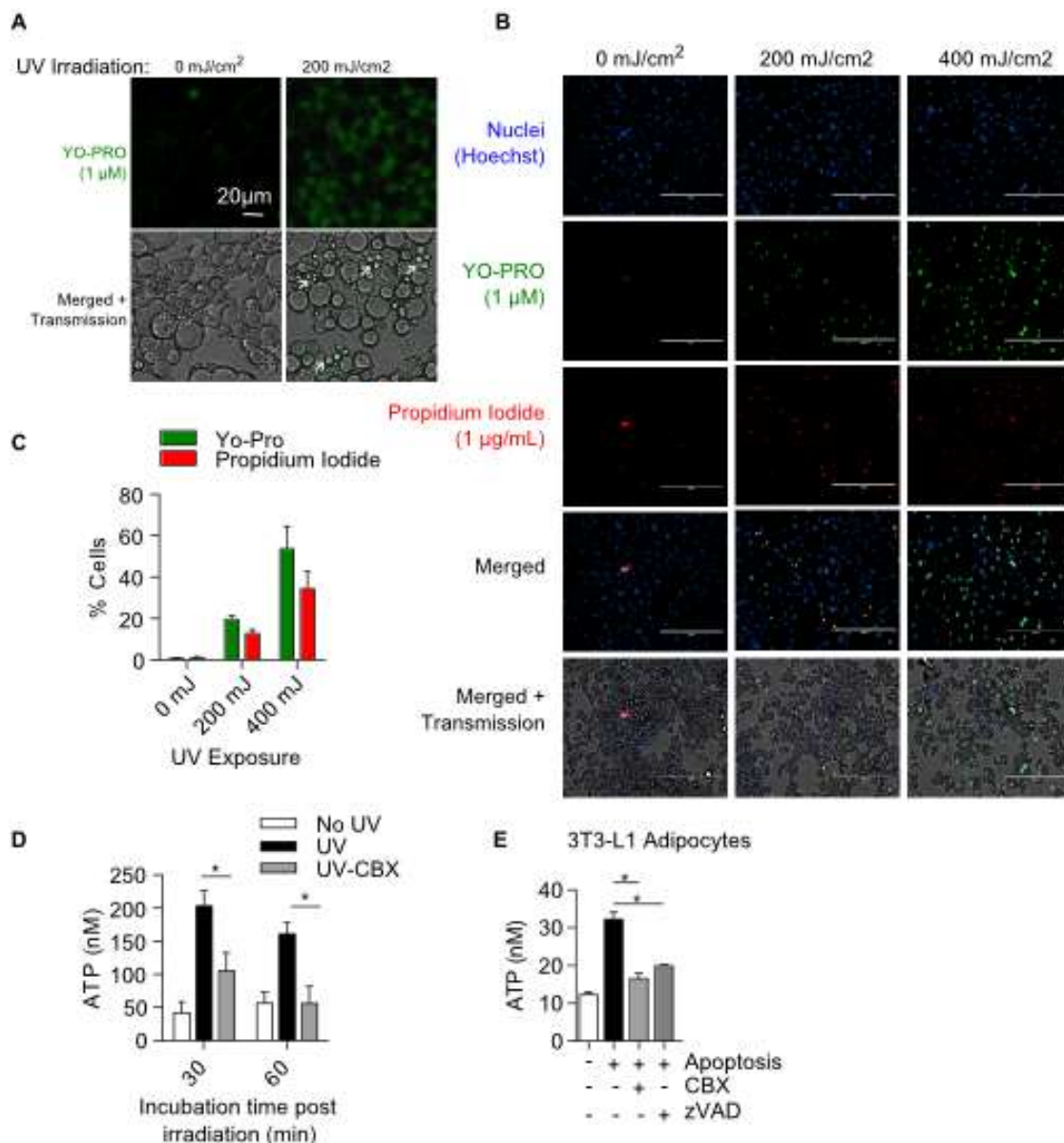


**Figure 3-4** UV irradiation of 3T3-L1 adipocytes causes apoptosis and the opening of Panx1 channels.

**Figure 3-4. UV irradiation of 3T3-L1 adipocytes causes apoptosis and the opening of Panx1 channels.**

(A) Exposure of 3T3-L1-adipocytes to 200 mJ/cm<sup>3</sup> UV irradiation induced apoptosis as evidenced by the uptake of YO-PRO dye (green) and the formation of apoptotic bodies as indicated by white arrows in transmission image.

(B) 3T3-L1 adipocytes were exposed to indicated doses of UV irradiation and stained with Hoechst to mark nuclei (blue) and the dyes YO-PRO (1 μM, green) and propidium iodide (PI, 1 μg/ml, red) which enter cells via activated Panx1 channels <sup>1</sup>.

(C) The percentage of YO-PRO and PI positive cells was quantified by counting YO-PRO and PI positive cells and dividing by Hoechst positive nuclei in at least 3 fields of triplicate analyses.

Data are expressed as mean +/-s.e.m.

(D) Apoptosis was induced in 3T3-L1-adipocytes by exposure to 200 mJ/cm<sup>3</sup> UV irradiation. Cells were treated with or without 400 μM carbenoxolone (CBX) and incubated for indicated times and ATP was measured from supernatants. Experiment was performed in quadruplicate. Data are expressed as mean +/- s.d. \*p<0.0001 by 2 way ANOVA with Sidak's multiple comparison test.

(E) 3T3-L1 adipocytes were exposed to 400 mJ/cm<sup>3</sup> UV irradiation (Stratalinker) to induce apoptosis and incubated with or without 400 μM carbenoxolone (CBX) or zVAD, a pan-caspase inhibitor (50 μM) for 1 h. ATP was measured in the supernatant by cell-titer glo assay (Promega). n=8. Data are expressed as mean +/-s.e.m. \*p<0.0001 by ANOVA with Tukey's multiple comparison test.

### 3.3.4 Insulin-mediated opening of Panx1 channels

Pannexin channels can be activated through several pathways including G protein coupled receptors.<sup>50,51</sup> Nitrosylation of Panx1 can also control channel activity.<sup>44</sup> The presence of putative phosphorylation sites on the channel suggests that perhaps phosphorylation may control channel opening. We observed a defect in insulin stimulated glucose uptake in Panx1 null adipocytes, which could be rescued by the addition of exogenous ATP (see chapter 5). This data suggested that insulin may activate Panx1 channels. To examine whether insulin activates Panx1 channels, we first assessed Panx1-dependent ATP release from primary adipocytes isolated from WT mice. Treatment with insulin for 30 minutes caused a significant increase in extracellular ATP, which was blocked by addition of the Panx1 inhibitor probenecid (Prob) (Fig 3.5A). Next, we tested the ability of insulin to activate Panx1 channels using HEK293 cells co-transfected with expression plasmids for the human insulin receptor (hIR) and murine Panx1. Insulin treatment evoked a current with Panx1-like voltage-dependent properties that was blocked by the Panx1 inhibitor carbenoxolone (CBX) (Fig 3.5B). Insulin-stimulated Panx1 currents were also seen in HEK293 cells co-transfected with expression plasmids for the human insulin receptor (hIR) and human Panx1 with a mutated caspase cleavage site<sup>52</sup> (Fig 3.5C). These data identify insulin as a novel mediator of Panx1 channel activation and show that insulin-induced activation of Panx1 is independent of caspase-mediated cleavage.

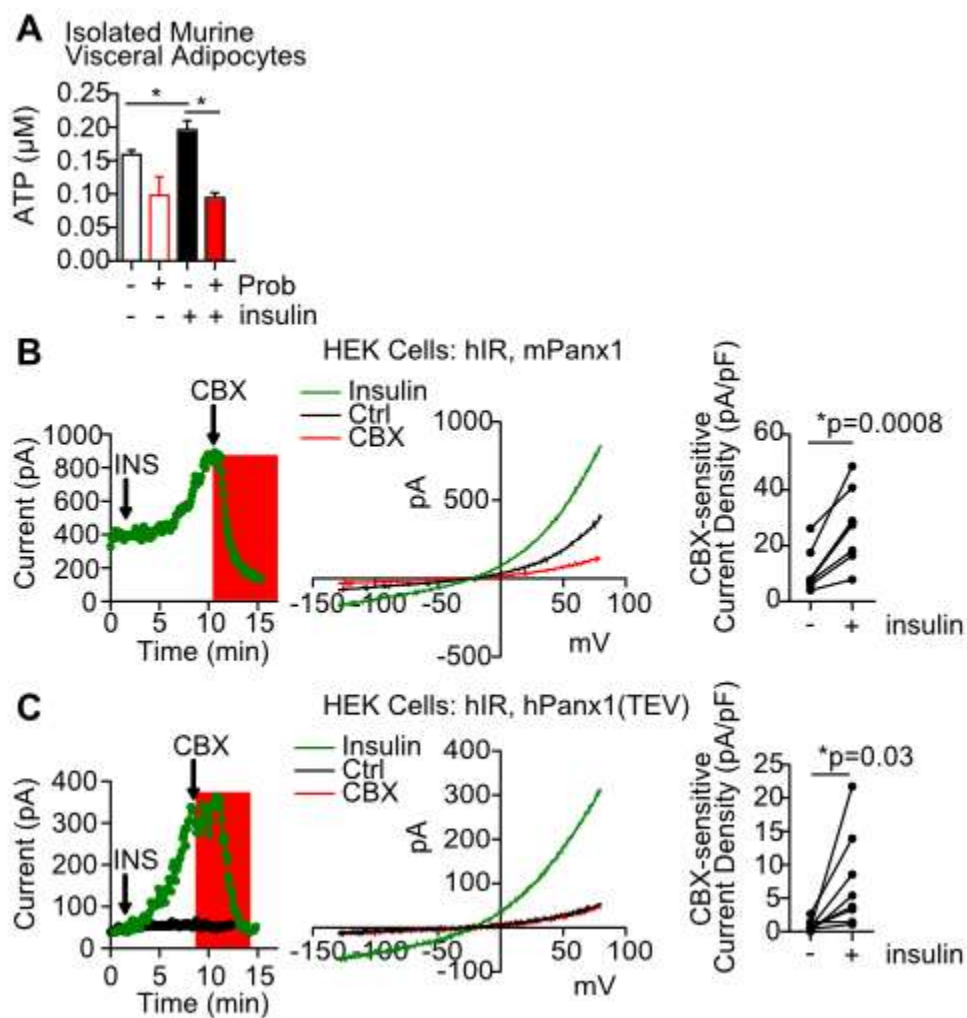


Figure 3-5 Insulin induces Panx1 channel activation and ATP release

**Figure 3-5. Insulin induces Panx1 channel activation and ATP release**

(A) Adipocytes isolated from perigonadal adipose tissue of WT mice release ATP upon insulin stimulation, which can be blocked by treatment with the Panx1 inhibitor probenecid. Data are expressed as mean  $\pm$  s.e.m. \* $p < 0.05$  by Student's t-test.

(B) Whole cell patch clamp of HEK cells transfected with human insulin receptor and mouse Panx1 reveals a Panx1 dependent current upon treatment with insulin that is abolished by addition of the Panx1 inhibitor carbenoxolone. Current-voltage relationship curve is shown in middle. Insulin treatment significantly increases CBX-sensitive current density (n=8 cells)

(C) Whole cell patch clamp of HEK cells transfected with human insulin receptor and human Panx1 in which the C-terminal caspase cleavage site has been replaced with a TEV protease cleavage site reveals a Panx1 dependent and CBX-sensitive current upon treatment with insulin. Current-voltage relationship curve is shown in middle. Insulin treatment significantly increases CBX-sensitive current density (n=8 cells). Recordings performed by Eva Chiu.

### 3.3.5 Panx1 expression during adipocyte differentiation

Extracellular ATP renders preadipocytes responsive to adipogenic hormones during the growth phase.<sup>69</sup> To determine whether there was any role for Panx1 in adipogenesis, I measured mRNA levels of Panx1 during different phases of 3T3-L1 adipocyte differentiation and saw that Panx1 mRNA levels drastically decreased during differentiation as did several other P2 purinergic receptors and the ectonucleotidase NT5E (Fig 3.6A). The master regulator PPAR $\gamma$  is greatly upregulated during differentiation, which suggested that perhaps this transcription factor might control Panx1 expression. A search for putative transcription factor binding sites in the mouse Panx1 promoter yielded PPAR binding sites among others (Fig 3.6B). We further tested whether PPAR $\gamma$  regulates Panx1 expression using a construct in which the Panx1 promoter drives luciferase expression and indeed HEK cells expressing the luciferase Panx1 promoter construct and PPAR $\gamma$  that were treated with the PPAR $\gamma$  agonist rosiglitazone showed a decrease in luminescence indicating a decrease in Panx1 transcription upon PPAR $\gamma$  activation (Fig 3.6C). These data suggest that PPAR $\gamma$  may negatively regulate Panx1 expression.

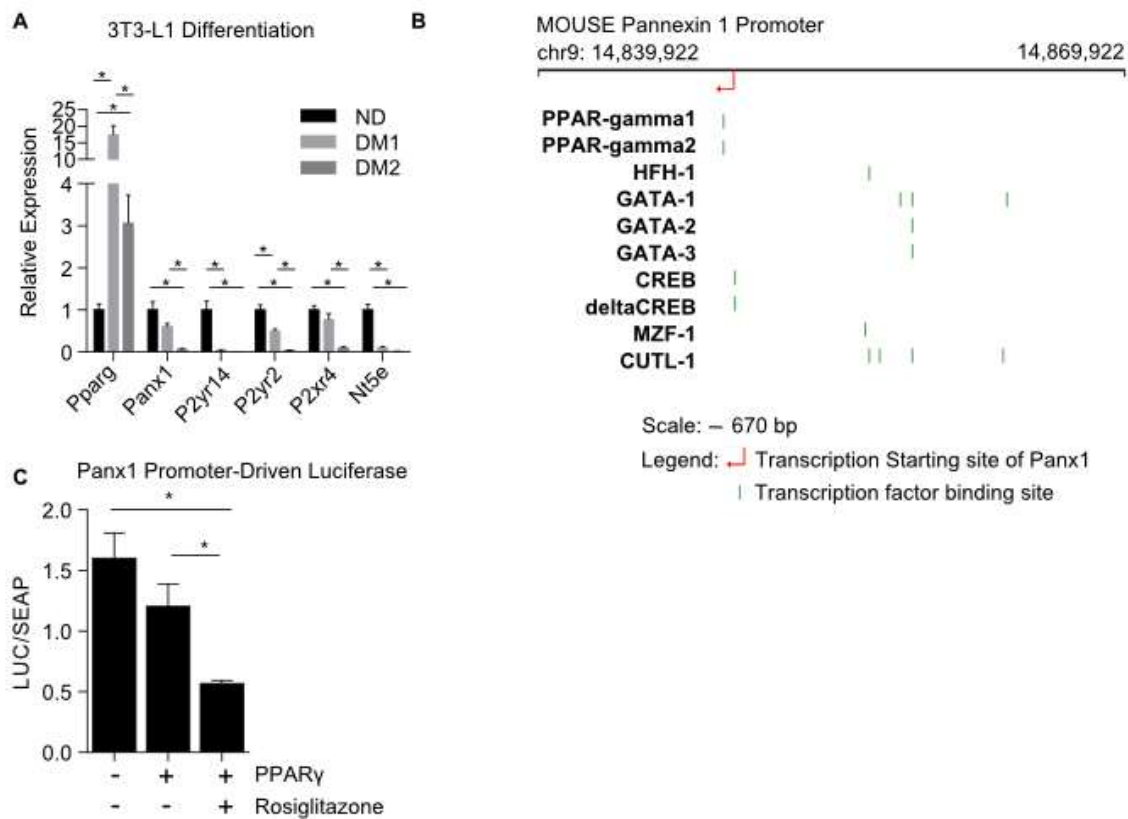


Figure 3-6 Panx1 expression during 3T3-L1 differentiation may be downregulated via PPAR $\gamma$

**Figure 3-6. Panx1 expression during 3T3-L1 differentiation may be downregulated via PPAR $\gamma$** 

(A) mRNA levels of Panx1 and other purinergic signaling proteins were measured during 3T3-L1 differentiation in non-differentiated fibroblasts (ND), cells that received differentiation media 1 for 3 days (DM1), and fully differentiated adipocytes which received DM1 as well as 3 days of differentiation media 2 (DM2).

(B) Predicted transcription factor binding sites on the Panx1 promoter were determined using SABiosciences' Champion ChiP Transcription Factor Search Portal and DECODE database. The Panx1 promoter is predicted by the UCSC Genome Browser.

(C) HEK cells were transfected for 48 hr with a dual-luciferase reporter construct in which secreted alkaline phosphatase (SEAP) is driven by the CMV promoter and Gaussia luciferase (also secreted) (LUC) is driven by the Panx1 promoter (GeneCopoeia, CS-MPRM19232-PG04, vector pEZX-PG04). Cell supernatants are collected and analyzed for LUC and SEAP, and results are expressed as the LUC to SEAP ratio because SEAP is an internal control for the level of plasmid expression. Cells were cotransfected with the PPAR $\gamma$  nuclear receptor and treated with 2  $\mu$ M rosiglitazone, a PPAR $\gamma$  agonist, as indicated.

### 3.4 DISCUSSION

Our data establish Panx1 channels as mediators of controlled extracellular nucleotide release from adipocytes. Furthermore, we identify insulin as a novel mediator of Panx1 channel activation.

Although pharmacologic Panx1 inhibitors such as carbenoxolone and probenidic are known to have off-target effects, the use of multiple inhibitors as well as genetic deletion of Panx1 in our study collectively support a role for Panx1 channels in ATP release from adipocytes. Together with highly specific electrophysiological channel recordings, YO-PRO® dye has been shown to enter apoptotic cells in a Panx1-dependent manner<sup>63</sup>, adding further evidence for Panx1 channel function in adipocytes.

While measuring ATP release from cultured cells is straight forward, determining the amount of ATP released from isolated primary adipocytes is quite tricky. Due to the isolation procedure and through the handling of the cells, which sometimes also results in disruption of cellular integrity, extracellular ATP levels can vary considerably between preparations even after final washing steps. Adipocytes from older mice or from larger adipose tissue depots tend to be larger and more fragile. The basal level of extracellular ATP is also dependent on the time between the final washing step and the initiation of the experiment as well as the number of cells used in the experiment. Together, differences are likely due to normal variation in adipocytes isolated from different mice and normal experimental variation. For our experiments, we typically only use preparations where the basal extracellular ATP concentrations range below 1  $\mu\text{M}$ . In order to compare responsiveness, preparations from wild type and knock out mice done in parallel need to demonstrate comparable basal extracellular ATP levels as well. Using these criteria, we can reproducibly measure responsiveness to phenylephrine or insulin-induced ATP release from isolated primary adipocytes.

The most widely studied molecule that is released by Panx1 channels is ATP; however, Panx1 channels have a pore size upon activation that can accommodate molecules of up to 1 kDa in size.<sup>41</sup> So it is conceivable that other molecules that could impact metabolic signaling in adipocytes in an autocrine fashion are also released via Panx1.

Our finding that insulin stimulates opening of Panx1 channels is intriguing and points to a novel mechanism by which the function of this channel is regulated. We demonstrate that insulin activates channel opening in a caspase-independent manner, pointing to a transient, reversible mechanism of activation. Utilizing an HEK293 heterologous expression system enabled us to explore insulin-mediated Panx1 channel activation by obtaining electrophysiologic data about Panx1 channel function. Feasibility of this approach is supported by previous reports that HEK293 cells express endogenous proteins involved in the insulin signaling pathway including Irs1<sup>70</sup>, Akt<sup>71,72</sup>, and mTOR<sup>73</sup>. Previous studies have identified putative phosphorylation sites on the Panx1 channel that may contribute to its function, suggesting that insulin-induced kinases may regulate channel opening. However, further studies are needed to elucidate this new mechanism of Panx1 channel activation.

Regulation of expression of Panx1 is not fully understood. Inflammatory signals such as IL1 $\beta$  have been reported to increase Panx1 expression.<sup>45</sup> And a study of the Panx1 promoter in rat epididymis revealed that both CREB and ETV4 transcriptionally regulate Panx1.<sup>66</sup> Indeed, we found that treatment of 3T3-L1 adipocytes with insulin, which activates the CREB transcription factor, increased expression of Panx1. Interestingly, Panx1 expression greatly decreased over the process of differentiation of 3T3-L1 fibroblasts into adipocytes and we found that agonism of the master regulator PPAR $\gamma$  with rosiglitazone in a heterologous expression system decreased luminescence from a Panx1 promoter construct driving luciferase expression. Although mRNA levels of Panx1 are quite low in differentiation 3T3-L1 adipocytes, that does not preclude

functional significance of channel function, as evidenced by our ability to observe a CBX-sensitive current in 3T3-L1 adipocytes treated with active caspase 3 (Fig. 3-3). Mechanisms of Panx1 channel regulation other than control of expression may be important such as post-translational modification of the channel or trafficking to the plasma membrane.

## **Chapter 4 Pannexin 1-P2Y2 receptor inflammatory signaling in obese adipose tissue**

### **4.1 ABSTRACT**

Infiltration of obese adipose tissue by macrophages and other immune cells greatly contributes to inflammation and insulin resistance. As adipose tissue expands, some adipocytes undergo apoptosis in response to hypoxic microenvironments.<sup>74</sup> ATP released from Panx1 channels on apoptotic cells can act as a “find-me” signal via P2Y2 receptors on phagocytes that are responsible for clearance of dying cells.<sup>63</sup> Here we investigate the hypothesis that Panx1 channels on apoptotic adipocytes release ATP that interacts with the purinergic receptor P2Y2 to attract macrophages. We subjected adipocyte specific Panx1 knockout mice generated in our laboratory as well as mice transplanted with either WT or P2Y2 receptor null bone marrow to high fat diet feeding and assessed insulin resistance and adipose tissue inflammation. We found that although adipocyte specific Panx1 KO mice were more insulin resistant compared to WT mice, this was independent of adipose tissue inflammation and macrophage infiltration. In contrast, WT mice reconstituted with P2Y2 receptor null bone marrow were equally insulin resistant as WT mice and had similar levels of macrophages in adipose tissue; however, macrophages in adipose tissue of WT mice reconstituted with P2Y2 receptor null bone marrow did not form crown like structures as were seen in WT mice. This data shows that macrophage P2Y2 receptor may be involved in crown-like structure formation; however, adipocyte Panx1 does not impact adipose tissue inflammation or macrophage infiltration.

### **4.2 INTRODUCTION**

During obesity, immune cell infiltration of adipose tissue produces inflammation which contributes to insulin resistance.<sup>75</sup> Immune cells such as T cells, eosinophils, neutrophils, and mast cells have been observed in obese adipose tissue; however, macrophages compose the largest proportion of immune cells within obese adipose tissue and are the most well-studied

(reviewed in <sup>76</sup>). As adipose tissue expands, some adipocytes undergo apoptosis in response to hypoxic microenvironments.<sup>74</sup> Indeed, sections of obese adipose show increased staining for activated caspase 3 and other apoptotic markers in adipocytes.<sup>77</sup> Secondary necrosis and spillage of content from adipocytes leads to exacerbated inflammation and additional macrophage infiltration. Cytokines such as TNF $\alpha$ , IL1 $\beta$ , and IL6 have been shown to be increased in obese adipose.<sup>77</sup> This inflammatory environment of low grade, chronic inflammation is thought to activate programs on macrophage infiltration into the tissue.

Chemokines like CCL2 recruit monocytes to adipose tissue<sup>78</sup>, and preventing macrophage infiltration into adipose tissue by blocking certain chemokine signaling pathways decreases inflammation and insulin resistance.<sup>79</sup> Within adipose tissue, inflammatory macrophages assemble around dying adipocytes, forming what are termed crown-like structures (CLS)<sup>80</sup>; however, little is known about the mechanisms of CLS formation. Recently, macrophage-inducible C-type lectin was shown to contribute to CLS formation and adipose tissue fibrosis<sup>81</sup>, but there are likely to be multiple signaling events that contribute to CLS formation. One assumption as to the function of macrophage assembly into CLS is to facilitate the clearance of dying adipocytes via phagocytosis. Clearance of dying adipocytes requires the digestion of the very large lipid droplets within adipocytes and the precise mechanism as to how this occurs is not known. One hypothesis is that adipose tissue macrophages secrete lipases which break down adipocyte lipids, a mechanism reminiscent of bone resorption by osteoclasts.<sup>82</sup> Another hypothesis is that adipocytes release vesicles<sup>83-85</sup> that contain lipids which are taken up by macrophages.

Extracellular ATP is an important signaling molecule throughout the inflammatory cascade, serving as a danger signal that causes activation of the inflammasome<sup>86</sup>, enhancement of immune cell infiltration<sup>87</sup>, and fine-tuning of several signaling cascades including those

important for the resolution of inflammation.<sup>88</sup> ATP signaling through the P2X7 receptor activates the inflammasome. However, it was recently reported that P2X7 null mice on high fat diet showed no change in metabolic phenotype or inflammasome activation when compared to WT mice on high fat diet.<sup>75</sup> Extracellular ATP released by Panx1 from apoptotic cells can act as a “find-me” signal via P2Y2 receptors on phagocytes that are responsible for clearance of dying cells.<sup>63</sup> Some groups have disputed that ATP-P2Y2 signaling induces directional migration over a long range, but they claim instead that ATP signaling enhances random chemokinesis and the development of lamellipodia which would likely impact phagocytosis capacity.<sup>89</sup> P2Y2 on macrophages may also contribute to expression of inflammatory mediators cyclo-oxygenase 2 and inducible nitric oxide synthase during inflammatory challenge.<sup>90</sup> Our hypothesis was that ATP released from adipocytes via Panx1 interacts with macrophage P2Y2 receptors to drive inflammation and CLS formation within obese adipose tissue.

## **4.3 RESULTS**

### **4.3.1 Adipocyte Panx1 function *in vitro* drives macrophage migration**

To determine whether adipocyte Panx1 had any effect on macrophage migration, supernatants from UV treated 3T3-adipocytes were applied to BMDM in a Boyden chamber, and migration was measured. Supernatants from UV treated 3T3-adipocytes induced migration of macrophages and blocking Panx1 in adipocytes with carbenoxolone abrogated migration (Fig. 4-1). This data suggested that adipocyte Panx1 function drives macrophage migration, most likely via the release of ATP which interacts with macrophage P2 receptors.

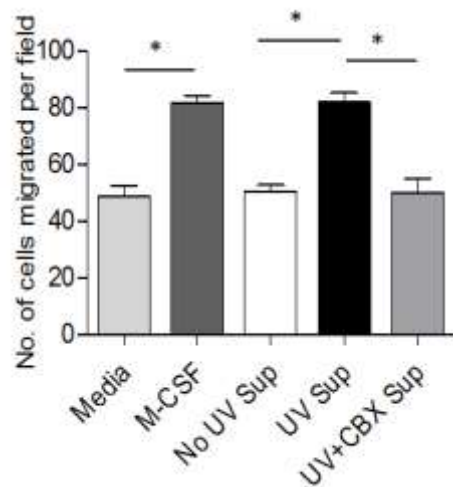


Figure 4-1 Adipocyte Panx1 function *in vitro* drives macrophage migration

**Figure 4-1. Adipocyte Panx1 function *in vitro* drives macrophage migration**

Apoptosis was induced in 3T3-adipocytes (200mJ UV) and ATP release was inhibited by treatment with CBX (500 mM). Supernatants (sup) of apoptotic adipocytes were used to test for chemotactic activity of bone marrow derived macrophages (BMDM) in Boyden chambers. Asterisk indicates significant difference by 1-way ANOVA. Data courtesy of Dr. Akshaya K. Meher.

#### 4.3.1 Generation of AdipPanx1 Mouse and BMT P2Y2

To explore the role of Panx1 in adipocytes *in vivo*, we crossed *Panx1<sup>F/F</sup>* mice with Adiponectin-Cre (*Adipq<sup>Cre+</sup>*) mice<sup>59</sup> to generate an adipocyte-specific Panx1 KO mouse (*AdipPanx1KO*). Excision of exon 3 of the Panx1 gene in *Panx1<sup>F/F</sup>Adipq<sup>Cre+</sup>* (*AdipPanx1KO*) mice was observed in adipose tissues including visceral, subcutaneous, and brown adipose tissue but not in liver, lung, pancreas, spleen, or brain (Fig 4.2A). Whole mount staining of visceral adipose tissue pieces from *WT* and *AdipPanx1KO* mice with an antibody specific for Panx1<sup>41</sup> and subsequent confocal microscopy demonstrated distinctive punctate Panx1 staining in adipocytes of *WT* mice, which was undetectable in adipocytes from *AdipPanx1KO* mice (Fig 4.2B). Unfortunately, we were not able to detect Panx1 protein in adipocyte and stromal vascular cell fractions although many attempts were made including membrane fraction enrichment, immunoprecipitation, and Biosorter analysis (similar to flow cytometry) of live adipocytes labelled with Panx1 antibody directed to the extracellular loop region with AF488 secondary antibody. Quantification of Panx1 mRNA in adipocyte and SVF fractions also proved extremely difficult. Panx1 mRNA levels in isolated adipocytes are low. Use of Panx1 Taqman probes gave counts of approximately 34 which were validated by standard curve and the use of global Panx1 KO adipocyte samples. Even small amounts of adipocyte fraction contamination by stromal vascular cells in *AdipPanx1 KO* mice gave high Panx1 mRNA signal and made data interpretation difficult. Nevertheless, functional differences in adipocytes isolated from *WT* and *AdipPanx1 KO* mice convinced us that our mice were indeed specifically lacking Panx1 in adipocytes.

To determine whether there were any developmental defects in adipose tissue in *AdipPanx1 KO* mice, we analyzed adipocyte cell size distribution. Panx1 deficiency in adipocytes did not affect cell size, as analysis via BioSorter® demonstrated that adipocytes isolated from

gonadal adipose tissue of WT and AdipPanx1KO mice showed identical cell size distribution (Fig 42C).

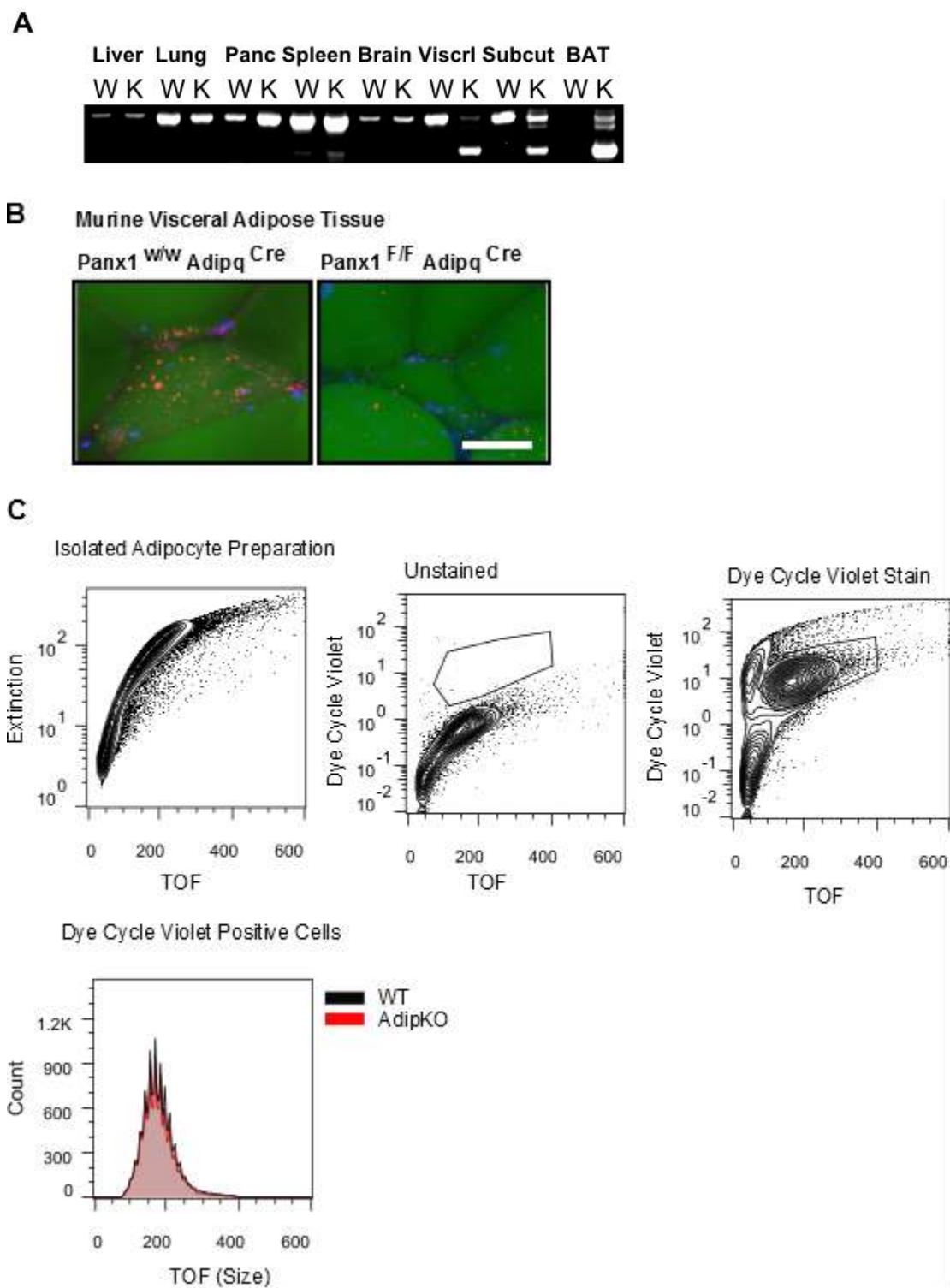


**Figure 4-2** Generation of adipocyte specific Pannexin 1 KO mouse

**Figure 4-2. Generation of adipocyte specific Pannexin 1 KO mouse**

(A) Genomic PCR was performed on various tissues including liver, lung, pancreas (Panc), spleen, brain, visceral fat (Viscrl), subcutaneous fat (Subcut), and brown adipose tissue (BAT) from WT ( $Panx1^{F/F}Adipoq^{Cre-}$ ) mice (W) or *AdipPanxKO* ( $Panx1^{F/F}Adipoq^{Cre+}$ ) mice (K). A null band (510 bp) indicating the excision of exon 3 appears only in adipose tissues, while all other tissues show a wild type band (379 bp), indicating the intact *Panx1* gene.

(B) Whole mount immunostaining of gonadal adipose tissue isolated from a WT ( $Panx1^{w/w}Adipoq^{Cre+}$ ) mouse or an *AdipPanxKO* ( $Panx1^{F/F}Adipoq^{Cre+}$ ) mouse. *Panx1* staining (red) is absent on adipocytes from the *AdipPanxKO* mouse. Neutral lipids stained with Bodipy (green), nuclei stained with DAPI (blue). Confocal image is at 63X magnification and is a composite z-stack. White bar is 20  $\mu$ m. Images were selected such that the surface of the central adipocyte is in view.

(C) Suspensions of isolated adipocytes from perigonadal adipose tissue from WT and *AdipPanxKO* mice were analyzed on a Biosorter (Union Biometrica) equipped with a 500  $\mu$ m metal-free FOCA (fluidic and optical core assembly) with PBS plus 0.1% BSA pH 7.4 as sheath fluid. Similar to a flow cytometer, objects are passed axially, one by one, through the focus of a laser beam. Relative size is determined by time of flight (TOF) measurement and optical density is determined by the extinction measurement. Cells were stained with Dye-Cycle Violet, a cell-permeable nuclear stain, in order to gate out non-cellular debris. Representative plots of extinction versus TOF and dye-cycle violet versus TOF of unstained and stained adipocyte suspensions are shown as contour plots with outliers. TOF histograms of dye-cycle violet positive adipocytes from WT and *AdipPanxKO* mice are superimposable, indicating identical cell size-distributions.

To investigate the contribution of macrophage P2Y2 receptor to adipose tissue inflammation during diet-induced obesity, we transplanted C57Bl/6 mice with bone marrow isolated from WT or global P2Y2<sup>-/-</sup> mice to obtain WT chimeric (WT-tp) mice and P2Y2<sup>-/-</sup> chimeric mice (P2Y2<sup>-/-</sup>-tp) (Fig 4.3A). We confirmed the bone marrow transplant by measuring P2y2r mRNA from blood from WT-tp and P2Y2<sup>-/-</sup>-tp mice and found significantly decreased P2y2r mRNA levels in blood from P2Y2<sup>-/-</sup>-tp mice compared to WT-tp mice (Fig 4.3B).

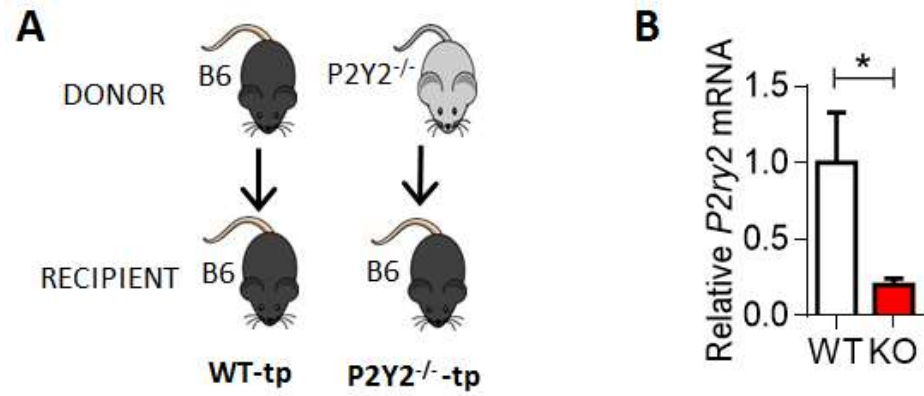


Figure 4-3 Generation of myeloid specific P2Y2 receptor KO mouse (P2Y2<sup>-/-</sup>-tp) by bone marrow transplantation.

**Figure 4-3. Generation of myeloid specific P2Y2 receptor KO mouse by bone marrow transplantation.**

(A) Schematic of bone marrow transplant.

(B) P2y2r mRNA levels in blood of WT-tp and P2Y2<sup>-/-</sup>-tp mice were measured by qRT-PCR and revealed a significant decrease in the mice transplanted with P2Y2 null marrow (N=12, mean +/- s.e.m., p<0.006 by Mann-Whitney test).

To confirm previous reports that mice deficient in P2Y2 receptor are protected in models of acute inflammation<sup>RW.ERROR - Unable to find reference:253</sup>, we dosed WT-tp and P2Y2<sup>-/-</sup>-tp mice intraperitoneally with either saline (SAL) or a sub-lethal dose of the gram-negative bacterial wall component lipopolysaccharide (LPS) for 24 hours. Indeed, P2Y2<sup>-/-</sup>-tp mice had significantly lower levels of the cytokines interleukin-6 (IL6) and tumor necrosis factor alpha (TNF $\alpha$ ) in serum (Fig 4.4A). One explanation for the protection of P2Y2 receptor deficient mice from acute inflammation is a decrease in leukocyte recruitment.<sup>RW.ERROR - Unable to find reference:253</sup> We analyzed blood from saline and LPS-treated WT-tp and P2Y2<sup>-/-</sup>-tp mice for white blood cell distribution and found that LPS treatment increased neutrophil (NE) content in blood and decreased lymphocyte (LY) and monocyte (MO) content in blood, but there was no significant difference between WT-tp and P2Y2<sup>-/-</sup>-tp mice (Fig 4.4B). *In vitro* treatment of macrophages with LPS increased P2y2r mRNA.<sup>90</sup> We tested whether LPS would mediate an increase in P2y2r mRNA *in vivo* by measuring P2y2r mRNA in blood from saline and LPS treated WT-tp mice; indeed, P2y2r mRNA levels were significantly increased in blood from LPS treated WT-tp mice compared to saline treated WT-tp mice (Fig 4.4C).

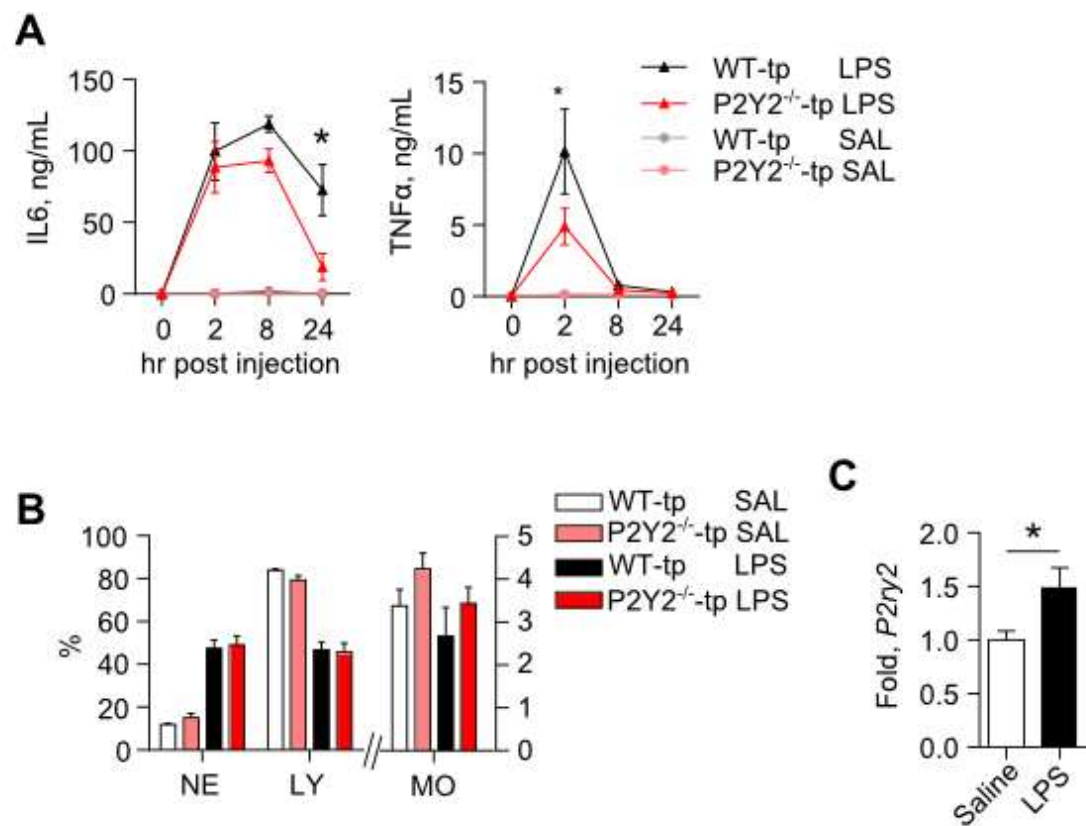


Figure 4-4 P2Y2<sup>-/-</sup>-tp mice challenged acutely with LPS are protected from inflammation.

**Figure 4-4. P2Y2<sup>-/-</sup>-tp mice challenged acutely with LPS are protected from inflammation.**

WT-tp and P2Y2<sup>-/-</sup>-tp mice were dosed i.p. with either saline or 2 mg/kg LPS for 24 hr.

(A) Serum IL6 and TNF $\alpha$  levels were measured by ELISA over the 24 hr period. P2Y2<sup>-/-</sup>-tp mice have significantly lower serum IL6 at 24 hr and significantly lower TNF $\alpha$  at 2 hr (N=6, mean +/- s.e.m., p<0.0001 by 2-Way repeated measures ANOVA with Tukey's multiple comparison test).

(B) Hemavet analysis of immune cells from blood reveals no difference between WT and P2Y2<sup>-/-</sup>-tp mice after 24 hr of LPS treatment (N=6, mean +/- s.e.m.).

(C) Expression of *P2y2r* mRNA was measured in blood from WT-tp mice and normalized to B2M revealing a significant increase in *P2y2r* mRNA upon LPS treatment (N=5, mean +/- s.e.m., p<0.05 by student's t-test).

#### 4.3.2 Characterization of high fat diet- and chow-fed *AdipPanx1* KO and *P2Y2*<sup>-/-</sup> mice.

We fed *WT* or *AdipPanx1KO* mice a diabetogenic high fat diet. The absence of Panx1 from adipocytes slightly, but significantly, exacerbated measures of insulin resistance, including glucose and insulin tolerance after 12 weeks of high fat diet feeding (Fig 4.5A and B). However, there was no difference in weight gain or adiposity was observed between the groups (Fig 4.5C and D). Serum free fatty acid levels were also similar between high fat diet-fed *WT* and *AdipPanx1KO* mice (Fig 4.5E). High fat feeding increased serum insulin levels in both *WT* and *AdipPanx1KO* mice but there was no difference between groups (Fig 4.5F).

Next, we investigated whether differences in insulin resistance in *AdipPanx1KO* mice could be a result from alterations in whole body energy expenditure. *AdipPanx1KO* mice on a high fat diet revealed small but non-significant decreases in light and dark cycle metabolic rates, compared to *WT* (Fig 4.5G- I), however, we did not observe differences in food intake (not shown), or overall mobility (Fig 4.5J). Chow fed *WT* and *AdipPanx1KO* mice had similar metabolic rates and mobility (Fig 4.5G- J)

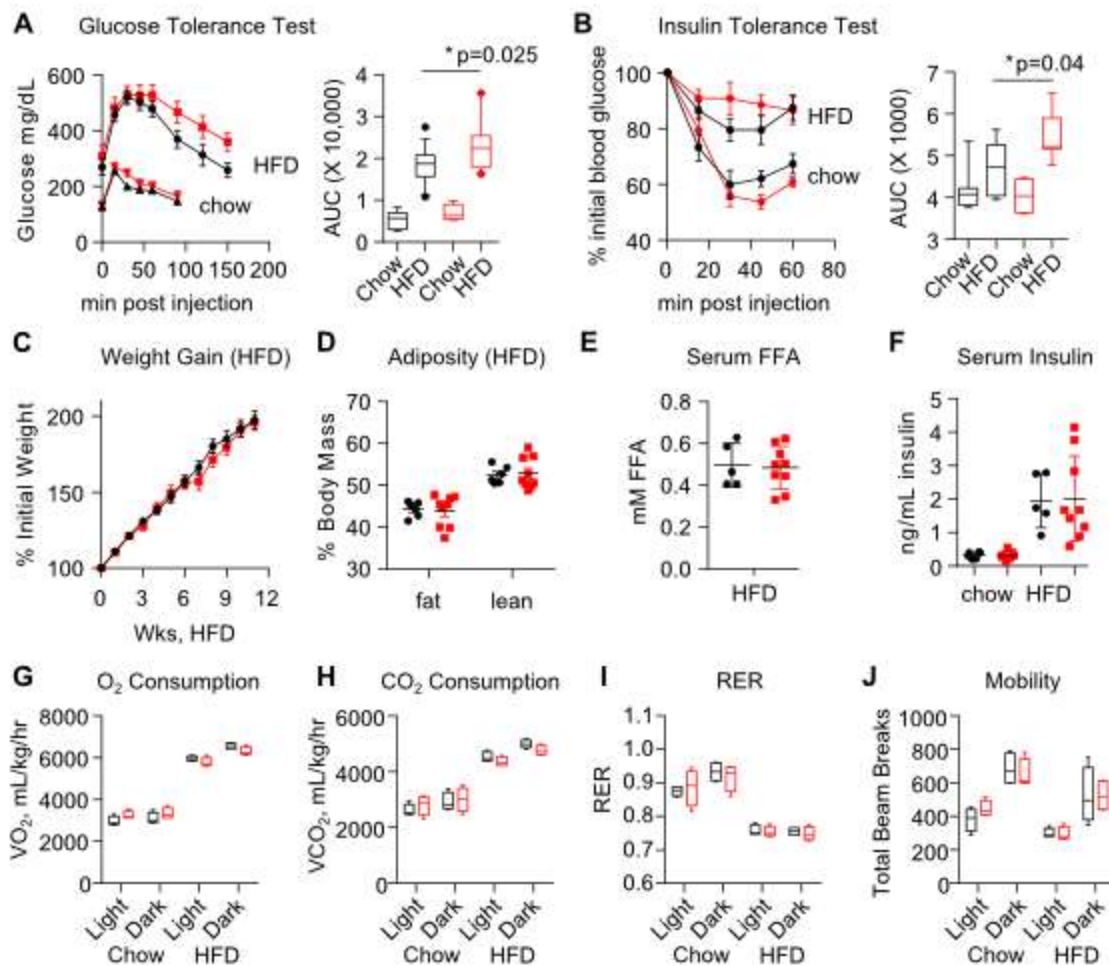


**Figure 4-5** Weight gain, energy expenditure, serum free fatty acids and insulin are not different between high fat fed WT and *AdipPanx1KO* mice.

**Figure 4-5. Weight gain, energy expenditure, serum free fatty acids and insulin are not different between high fat fed WT and *AdipPanx1KO* mice.**

(A) Intraperitoneal glucose tolerance test was performed on age-matched, male, WT and *AdipPanxKO* littermates that had been fed chow or high fat diet (60% fat) for 12 weeks. Mice were injected i.p. with 1 mg/kg glucose and blood glucose was measured in tail vein blood via glucometer (One Touch Ultra). Data are presented as mean +/-s.e.m and representative of 3 independent experiments (WT HFD n=6, KO HFD n=9, WT chow n=7, KO chow n=6). Combined area under the curve (AUC) analysis of glucose tolerance tests reveals that *AdipPanxKO* mice are significantly more glucose intolerant after high fat feeding compared to WT mice (WT HFD n=18, KO HFD n=14, WT chow n=7, KO chow n=4); \*p = 0.025 by 2-tailed Student's t-test. Box plots represent the 10th to 90th percentile. Three mice in the high fat diet group (WT n=1, KO n=2) did not respond to diet as evidenced by AUC not being different from chow groups and thus were excluded from the analysis. One data point (WT n=1) was greater than 2 standard deviations from the mean and thus was excluded.

(B) Intraperitoneal insulin tolerance tests (0.75 U/kg) was performed on age-matched, male, WT and *AdipPanxKO* littermates that had been fed chow or high fat diet (60% fat) for 12 weeks. n=6-7 mice per group. Data are expressed as mean + s.e.m. Box plots represent the 10th to 90th percentile. \*p < 0.05 by Student's t-test.

(C,D) Male WT and *AdipPanx1KO* littermates were fed a high fat diet (60% fat) for 12 weeks. Mice on a high fat diet were weighed weekly. Adiposity (%fat) and lean mass (%lean) were assessed by echo MRI. Data are representative of 3 independent experiments, n=6 WT, n=9 *AdipPanx1KO*. Data are expressed as mean +/-s.e.m.

(E) Serum free fatty acids (FFA) were measured after 12 weeks of high fat feeding in WT and *AdipPanxKO* mice using the colorimetric FFA kit from Wako. (n=5 WT, n=9 KO). Data are expressed as mean +/-s.d.

(F) Serum insulin in WT and *AdipPanxKO* mice that were either fed chow diet or HFD for 12 weeks were measured after a 5 hour fast. (n=6 WT chow, n=7 *AdipPanxKO* chow, n=5 WT high fat diet, n=9 *AdipPanxKO* high fat diet). Data are expressed as mean +/-s.d.

(G-I) High fat diet-fed (12 weeks) and chow-fed WT and *AdipPanx1KO* mice (n=4 per group) were placed in metabolic cages for 72 h. Average  $VO_2$  consumption,  $VCO_2$ , and respiratory exchange ratio (RER) by animal are shown for light and dark periods. The initial 4 h of readings were not part of average light values as this was time for mice to acclimate. Box plots represent the 10th to 90th percentile.

(J) Locomotion was recorded as X- and Y-axis beam breaks during light and dark cycle. Total beam breaks were not different between WT and *AdipPanx1KO* mice indicating no overall difference in locomotion. Box plots represent the 10th to 90th percentile.

To determine whether P2Y2 receptor on myeloid cells plays a role in chronic inflammation, we fed WT-tp and P2Y2<sup>-/-</sup>-tp mice a high fat diet (HFD) (60% kcal from fat) for up to 20 weeks. Although HFD significantly increased weight gain and adiposity, there was no difference between WT-tp and P2Y2<sup>-/-</sup>-tp mice, nor was there any difference in food intake (Fig 4.6A-C). Glucose tolerance tests revealed that high fat diet feeding decreased glucose tolerance at both 4 and 10 weeks, but there was no difference between WT-tp and P2Y2<sup>-/-</sup>-tp mice (Fig 4.6D). Serum insulin levels were increased with high fat diet feeding but not different between WT-tp and P2Y2<sup>-/-</sup>-tp mice (Fig 4.6E). Taken together, this data shows that while high fat fed AdipPanx1 KO mice have increased insulin resistance compared to WT mice, P2Y2<sup>-/-</sup>-tp mice show no difference in insulin resistance compared to WT.

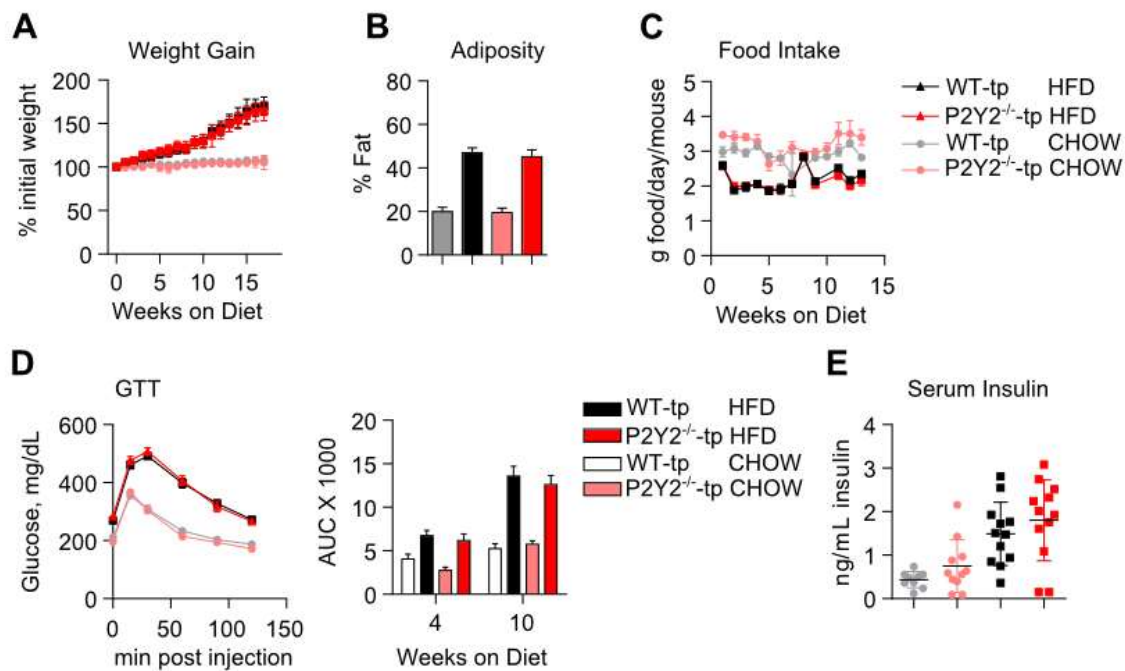


**Figure 4-6 High fat fed P2Y2<sup>-/-</sup>-tp mice show weight gain, adiposity, and glucose intolerance similar to high fat fed WT-tp**

**Figure 4-6. High fat fed P2Y<sub>2</sub>R<sup>-/-</sup>-tp mice show weight gain, adiposity, and glucose intolerance similar to high fat fed WT-tp**

WT and P2Y<sub>2</sub>R<sup>-/-</sup> chimeric mice were fed either a regular chow diet (Teklad) or high fat diet (60% kcals from fat with 0.2% cholesterol, Bioserv) for up to 20 weeks.

(A) Mice were weighed weekly to reveal no difference between WT and P2Y<sub>2</sub>R<sup>-/-</sup> chimeric mice weight gain on high fat diet (N=12, mean +/- s.d.).

(B) Adiposity was determined for WT and P2Y<sub>2</sub>R<sup>-/-</sup> chimeric mice after 17 weeks of diet by DEXA scan (N=12, mean +/- s.d., p<0.0001 by 1-way ANOVA with Sidak's multiple comparison test).

(C) Food intake was determined for WT and P2Y<sub>2</sub>R<sup>-/-</sup> chimeric mice by determining food weight weekly per cage of 4 mice (N=3 cages of 4 mice, mean +/- s.e.m.).

(D) Whole body glucose tolerance was assessed by glucose tolerance test in which mice were fasted for 6 h and then dosed intraperitoneally with 2g/kg glucose in saline. Blood glucose was measured by handheld glucometer (One Touch Ultra) for up to 2 h. Blood glucose curve is shown for glucose tolerance test performed after 10 weeks on diet. (N=11-12, mean +/- s.e.m. Quantification of area under the curve is shown at the right for glucose tolerance tests performed after 4 weeks and 10 weeks of diet. (N=11-12, mean +/- s.e.m.).

(E) Insulin levels were measured by ELISA in serum obtained from 6 h fasted WT and P2Y<sub>2</sub>R<sup>-/-</sup> chimeric mice after 10 weeks on diet. (N=9-12, each point represents one mouse, mean +/- s.d.).

### 4.3.3 Analysis of adipose tissue inflammation and macrophage infiltration in obese

#### AdipPanx1KO mice and P2Y2<sup>-/-</sup>-tp mice.

To determine whether increased insulin resistance observed in AdipPanx1 KO mice is due to differences in adipose tissue inflammation and macrophage infiltration, we analyzed cytokine expression in the stromal vascular fraction and also performed flow cytometry analysis to quantify macrophage content. Analysis of the stromal vascular fractions of perigonadal adipose tissue from high fat-fed WT and AdipPanx1KO mice by flow cytometry revealed no difference in absolute numbers of CD45<sup>+</sup>/CD11b<sup>+</sup> cells, which include macrophages. There was also no difference in the relative abundance of phenotypically polarized macrophage subsets M1 (CD11b<sup>+</sup>/CD11c<sup>+</sup>) and M2 (CD11b<sup>+</sup>/CD206<sup>+</sup>) (Fig 4.7A). Moreover, analyses of mRNA levels of several pro and anti-inflammatory cytokines in the stromal vascular fraction of perigonadal adipose tissue from high fat fed WT and AdipPanx1KO mice, including *tnfa*, *il1b*, *il18*, *ifnγ*, and *mcp1* as well as *il4*, *arg1*, *mg1*, *il10*, and *ym1* revealed no significant difference (Fig 4.7B), except for *mg1* mRNA levels, which were significantly lower in SVF from AdipPanx1KO mice. We conclude from these data that the greater propensity to develop insulin resistance in high fat-fed AdipPanx1KO mice is not due to adipose tissue inflammation.

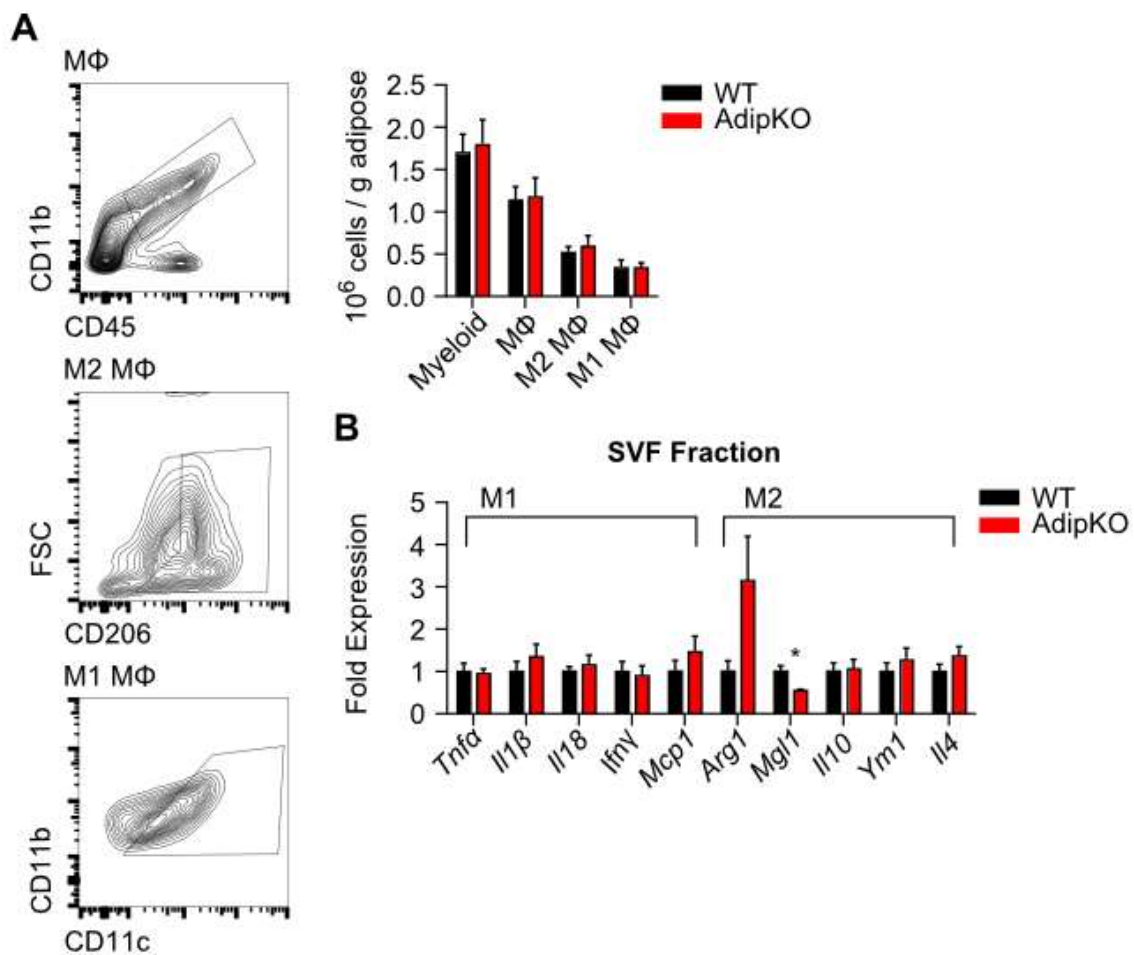


Figure 4-7 Adipose tissue inflammation is not different between high fat fed WT and AdipPanx1KO mice.

**Figure 4-7. Adipose tissue inflammation is not different between high fat fed WT and AdipPanx1KO mice.**

(A) Flow cytometric analysis of stromal vascular fractions (SVF) isolated from perigonadal adipose tissue of 12 week high fat diet-fed WT and *AdipPanxKO* mice. Gating strategy for flow cytometry is shown. CD11b<sup>+</sup>/CD45<sup>+</sup> cells in the SVF were further gated on M2 and M1 macrophage markers CD206<sup>+</sup> and CD11c<sup>+</sup>, respectively. Abundance of total myeloid cells (CD45<sup>+</sup>), CD45<sup>+</sup>/CD11b<sup>+</sup> cells, M2 (CD45<sup>+</sup>/CD11b<sup>+</sup>/CD206<sup>+</sup>) cells and M1 (CD45<sup>+</sup>/CD11b<sup>+</sup>/CD11c<sup>+</sup>) cells are shown in bar graph on the right. n= 6 mice per group. Data are expressed as mean +/- s.e.m.

(B) mRNA expression of inflammatory (M1) and anti-inflammatory (M2) cytokines in the stromal vascular fraction (SVF) from perigonadal adipose tissue of 12 week high fat diet-fed WT and *AdipPanxKO* mice was measured by qPCR. n=7 WT, n=8 *AdipPanxKO* mice. Data are normalized to beta-2 microglobulin and the WT average was set to 1 for each cytokine. Data are expressed as mean +/-s.e.m. \*p<0.05 by Student's t-test.

Unlike in the acute endotoxemia model, high fat fed P2Y2<sup>-/-</sup>-tp mice showed no difference in levels of serum cytokines including TNF $\alpha$ , IL6, and IL10 compared to WT-tp (Fig 4.8A). Confocal microscopy of perigonadal adipose tissue from WT-tp and P2Y2<sup>-/-</sup>-tp mice showed the presence of CD68+ macrophages (blue) in both groups; however, while CD68+ macrophages in adipose tissue from WT-tp mice were observed to surround adipocytes in crown-like structures (CLS), CD68+ macrophages in adipose tissue from P2Y2<sup>-/-</sup>-tp mice were dispersed among adipocytes but did not seem to form crown-like structures (Fig 4.8B). Quantification of CLS showed that after 12 weeks of high fat diet feeding, CLS were frequently observed in WT-tp adipose tissue but no CLS were observed in adipose tissue from P2Y2<sup>-/-</sup>-tp (Fig 4.8C). By 20 weeks of high fat diet feeding, CLS were observed in adipose tissue from P2Y2<sup>-/-</sup>-tp mice but were not observed as frequently as in adipose tissue from WT-tp mice (Fig 4.8C). The difference in the presence of CLS was independent of overall immune cell infiltration into the adipose tissue as equivalent numbers of cells in the stromal vascular fraction (SVF) which include macrophages and other immune cells were observed in perigonadal adipose tissue from WT-tp and P2Y2<sup>-/-</sup>-tp mice (Fig 4.8D). Taken together, this data indicates that myeloid P2Y2 receptor does not affect diet-induced insulin resistance in mice, but may play a role in the formation of crown-like structures within adipose tissue.

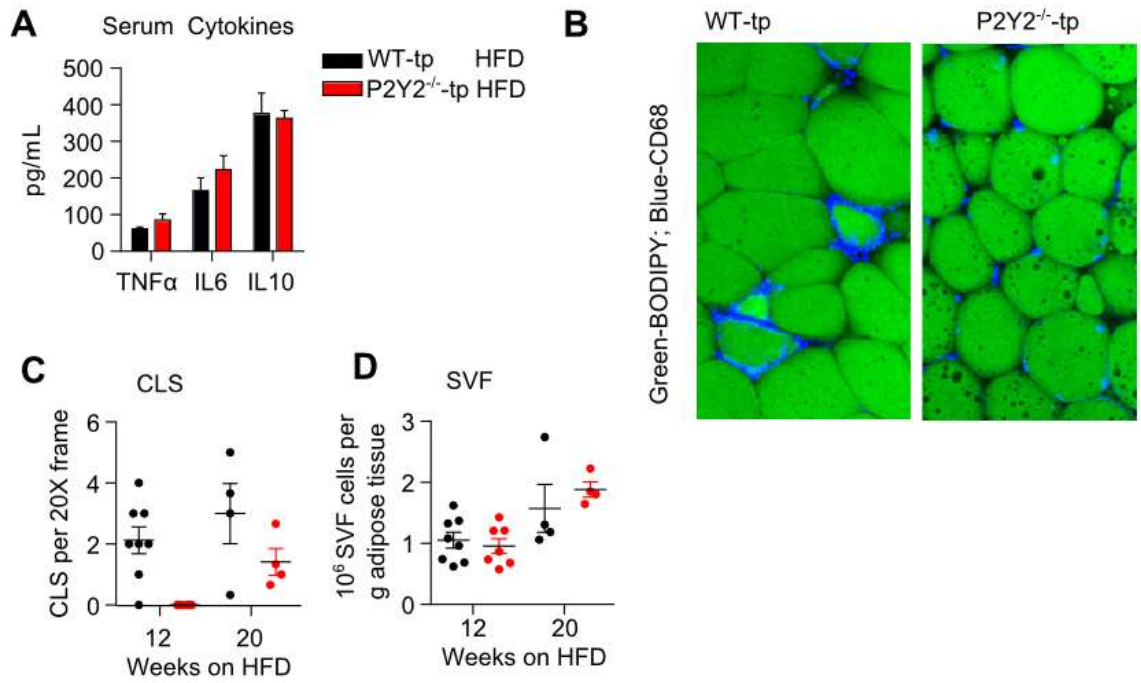


**Figure 4-8** High fat fed P2Y2<sup>-/-</sup>-tp mice have decreased formation of crown-like structures in adipose tissue.

**Figure 4-8. High fat fed P2Y2<sup>-/-</sup>-tp mice have decreased formation of crown-like structures in adipose tissue.**

(A) TNF $\alpha$ , IL6, and IL10 levels were measured by ELISA in serum obtained from WT-tp and P2Y2<sup>-/-</sup>-tp mice after 12 weeks on high fat diet. (N=7, each point represents one mouse, mean +/- s.e.m.).

(B) Whole mount immunostaining of gonadal adipose tissue isolated from WT-tp and P2Y2<sup>-/-</sup>-tp mice. Macrophages (blue, CD68) form crown like structures in adipose tissue from WT-tp mice, but not in P2Y2<sup>-/-</sup>-tp mice. Neutral lipids stained with Bodipy (green). Confocal image is at 20X magnification and is a composite z-stack.

(C) Quantification of CLS in perigonadal adipose tissue from WT-tp and P2Y2<sup>-/-</sup>-tp mice after 12 and 20 weeks on high fat diet. Three 20X images were quantified per mouse and averaged by 3 independent observers. Each point represents one mouse. Data presented as mean +/- s.e.m.

(D) Stromal vascular cells isolated from perigonadal adipose tissue from WT-tp and P2Y2<sup>-/-</sup>-tp mice after 12 and 20 weeks on high fat diet were quantified by hemocytomer. Each point represents one mouse. Data presented as mean +/- s.e.m.

#### **4.3.4 Pannexin 1 expression in human adipose tissue correlates with obesity and insulin resistance**

Neither expression levels nor potential functional roles of Panx1 in adipose tissue have been reported in the context of human pathology. A previous study compared global gene expression in subcutaneous adipose tissue between lean and obese Pima Indians using gene arrays<sup>49</sup>. Data extracted from the data sets deposited at NCBI (GDS1498[ACCN]) demonstrate that Panx1 expression in both males and females was significantly increased in obese compared to lean subjects (Fig 4.9A). We then examined Panx1 expression in visceral adipose tissue obtained from 23 morbidly obese patients during bariatric surgery. We found that relative Panx1 mRNA expression levels significantly correlated with fasting blood glucose levels, and this correlation was especially strong in Caucasian females (Fig 4.9B). Subjects in the tertile with the highest relative Panx1 mRNA levels also had significantly higher HOMA-IR scores (a measure of insulin resistance) (Fig 4.9C). These data suggest that Panx1 may also play a role in adipocyte metabolism in humans, in a way that increased Panx1 expression may help counterbalance decreasing insulin sensitivity.

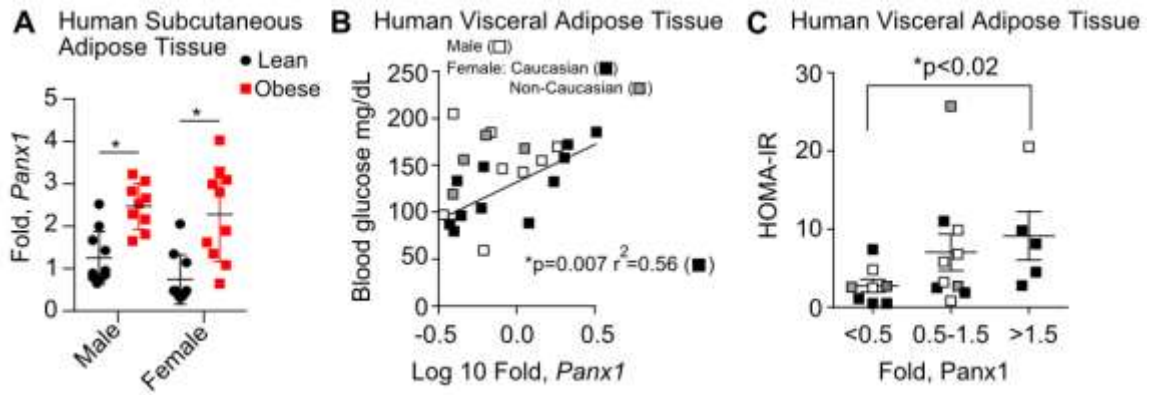


**Figure 4-9 Pannexin 1 expression in human adipose tissue is associated with obesity and insulin resistance.**

**Figure 4-9. Pannexin 1 expression in human adipose tissue is associated with obesity and insulin resistance**

(A) Data from NCBI gene array (GDS1498[ACCN])<sup>49</sup> were analyzed for Panx1 expression in subcutaneous adipose tissue from lean male (n=10), lean female (n=10), and obese male (n=9) and obese female (n=10) human subjects. Data are normalized to lean samples, each point represents one human subject, error bars indicate s.d. \*p<0.0001 by 2 way ANOVA with Sidak's multiple comparison test.

(B) Omental fat samples were obtained from human subjects prior to bariatric surgery and analyzed for Panx1 mRNA levels normalized to 18S mRNA. The average of all samples was set to 1 and log 10 values of Panx1 mRNA were plotted against the blood glucose levels of patients at time of surgery, revealing a positive and significant correlation ( $r^2=0.181$  and  $p=0.04$  by linear regression, grey line). The correlation of Panx1 levels with blood glucose levels was particularly pronounced in Caucasian females ( $r^2=0.56$ ,  $n=11$ , black line). Each point represents one human subject, female subjects are shown as grey (non-Caucasian) and black (Caucasian) squares, male subjects as white squares.

(C) Samples from B were grouped into tertiles based on low (<0.5 fold, n=8), medium (0.5-1.5 fold, n=10), and high Panx1 expression (>1.5 fold, n=5) and plotted against HOMA-IR, a clinical measure of insulin resistance. \*p<0.02 by Student's t-test. Each point represents one human subject; error bars represent s.e.m.

#### 4.4 DISCUSSION

We investigated whether release of ATP from adipocytes via Panx1 signals to macrophage P2Y2 receptors to impact inflammation, crown-like structure formation, and insulin resistance by feeding a high fat diet to adipocyte specific Panx1 KO mice and myeloid specific P2Y2 receptor knockout mice (generated via bone marrow transplant). We found that while AdipPanx1 KO mice were significantly more insulin resistance compared to WT mice, it was independent of macrophage infiltration and inflammation as determined by qRT-PCR and flow cytometry analysis of stromal vascular cells from perigonadal adipose tissue. We determined that increased insulin resistance in AdipPanx1 KO mice is due do defective insulin-stimulated glucose uptake in adipocytes (see Chapter 5). P2Y2<sup>-/-</sup>-tp mice were equally glucose intolerant as WT-tp mice; however, confocal microscopy of perigonadal adipose tissue revealed a lack of CLS formation without a difference in total adipose tissue macrophage content. This data suggests that Panx1-mediated ATP release from adipocytes does not impact overall adipose tissue macrophage accumulation and inflammatory status. Indeed, the ATP-P2X7 signaling axis was shown to be dispensable for obesity-associated inflammasome activation.<sup>75</sup> In terms of macrophage migration and inflammation, it is likely that other cytokine and chemokine signals overshadow any impact of extracellular ATP signaling. There may also be alternative mechanisms of ATP release from adipocytes such as vesicular release.

The generation of adipocyte-specific Panx1 KO mice was successful; however, as described above the detection of Panx1 protein by western blot proved extremely difficult. Several Panx1 antibodies are currently available which are specific to the C-terminal region, N-terminal region, and extracellular loop region, and while overexpressed Panx1 protein is easily detected by most of these antibodies, detection of Panx1 in whole tissue lysates, especially of adipose tissue, was difficult. The levels of Panx1 protein in adipocytes may be low; however this

does not preclude a functional relevance of the channel. Perhaps in the future better antibodies will be available. The AdipPanx1 KO line suffered from germline leakiness of the Cre; however, by analysis of genomic DNA for the deletion of Panx1 exon 3 we were able to exclude mice which were carrying a deletion allele. The adiponectin-Cre we used was produced in the laboratory of Dr. Phil Scherer<sup>59</sup> and has been used to successfully overexpress genetic material in adipocytes in several publications.<sup>92-98</sup> This mouse has been used to specifically delete genetic material from adipocytes in four publications<sup>99-102</sup>, only two of which analyze tissues other than adipose for expression of the protein of interest. Additionally one of those publications<sup>102</sup> confusingly reports in the results section that the adiponectin-Cre mouse utilized was the BAC mouse generated in Dr. Evan Rosen's laboratory (described below), while in the methods section of the paper they report that the adiponectin-Cre mouse utilized was from Dr. Scherer's laboratory. Another adiponectin-Cre is available from Jackson Labs that was generated by the BAC method in the lab of Dr. Evan Rosen<sup>103</sup> and has been used more extensively for adipocyte-specific deletion of genetic material.<sup>104-140</sup> This adiponectin-Cre mouse has also been used for overexpression of genetic material including fluorescent reporter genes.<sup>133,141-147</sup> The adiponectin-Cre is superior to the ap2-cre utilized in the past which has been shown to delete in macrophages as well as adipocytes.<sup>148,149</sup> A tamoxifen-inducible adiponectin-Cre mouse<sup>150</sup> has been used by a few groups<sup>151-153</sup> to date and will certainly be a valuable tool for future studies of adipose tissue function *in vivo*.

The generation of myeloid-specific P2Y2 receptor KO mice by bone marrow transplantation was complicated by the fact that the P2Y2 global KO donor mice were only partially on a C57Bl/6 background. We observed no sign of graft rejection during our study. The data generated by the high fat feeding study is validated insofar as WT-tp and P2Y2<sup>-/-</sup>-tp mice responded to acute endotoxemia as expected based on reported literature of global P2Y2

receptor KO mice and yet no difference was observed in glucose tolerance after high fat feeding. *In vitro* studies have utilized bone marrow derived macrophages from C57Bl/6 mice as controls for BMDM studies with cells isolated from P2Y2 global KO mice.<sup>63</sup> Future studies with specific genetic deletion of P2Y2 receptor in macrophages may help to clarify our findings. Although our findings show that although macrophage P2Y2 receptor may have some role in CLS formation, overall whole body glucose tolerance was not changed. There are several other P2 receptor family members that may play a role in insulin resistance. Indeed, the P2Y14 receptor (also known as GPR 105) which is a receptor for UDP-glucose was shown to facilitate macrophage infiltration and inflammation.<sup>154</sup>

Our observation of an association of Panx1 expression with obesity and insulin resistance in humans supports a role for Panx1 in metabolic homeostasis. Upregulation of Panx1 expression in response to obesity and insulin resistance may reflect a protective mechanism by which decreased insulin sensitivity is counteracted by an increased ability of the tissue to release bioactive nucleotides. However, further studies particularly in human subjects are required to definitively support this hypothesis.

## Chapter 5 Pannexin 1 and Adipocyte Metabolic Function

### 5.1 ABSTRACT

Defective glucose uptake in adipocytes leads to impaired metabolic homeostasis and insulin resistance, hallmarks of type 2 diabetes. Extracellular ATP-derived nucleotides and nucleosides are important regulators of adipocyte function. Glucose uptake in cultured 3T3-L1 adipocytes was measured in the presence of Panx1 pharmacologic inhibitors and in adipocytes isolated from white adipose tissue from wildtype (WT) or adipocyte-specific Panx1 knockout (AdipPanx1 KO) mice generated in our laboratory. We performed *in vivo* glucose uptake studies in chow fed WT and AdipPanx1 KO mice. Pharmacologic inhibition or selective genetic deletion of Panx1 from adipocytes decreased insulin-induced glucose uptake *in vitro* and *in vivo*. We also performed lipidomic analysis on perigonadal adipose tissue from chow- and high fat diet-fed WT and AdipPanx1 KO mice to determine phospholipid levels.

### 5.2 INTRODUCTION

Adipose tissue is renowned for its function in lipid storage, but it is also a key endocrine organ and metabolic dysfunction of adipocytes exacerbates insulin resistance<sup>13</sup>. In healthy adipose tissue, insulin stimulates glucose uptake and lipogenesis while inhibiting lipolysis, but these effects are blunted during insulin resistance<sup>13</sup>. Furthermore, glucose uptake in adipocytes is a major contributor to whole body insulin sensitivity<sup>15</sup>.

The purine nucleoside adenosine accumulates extracellularly in isolated adipocyte suspensions<sup>18-20</sup> and is thought to be derived from degradation of extracellular ATP. Adenosine can impact adipocyte metabolic function by inhibiting lipolysis<sup>21</sup>, increasing glucose uptake<sup>22,23</sup>, enhancing insulin action to stimulate glucose oxidation<sup>24</sup>, and by regulating adipose tissue blood flow<sup>25</sup>. In addition to adenosine, extracellular nucleotides such as ATP or UTP have autocrine effects on adipocytes. They signal through the purinergic P2 receptor family, which includes

ATP-gated cation channels P2X<sub>1-7</sub> and G-protein-coupled P2Y<sub>1,2,4,6,11-14</sub> receptors<sup>26</sup>. In brown adipose tissue, extracellular ATP caused mobilization of intracellular calcium stores, consistent with nucleotide signaling through purinergic P2 receptors<sup>27</sup>. Extracellular ATP also led to increased cell membrane capacitance in adipocytes<sup>28,29</sup> and it was suggested that ATP activates exocytosis<sup>30</sup>. In white adipocytes, micromolar concentrations of ATP inhibit glucose oxidation<sup>31</sup>, but increase glycogen synthesis<sup>32</sup> and lipogenesis<sup>33</sup>. However, the effect of exogenous ATP on basal and insulin-induced glucose uptake in adipocytes is still a matter of controversy: ATP was shown in some studies to be inhibitory at millimolar concentrations<sup>34,35</sup>, while in other work no effect of ATP was observed<sup>33</sup>.

Extracellular ATP and related nucleotides and nucleosides also impact lipid metabolism. It has long been known that adenosine suppresses adipocyte lipolysis. Extracellular ATP and other nucleotides can stimulate the hydrolysis of phosphatidylethanolamine<sup>155</sup>, while UTP and ATP were observed to activate phospholipase D, resulting in phosphatidylcholine hydrolysis.<sup>156</sup> The ratio of phosphatidylcholine to phosphatidylethanolamine was observed to decrease as lipid droplet formation occurs in 3T3-L1 adipocytes.<sup>157</sup>

We sought to determine whether adipocyte Panx1 controls adipocyte glucose and lipid homeostasis.

## 5.3 RESULTS

### 5.3.1 Glucose uptake in WT and Panx1 KO adipocytes

To examine a role for Panx1 in glucose uptake in adipocytes, we treated cultured or primary adipocytes with insulin for 15 minutes and basal and insulin-stimulated glucose uptake was measured in the presence and absence of two distinct pharmacological Panx1 inhibitors. Glucose uptake into cultured 3T3-L1 adipocytes was significantly increased after treatment with insulin; notably, pretreatment with carbenoxolone (CBX) or probenecid (Prob) resulted in

significantly blunted insulin-stimulated glucose uptake (Fig 5.1A). In addition, insulin-stimulated glucose uptake was significantly impaired in adipocytes isolated from *AdipPanx1KO* mice compared to adipocytes isolated from *WT* mice (Fig 5.1B). Since pharmacological as well as genetic inhibition of Panx1 in adipocytes resulted in blunted insulin-stimulated glucose uptake, we hypothesized that Panx1-mediated ATP release was responsible for the effect. Indeed, the addition of exogenous ATP rescued the compromised insulin-stimulated glucose uptake in *Panx1*-deficient adipocytes (Fig 5.1B).

To test whether a lack of adipocyte Panx1 would inhibit glucose uptake *in vivo*, lean *WT* and *AdipPanx1KO* mice were given a bolus of glucose containing a trace amount of radioactive [<sup>3</sup>H] 2-deoxy-D-glucose such that organs harvested at the end of the study could be assessed for glucose uptake. While the rate of glucose uptake was similar in gastrocnemius muscle from *WT* and *AdipPanx1KO* mice, the absence of Panx1 in adipocytes resulted in a 20% decreased rate of glucose uptake in perigonadal white adipose tissue (Fig 5.1C).

These results demonstrate that Panx1-dependent ATP release is required for insulin-stimulated glucose uptake in adipocytes, and they suggest a potentially novel mechanism of Panx1 channel activation by insulin (see Chapter 3 Section 3.3.4). Defective insulin-stimulated glucose uptake in adipocytes also explains why high fat diet fed *AdipPanx1 KO* mice are significantly more insulin resistance than *WT* mice because a deficit in glucose uptake in adipocytes may begin to manifest in whole body glucose tolerance over time<sup>15</sup>.

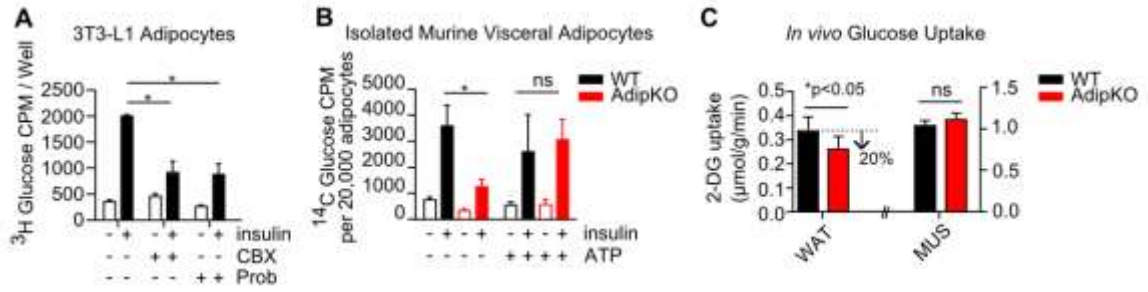


**Figure 5-1 Full activation of insulin-stimulated glucose uptake in adipocytes requires ATP**

**release by Panx1 channels**

**Figure 5-1. Full activation of insulin-stimulated glucose uptake in adipocytes requires ATP release by Panx1 channels**

(A) Blockade of Pannexin-1 channels with carbenoxolone (100  $\mu$ M, CBX) or probenecid (1 mM, Prob) significantly decreases insulin-stimulated  $^3$ H-glucose uptake in 3T3L1-adipocytes. Data are expressed as mean  $\pm$ s.e.m. \* $p$ <0.001 by 2 way ANOVA with Tukey's multiple comparisons test.

(B) Insulin-stimulated glucose uptake is significantly decreased in adipocytes isolated from perigonadal adipose tissue of adipocyte-specific Pannexin-1 null mice. Addition of exogenous ATP (50  $\mu$ M) restores insulin-stimulated  $^{14}$ C-glucose uptake in adipocytes isolated from *Panx1* null mice. Data are expressed as mean  $\pm$ s.e.m. \* $p$ <0.003 by 1 way ANOVA with Tukey's multiple comparisons test.

(C) *In vivo* [ $^3$ H] 2-deoxy-D-glucose uptake was assessed in perigonadal white adipose tissue (WAT) and gastrocnemius muscle (MUS) in age-matched, male, chow fed WT and *AdipPanxKO* littermates (n=6). Data are presented as mean  $\pm$ s.e.m. \* $p$ <0.05 by paired t-test. Dotted line indicates the 20% decrease in glucose uptake in WAT in *AdipPanxKO* mice compared to WT.

### 5.3.2 Lipid genes and Lipidomics

We analyzed adipocytes isolated from perigonadal adipose tissue from chow- and high fat diet-fed WT and AdipPanx1 KO mice for mRNA expression of metabolic genes. There was no significant difference in the fatty acid transport protein FATP1 (also called Slc27a1), the glucose transporter Glut1 (also called Slc2a1), or the diacylglycerol acyltransferase Dgat1 in adipocytes isolated from chow fed WT and AdipPanx1 KO mice. However, in adipocytes isolated from high fat fed mice, both FATP1 and Dgat1 had significantly lower expression in adipocytes isolated from perigonadal adipose tissue from AdipPanx1 KO mice compared to WT mice. In adipocytes isolated from obese mice, expression of acyl-CoA synthetase Acsl1 was significantly lower in adipocytes isolated from AdipPanx1 KO mice compared to WT mice, with no significant difference in the master transcriptional regulator Ppar $\gamma$ , the glucose transporter Glut4 (also called Slc2a4), the monoacylglycerol acyltransferase Mogat1, the adipokines leptin and adiponectin, or preadipocyte factor 1 Pref1. This data suggested that Panx1 null adipocytes may have altered lipid metabolism so we used mass spectrometry to assess the lipid content in perigonadal adipose tissue from chow and high fat diet fed WT and AdipPanx1 KO mice.

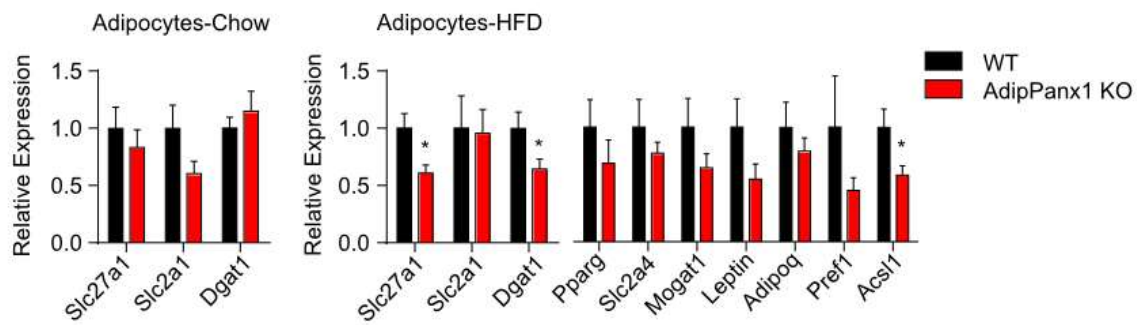


Figure 5-2 Expression of metabolism genes in adipocytes from WT and AdipPanx1 KO mice.

**Figure 5-2. Expression of metabolism genes in adipocytes from WT and AdipPanx1 KO mice.**

Adipocytes isolated from perigonadal adipose tissue from chow and high fat diet fed WT and AdipPanx1 KO mice were analyzed for mRNA expression of metabolic genes. N=13,11 for adipocytes from chow fed WT and AdipPanx1 KO mice. N=7,8 for adipocytes from high fat diet fed WT and AdipPanx1 KO mice. Data expressed as mean +/- s.e.m. \*p<0.05 by student's t-test.

Perigonadal adipose tissue from chow fed WT and AdipPanx1 KO mice was analyzed by mass spectrometry for lipids. There was no difference between the levels of phosphatidylcholine (PC) and phosphatidylethanolamine (PE) between high fat diet fed WT and AdipPanx1 KO mice; however, there was a trend for increased total levels of PC and decreased total levels of PE in chow fed AdipPanx1 KO mice compared to chow fed WT mice (Fig 5-3). Indeed, when comparing the PC:PE ratio in adipose tissue from chow fed WT and AdipPanx1 KO mice, there was a significant increase (\* $p=0.004$ ) in the PC:PE ratio in adipose tissue from AdipPanx1 KO mice compared to WT. This finding is intriguing because the PC:PE ratio may be important for lipid droplet synthesis in adipocytes.<sup>157</sup>



**Figure 5-3. Phosphatidylcholine and phosphatidylethanolamine content in adipose tissue from chow and high fat diet-fed WT and AdipPanx1 KO mice.**

Lipids were extracted from perigonadal adipose tissue from chow and high fat diet fed WT and AdipPanx1 KO mice and analyzed by mass spectroscopy. Samples were normalized to a C17 LPA standard. Individual species of phosphatidylcholine and phosphatidylethanolamine are shown as box and whisker plots representing the min to max. Lipid species which are preceded by an asterisk are those which have a mass identical to other lipid species and are thus nonresolvable by mass spectroscopy and are listed vertically at the bottom of the figure. Insets show total  $\mu\text{mol}$  of phosphatidylcholine and phosphatidylethanolamine per mg adipose tissue processed, which was calculated by addition of all species measured per mouse. Each dot represents one mouse. Data is expressed as mean  $\pm$  s.e.m. The PC:PE ratio is also shown which is calculated by dividing total PC by total PE content for each mouse. N=4 per chow fed group and n=6 per high fat diet fed group.

The synthesis of PC and PE in cells requires diacylglycerol (DAG) as a substrate. Alternatively, PE can be converted to PC by the enzyme PEMT. PE can also be synthesized by the conversion of phosphatidylserine (PS) into PE by PS decarboxylase. We measured both DAG and PS levels in adipose tissue from chow and high fat diet fed WT and AdipPanx1 KO mice. We found no significant difference in DAG levels between WT and AdipPanx1 KO mice (Fig 5-4). However, there were some differences between the chow groups compared to the high fat diet fed groups. For example, 16:0 18:2 DAG was decreased in adipose tissue from high fat diet fed mice compared to chow fed mice, while 18:1 18:1 DAG was increased in in adipose tissue from high fat diet fed mice compared to chow fed mice (Fig 5-4). There were no significant differences in phosphatidylserine content of adipose tissue from high fat diet fed WT and AdipPanx1 KO mice, but similar to PE, there was a trend towards decreased PS levels in chow fed AdipPanx1 KO mice compared to chow fed WT mice. This data suggests that lower PE levels in chow fed AdipPanx1 KO mice compared to chow fed WT mice may be driven by lower levels of PS since PS can be converted to PE in the mitochondria by PS decarboxylase.



**Figure 5-4. Phosphatidylserine and diacylglycerol content in adipose tissue from chow and high fat diet-fed WT and AdipPanx1 KO mice.**

Lipids were extracted from perigonadal adipose tissue from chow and high fat diet fed WT and AdipPanx1 KO mice and analyzed by mass spectroscopy. Samples were normalized to a C17 LPA standard. Individual species of phosphatidylserine and diacylglycerol are shown as box and whisker plots representing the min to max. Phosphatidylserine species which are preceded by an asterisk are those which have a mass identical to other lipid species and are thus nonresolvable by mass spectroscopy and are listed vertically at the bottom of the figure. Insets show total nmol and  $\mu\text{mol}$  of phosphatidylserine and diacylglycerol, respectively, per mg adipose tissue processed which was calculated by addition of all species measured per mouse. Each dot represents one mouse. Data is expressed as mean  $\pm$  s.e.m. N=4 per chow fed group and n=6 per high fat diet fed group.

We also measured phosphatidic acid (PA) levels in perigonadal adipose tissue from chow and high fat diet fed WT and AdipPanx1 KO mice. PA is a precursor of DAG so since we saw no difference in DAG levels between genotypes we did not expect a difference in PA levels. And indeed, we saw no significant difference in PA levels between WT and AdipPanx1 KO mice (Fig 5-5). We were unable to measure lyso-phosphatidic acid species (a precursor of PA) due to technical difficulties and high background signal on the mass spectrometer.

Taken together, this data suggests that the absence of Panx1 in adipocytes results in slight alterations in lipid species in the adipose tissue, particularly an increase in the PC:PE due to slightly increased PC and slightly decreased PE. PS, a precursor of PE, was also slightly decreased. To further understand these observations, it would be helpful to measure levels of enzymes involved in the synthesis pathways of these lipids. Many of these synthetic steps occur at the ER membrane, and Panx1 has been observed to be present on these membranes so it would be interesting to determine whether Panx1 functionality at the ER membrane might be important for the production of these lipids or whether these differences are in response to other alterations in adipocyte metabolic homeostasis.

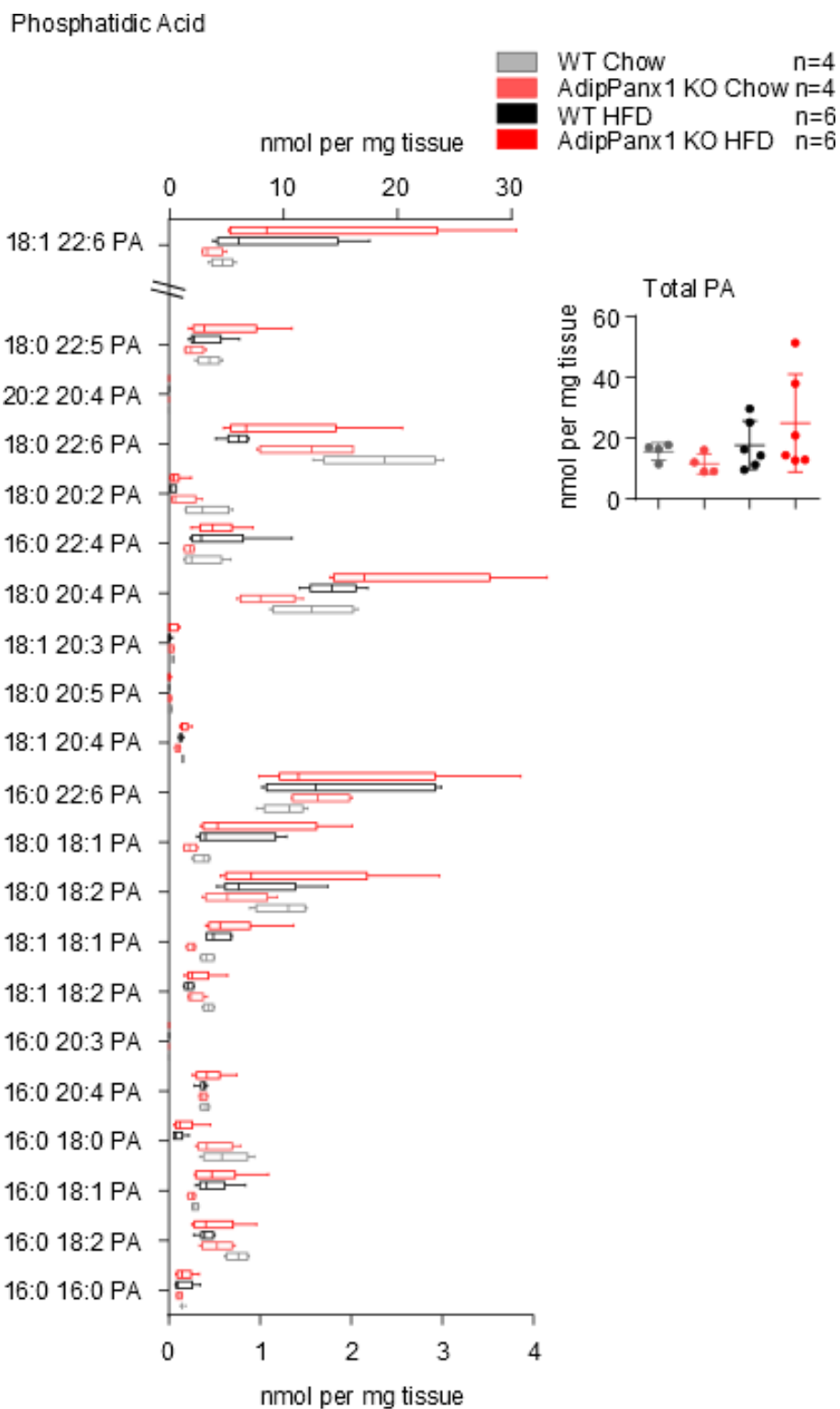


**Figure 5-5 Phosphatidic acid content in adipose tissue from chow and high fat diet-fed WT and AdipPanx1 KO mice.**

**Figure 5-5. Phosphatidic acid content in adipose tissue from chow and high fat diet-fed WT and AdipPanx1 KO mice.**

Lipids were extracted from perigonadal adipose tissue from chow and high fat diet fed WT and AdipPanx1 KO mice and analyzed by mass spectroscopy. Samples were normalized to a C17 LPA standard. Individual species of phosphatidic acid are shown as box and whisker plots representing the min to max. Inset shows total nmol and  $\mu\text{mol}$  of phosphatidic acid per mg adipose tissue processed which was calculated by addition of all species measured per mouse. Each dot represents one mouse. Data is expressed as mean  $\pm$  s.e.m. N=4 per chow fed group and n=6 per high fat diet fed group.

## 5.4 DISCUSSION

Our finding that addition of exogenous ATP to Panx1-deficient adipocytes rescues inhibited insulin-induced glucose uptake strongly suggests a role for ATP or its metabolites in this context. Extracellular ATP is rapidly metabolized and we calculated an approximately 6 minute half-life of exogenous ATP added to 3T3-L1 adipocytes (data not shown). The degradation of ATP by ectonucleotidases including CD39 and CD73, which are expressed on adipocytes<sup>158</sup>, provides ligands for a variety of purinergic receptors and adenosine, which was shown to enhance glucose uptake and block lipolysis<sup>22,23</sup>. Further studies are needed to identify the autocrine purinergic signaling pathways that are activated subsequently to Panx1 channel opening in adipocytes. Although we see no overt changes in lean, chow-fed AdipPanx1KO mice in the glucose tolerance test, we did observe decreased glucose uptake specifically in white adipose tissue. Upon high fat diet challenge, a deficit in glucose uptake in adipocytes may begin to manifest in whole body glucose tolerance over time<sup>15</sup>.

We observed decreased gene expression of certain metabolic genes in adipose tissue from AdipPanx1 KO mice including the acyl-CoA synthetase *Acs1*, the fatty acid transporter *FATP1*, and the diacylglycerol acyltransferase *Dgat1* all of which are involved in the cycle of fatty acid uptake and lipogenesis. We measured individual lipid species including phosphatidic acid, diacylglycerol, phosphatidylserine, phosphatidylcholine, and phosphatidylethanolamine by mass spectrometry and observed slight differences in the adipose tissue from chow fed WT and AdipPanx1 KO mice, which suggests that Panx1 may play a role in lipid metabolism within the adipocyte.

## Chapter 6 DISCUSSION

### 6.1 SUMMARY OF FINDINGS

These studies show that adipocytes express functional Pannexin 1 (Panx1) channels that can be activated to release ATP by known mechanisms including alpha-adrenergic stimulation and caspase-mediated C-terminal cleavage. Further, we identify insulin as a novel activator of Panx1 channels. Pharmacologic inhibition or selective genetic deletion of Panx1 from adipocytes decreased insulin-induced glucose uptake *in vitro* and *in vivo* and exacerbated diet-induced insulin resistance in mice. In obese humans Panx1 expression in adipose tissue is increased and correlates with the degree of insulin resistance.

Although in other systems, extracellular ATP has been shown to be chemotactic for immune cells such as macrophages, we saw no difference in the level of macrophage infiltration or inflammation in adipose tissue of diet-induced obese, insulin resistance AdipPanx1 KO mice. We also observed that deficiency of the ATP receptor P2Y2 on myeloid cells did not affect glucose tolerance in a mouse model of diet-induced obesity and insulin resistance. However, mice which lack P2Y2 receptor in myeloid cells show decreased crown like structure formation in perigonadal adipose tissue although the amount of macrophages within the tissue are not different from WT mice.

We also observed slight differences in adipose tissue lipids and decreased expression of certain metabolic genes in AdipPanx1 KO mice, suggesting that Panx1 may also play a role in lipid metabolism within adipocytes. Moreover, we found that Panx1 expression may be negatively regulated by PPAR $\gamma$ .

In conclusion, Panx1 channel activity controls metabolic homeostasis in adipocytes, namely through the regulation of insulin-stimulated glucose uptake (Fig. 6-1).

## 6.2 SIGNIFICANCE AND FUTURE DIRECTIONS

The prevalence of obesity is continuing to increase concomitantly with other risk factors such as diabetes, high blood pressure, and cardiovascular disease. According to the American Heart Association, metabolic syndrome affects 34% of adults. Many organ systems are involved in these pathologies including adipose tissue. Understanding the pathology of insulin resistance, especially in the context of obesity, will lead to novel therapies for the treatment of diabetes.

Adipocytes are surrounded by many other cells types within adipose tissue including macrophages, endothelial cells, neurons, and others and cross talk between the cells types allows the organ to maintain homeostasis and can also exacerbate pathology. Additionally, autocrine and paracrine signaling between adipocytes also functions to maintain homeostasis or exacerbate pathology. Extracellular ATP when released by cells in a controlled manner by Panx1 channels can fulfill this role as a mediator of cellular crosstalk. Our studies show that while Panx1-mediated ATP release from adipocytes had no effect on adipose tissue macrophage infiltration or inflammation in the setting of diet-induced obesity, adipocyte Panx1 function allowed for full activation of insulin-stimulated glucose uptake which may be an autocrine effect or a paracrine effect among neighboring adipocytes. ATP released by cells can be converted into adenosine by the action of ectonucleotidases CD39 (ENTPD1; nucleoside triphosphate diphosphorylase 1) and CD73 (NT5E; ecto-5'-nucleotidase). These ectonucleotidases are present on adipocytes and are also abundantly expressed on immune cells such as macrophages that are present in adipose tissue. ATP released by adipocytes may be converted to adenosine through the action of ectonucleotidases present on neighboring cells, creating an intricate network of cellular crosstalk.

The observation that adipocyte-specific Panx1 knockout mice experienced worsened insulin resistance in a model of diet-induced obesity suggests that it would be unwise to inhibit Panx1 in diabetic patients. Perhaps activating Panx1 channels might improve adipose tissue insulin sensitivity; however, this would likely result in many other physiologic effects given the variety of functions of Panx1 channels reported in many tissues. At present, there are no known Panx1 agonists; however, Dr. Kodi Ravichandran and colleagues have completed drug screens to discover novel compounds that impact Panx1 function such as the broad spectrum antibiotic trovafloxacin that they found to be a potent inhibitor of Panx1.<sup>48</sup>

An open question remains as to the exact mechanism by which adipocyte Panx1 channels allow for full activation of insulin-stimulated glucose uptake. Our data suggests that Panx1-mediated ATP release impacts glucose uptake. ATP may signal through purinergic P2 receptors to mediate this effect but future studies are needed to confirm this. ATP binding to P2Y receptors generally leads to PLC $\beta$  (phospholipase C beta) activation and decreased cAMP as most P2Y receptors are G<sub>q/11</sub> coupled. Phospholipase C has been suggested to play a role in glucose uptake<sup>159</sup> and may contribute to the mechanism of how Panx1-mediated ATP release may impact glucose uptake. ATP released by Panx1 could also activate P2X receptors, resulting in the influx of cations such as calcium. Calcium-mobilizing second messengers have been implicated in insulin-stimulated glucose uptake.<sup>160,161</sup>

In adipocytes, insulin-stimulated glucose uptake requires the presence of Glut4 (glucose transporter type 4) at the plasma membrane. Vesicles containing Glut4 are sequestered in the cytoplasm until insulin stimulates Glut4 vesicle exocytosis which requires several steps including translocation of vesicles to the cell periphery, targeting of vesicles to the plasma membrane, and fusion of vesicles with the plasma membrane.<sup>162</sup> Small GTPases are integral in coordinating these vesicular processes along with guanine nucleotide exchange factors (GEFs) and GTPase

activating proteins (GAPs) which control the cycling of GTPases between the “active” GTP-bound state and “inactive” GDP-bound state.<sup>162</sup> Glut4 vesicles are transported along cytoskeletal tracks by motor proteins. For example, the actin-based myosin motor protein MYO1C interacts with the small GTPase, RALA, to deliver Glut4 vesicles to targeting sites on the plasma membrane.<sup>163,164</sup> Calmodulin may play a role in regulating this process<sup>164</sup> which suggests that control of intracellular calcium may be important for glucose uptake in adipocytes. Glut4 vesicle fusion to the plasma membrane involves SNARE complexes. A protein called CDP138 is an Akt substrate that positively regulates Glut4 insertion into the plasma membrane in adipocytes potentially by binding to lipids in a calcium-dependent manner to induce membrane curvature.<sup>165,166</sup> Panx1 channel function may control calcium that contributes to these processes either by ion flux through activated Panx1 channels or by ATP released from Panx1 that may act back on purinergic receptors.

Adipocyte glucose uptake studies utilizing purinergic receptor antagonists or adipocytes isolated from various knockout mice lacking specific P2Y or P2X receptors would be useful. The pan-purinergic receptor antagonists suramin and PPADS have off-target effects, but have utility as a first step towards determining a role for purinergic receptors. More selective P2 receptor inhibitors and agonists exist for specific P2 receptors. Indeed, P2Y12 antagonists are routinely used in the clinic as antithrombotic drugs. Purinergic signaling in endocrine organs has been a major research focus [reviewed by<sup>36</sup>] and novel therapies based on purinergic receptors as potential drug targets for type II diabetes have been suggested<sup>37-39</sup>. At present, the most promising therapeutic possibility for purinergic receptor modulation is the activation of P2Y receptors in pancreatic beta cells to enhance insulin secretion. There are many promising areas of research about the role of purinergic receptors in other tissues involved in diabetes. However, modulating ATP release could represent an additional or alternative therapeutic

strategy. In terms of Pannexin 1, although our evidence suggests that Panx1 positively regulates glucose uptake, it may have a more detrimental role in some pathological conditions that are known sequelae of diabetes including neuropathic pain and bladder dysfunction.<sup>45,53</sup>

The mechanism of how Panx1 impacts insulin-stimulated glucose uptake may involve adenosine signaling through adenosine receptors, as released ATP is converted into adenosine by ectonucleotidases. Adenosine has long been known to impact glucose homeostasis and lipid metabolism.<sup>167</sup> Specifically in adipocytes, adenosine was observed to increase glucose transport activity of Glut4<sup>168</sup>; however, the exact mechanism is unknown.

We observed a correlation of adipose tissue Panx1 expression and obesity and insulin resistance in humans which may reflect a protective mechanism by which decreased insulin sensitivity is counteracted by an increased ability of the tissue to release bioactive nucleotides. Panx1 expression on cells in adipose tissue other than adipocytes could influence the correlation, so determining Panx1 expression from human isolated adipocytes would be beneficial. Furthermore, it would be interesting to determine whether certain single-nucleotide polymorphisms (SNPs) in Pannexin 1 are associated with obesity and insulin resistance in human patients. To further establish the functional role of Panx1 in controlling full activation of insulin stimulated glucose in adipocytes, our glucose uptake studies need to be repeated in human adipocytes either isolated from patients or at the very least in human-derived cultured adipocytes.

In addition to many open questions as to the therapeutic relevance of Panx1 and purinergic receptors for diabetes and obesity, many opportunities remain for further investigation into the role of Pannexin 1 in adipocytes. We showed that adipocyte Panx1 could be activated by alpha-adrenergic stimulation and caspase-mediated C-terminal cleavage during apoptosis. It would be interesting to investigate whether adipocyte Panx1 is important for

adipocyte function in physiologic situations where those stimuli are present. For example, stimulation of beta-3-adrenergic receptors by norepinephrine induces lipolysis in adipose tissue, but norepinephrine also activates alpha-adrenergic receptors potentially activating Panx1 channels. This scenario begs the question: does Panx1 impact adipocyte lipolysis? Adenosine is known to suppress lipolysis, but whether ATP release by Panx1 is a source of this adenosine is unknown. Preliminary studies measuring glycerol release in response to lipolytic stimuli in isolated WT and Panx1 KO adipocytes did not show a difference (data not shown), but more work needs to be done to confirm this.

We initially hypothesized that caspase-mediated activation of Panx1 in dying adipocytes in obese adipose tissue would be important for cellular crosstalk between adipocytes and infiltrating macrophages, but our data suggests that this is not the case. Nevertheless, Panx1 activation by caspase cleavage may be physiologically important in other situations where adipocytes experience apoptosis. One such situation may be during infection with *Trypanosoma cruzi*, a protozoan parasite that causes Chagas disease and can infect adipocytes and persist in adipose tissue during the chronic phase of infection.<sup>169,170</sup> Following plastic surgery, adipocytes experience hypoxia and cell death while adipose-derived progenitor cells are activated and contribute to adipose tissue repair.<sup>171</sup> Panx1 is likely activated by caspase cleavage in this situation, and extracellular ATP may play a role in preadipocyte migration and adipocyte differentiation.<sup>69</sup> Studies to determine whether adipocyte Panx1 affects adipocyte physiology in these situations could be done utilizing our adipocyte-specific Panx1 KO mice.

Our data demonstrate insulin as a novel activator of Panx1 channels, but the precise mechanism of this activation has yet to be determined. Using the Panx1 (TEV) construct, we were able to determine that insulin activation of Panx1 does not involve cleavage of the C-terminal tail. We can use our heterologous expression system to obtain recordings of CBX-

dependent currents upon insulin stimulation while systematically blocking kinases pharmacologically within the insulin signaling pathway. Phosphorylation site mutants of Panx1 are available and could be used to determine whether phosphorylation of Panx1 occurs when activated by insulin stimulation. It has been suggested that there may be a role for Rho GTPases in activating Panx1 (ongoing work by Dr. Eva Chiu). In addition to PI3K signaling pathways, insulin also induces the recruitment of the adaptor protein APS which leads to the activation of TC10, a Rho-family GTPase.<sup>162</sup> Perhaps TC10 may be involved in the mechanism of Panx1 activation by insulin stimulation.

Another important question is whether Panx1 control of full activation of insulin stimulated glucose uptake occurs in other insulin-sensitive tissues such as liver, muscle, or brown adipose tissue. Given the fact that glucose tolerance in lean or obese global Panx1 KO mice is equivalent to WT mice (data not shown), it seems unlikely that there is any appreciable effect of Panx1 on glucose uptake in skeletal muscle, since muscle accounts for the majority of glucose uptake. Our laboratory has generated liver-specific Panx1 KO mice, and studies are underway. Preliminary data shows that lean, male liver Panx1 KO mice have fasting glucose levels and whole body glucose clearance equivalent to WT mice (data not shown).

[<sup>3</sup>H]-2-deoxy-D-Glucose uptake in brown adipose tissue (BAT) was similar between WT and adipocyte-specific Panx1 KO mice (data not shown), suggesting differential roles for Panx1 in white versus brown adipose tissue. However, since brown adipose tissue plays a major role in thermogenesis, it would be interesting to see whether adipocyte-specific Panx1 KO mice respond differently to activation of the thermogenic program by cold exposure. WT and adipocyte-specific Panx1 KO mice were exposed to 4°C for 4 hrs in preliminary studies, and analysis of gene expression in BAT showed a significant increase in PGC1 $\alpha$  and UCP1 upon cold exposure but no difference between WT and adipocyte-specific Panx1 KO mice. Future studies

may require longer exposures, housing mice at thermoneutrality, or acclimating mice to colder housing temperatures for additional study. A very exciting emerging field is the “browning” of adipose tissue during which expression programs are activated that cause white adipocytes to take on characteristics of brown adipocytes, namely thermogenic capacity. Recently, it was shown that adenosine activates BAT and recruits beige adipocytes.<sup>172</sup> And extracellular ATP has also been shown to impact brown adipocytes.<sup>27,30</sup> Panx1 in brown adipocytes might affect their physiology in important ways.

Lastly, we observed that Panx1 null adipose had decreased expression of certain lipid metabolism genes including free fatty acid transporters and acyl-coA synthetases. To further understand whether these changes represent important physiologic differences, additional experiments are warranted. Using the Biosorter, we saw no difference in size distribution of adipocytes isolated from WT and adipocyte-specific Panx1 KO mice, suggesting that there is not a significant difference in lipid droplet size. Nevertheless, there may be slight differences in free fatty acid uptake or fatty acid beta-oxidation or lipogenesis which can be experimentally investigated. A more extensive analysis of gene expression of lipid metabolism genes using RNAseq may be helpful in understanding which pathways, if any, require Panx1.

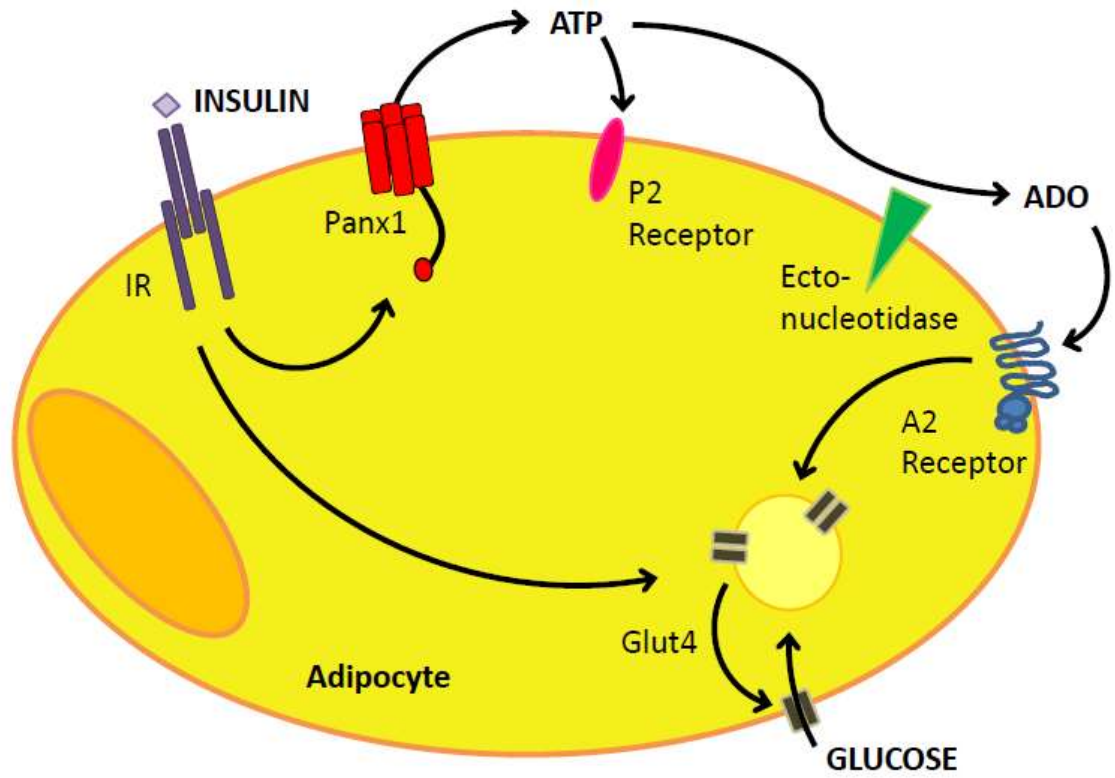


Figure 6-1 Adipocyte Panx1 is required for full activation of insulin-stimulated glucose uptake

**Figure 6-1. Adipocyte Panx1 is required for full activation of insulin-stimulated glucose uptake**

Schematic represents Panx1 activation in adipocytes upon insulin stimulation, resulting in ATP release which allows for full activation of glucose uptake. ATP may act via purinergic P2 receptors or can be further broken down by ectonucleotidases into adenosine (ADO) that acts on adenosine A2 receptors to enhance insulin-stimulated glucose uptake.

## REFERENCES

1. Centers for Disease Control and Prevention. Facts about county-level estimates of diagnosed diabetes and obesity, 2007. <http://www.cdc.gov/diabetes/pubs/factsheets/countyvllestimates.htm>. Updated 2011.
2. American Diabetes Association. Economic costs of diabetes in the U.S. in 2012. <http://www.diabetes.org/advocate/resources/cost-of-diabetes.html>. Updated 2013.
3. Centers for Disease Control and Prevention. Defining adult overweight and obesity. <http://www.cdc.gov/obesity/adult/defining.html>. Updated April 27, 2012/2015.
4. Flegal KM, Kit BK, Orpana H, Graubard BI. Association of all-cause mortality with overweight and obesity using standard body mass index categories: A systematic review and meta-analysis. *JAMA*. 2013;309(1):71-82. doi: 10.1001/jama.2012.113905 [doi].
5. Flegal KM, Graubard BI, Williamson DF, Gail MH. Excess deaths associated with underweight, overweight, and obesity. *JAMA*. 2005;293(15):1861-1867. doi: 293/15/1861 [pii].
6. Prospective Studies Collaboration, Whitlock G, Lewington S, et al. Body-mass index and cause-specific mortality in 900 000 adults: Collaborative analyses of 57 prospective studies. *Lancet*. 2009;373(9669):1083-1096. doi: 10.1016/S0140-6736(09)60318-4 [doi].
7. Shah RV, Murthy VL, Abbasi SA, et al. Visceral adiposity and the risk of metabolic syndrome across body mass index: The MESA study. *JACC Cardiovasc Imaging*. 2014;7(12):1221-1235. doi: 10.1016/j.jcmg.2014.07.017 [doi].
8. Neeland IJ, Turer AT, Ayers CR, et al. Dysfunctional adiposity and the risk of prediabetes and type 2 diabetes in obese adults. *JAMA*. 2012;308(11):1150-1159. doi: 1360863 [pii].
9. Janssen I, Katzmarzyk PT, Ross R. Body mass index, waist circumference, and health risk: Evidence in support of current national institutes of health guidelines. *Arch Intern Med*. 2002;162(18):2074-2079. doi: 10.1001/archinternmed.2002.10789 [pii].
10. Emerging Risk Factors Collaboration, Wormser D, Kaptoge S, et al. Separate and combined associations of body-mass index and abdominal adiposity with cardiovascular disease: Collaborative analysis of 58 prospective studies. *Lancet*. 2011;377(9771):1085-1095. doi: 10.1016/S0140-6736(11)60105-0 [doi].
11. Han JM, Levings MK. Immune regulation in obesity-associated adipose inflammation. *J Immunol*. 2013;191(2):527-532. doi: 10.1093/jimmunol.1301035 [doi].
12. Giralt M, Villarroya F. White, brown, beige/brite: Different adipose cells for different functions? *Endocrinology*. 2013;154(9):2992-3000. doi: 10.1210/en.2013-1403 [doi].
13. Samuel VT, Shulman GI. Mechanisms for insulin resistance: Common threads and missing links. *Cell*. 2012;148(5):852-871. doi: 10.1016/j.cell.2012.02.017 [doi].

14. Fasshauer M, Bluher M. Adipokines in health and disease. *Trends Pharmacol Sci*. 2015;36(7):461-470. doi: 10.1016/j.tips.2015.04.014 [doi].
15. Shepherd PR, Kahn BB. Glucose transporters and insulin action--implications for insulin resistance and diabetes mellitus. *N Engl J Med*. 1999;341(4):248-257. doi: 10.1056/NEJM199907223410406 [doi].
16. National Heart, Lung, and Blood Institute. "What is metabolic syndrome?". <http://www.nhlbi.nih.gov/health/health-topics/topics/ms>. Updated November 3, 2011.
17. Scherer PE. Nature medicine metabolic syndrome ePoster adipose tissue sponsored by Takeda global research & development center, inc. [http://www.nature.com/nm/e-poster/eposter\\_full.html](http://www.nature.com/nm/e-poster/eposter_full.html). Updated October 5, 2012.
18. Turpin BP, Duckworth WC, Solomon SS. Perfusion of isolated rat adipose cells. modulation of lipolysis by adenosine. *J Clin Invest*. 1977;60(2):442-448. doi: 10.1172/JCI108794 [doi].
19. Kather H. Purine accumulation in human fat cell suspensions. evidence that human adipocytes release inosine and hypoxanthine rather than adenosine. *J Biol Chem*. 1988;263(18):8803-8809.
20. Schwabe U, Ebert R, Erbiler HC. Adenosine release from isolated fat cells and its significance for the effects of hormones on cyclic 3',5'-AMP levels and lipolysis. *Naunyn Schmiedebergs Arch Pharmacol*. 1973;276(2):133-148.
21. Dhalla AK, Chisholm JW, Reaven GM, Belardinelli L. A1 adenosine receptor: Role in diabetes and obesity. *Handb Exp Pharmacol*. 2009;(193):271-95. doi(193):271-295. doi: 10.1007/978-3-540-89615-9\_9 [doi].
22. Martin SE, Bockman EL. Adenosine regulates blood flow and glucose uptake in adipose tissue of dogs. *Am J Physiol*. 1986;250(6 Pt 2):H1127-35.
23. Green A. Catecholamines inhibit insulin-stimulated glucose transport in adipocytes, in the presence of adenosine deaminase. *FEBS Lett*. 1983;152(2):261-264. doi: 0014-5793(83)80392-5 [pii].
24. Schwabe U, Schonhofer PS, Ebert R. Facilitation by adenosine of the action of insulin on the accumulation of adenosine 3':5'-monophosphate, lipolysis, and glucose oxidation in isolated fat cells. *Eur J Biochem*. 1974;46(3):537-545.
25. Martin SE, Lenhard SD, Schmarkey LS, Offenbacher S, Odle BM. Adenosine regulates coronary blood flow during increased work and decreased supply. *Am J Physiol*. 1993;264(5 Pt 2):H1438-46.
26. Junger WG. Immune cell regulation by autocrine purinergic signalling. *Nat Rev Immunol*. 2011;11(3):201-212. doi: 10.1038/nri2938 [doi].

27. Lee SC, Pappone PA. Effects of P2 purinergic receptor stimulation in brown adipocytes. *Am J Physiol.* 1997;273(2 Pt 1):C679-86.
28. Chowdhury HH, Grilc S, Zorec R. Correlated ATP-induced changes in membrane area and membrane conductance in single rat adipocytes. *Ann N Y Acad Sci.* 2005;1048:281-286. doi: 1048/1/281 [pii].
29. Lee SC, Pappone PA. Membrane responses to extracellular ATP in rat isolated white adipocytes. *Pflugers Arch.* 1997;434(4):422-428.
30. Lee SC, Pappone PA. ATP can stimulate exocytosis in rat brown adipocytes without apparent increases in cytosolic Ca<sup>2+</sup> or G protein activation. *Biophys J.* 1999;76(4):2297-2306. doi: S0006-3495(99)77385-6 [pii].
31. Chang KJ, Cuatrecasas P. Adenosine triphosphate-dependent inhibition of insulin-stimulated glucose transport in fat cells. possible role of membrane phosphorylation. *J Biol Chem.* 1974;249(10):3170-3180.
32. Tamura S, Dubler RE, Larner J. Stimulation of maximal intracellular insulin action on glycogen synthase by preincubation of adipocytes with adenosine 5'-triphosphate. *J Biol Chem.* 1983;258(2):719-724.
33. Schodel J, Weise I, Klinger R, Schmidt M. Stimulation of lipogenesis in rat adipocytes by ATP, a ligand for P2-receptors. *Biochem Biophys Res Commun.* 2004;321(4):767-773. doi: 10.1016/j.bbrc.2004.06.179 [doi].
34. Hashimoto N, Robinson FW, Shibata Y, Flanagan JE, Kono T. Diversity in the effects of extracellular ATP and adenosine on the cellular processing and physiologic actions of insulin in rat adipocytes. *J Biol Chem.* 1987;262(31):15026-15032.
35. Yu Z, Jin T. Extracellular high dosages of adenosine triphosphate induce inflammatory response and insulin resistance in rat adipocytes. *Biochem Biophys Res Commun.* 2010;402(3):455-460. doi: 10.1016/j.bbrc.2010.10.028 [doi].
36. Burnstock G. Purinergic signalling in endocrine organs. *Purinergic Signal.* 2014;10(1):189-231. doi: 10.1007/s11302-013-9396-x [doi].
37. Yelovitch S, Barr HM, Camden J, et al. Identification of a promising drug candidate for the treatment of type 2 diabetes based on a P2Y(1) receptor agonist. *J Med Chem.* 2012;55(17):7623-7635. doi: 10.1021/jm3006355 [doi].
38. Pacheco PA, Ferreira LG, Alves LA, Faria RX. Modulation of P2 receptors on pancreatic beta-cells by agonists and antagonists: A molecular target for type 2 diabetes treatment. *Curr Diabetes Rev.* 2013;9(3):228-236. doi: CDR-EPUB-20130314-4 [pii].

39. Piwkowska A, Rogacka D, Jankowski M, Angielski S. Metformin reduces NAD(P)H oxidase activity in mouse cultured podocytes through purinergic dependent mechanism by increasing extracellular ATP concentration. *Acta Biochim Pol.* 2013;60(4):607-612. doi: 2013\_607-612 [pii].
40. Sosinsky GE, Boassa D, Dermietzel R, et al. Pannexin channels are not gap junction hemichannels. *Channels (Austin).* 2011;5(3):193-197. doi: 15765 [pii].
41. Penuela S, Gehi R, Laird DW. The biochemistry and function of pannexin channels. *Biochim Biophys Acta.* 2013;1828(1):15-22. doi: 10.1016/j.bbamem.2012.01.017 [doi].
42. D'hondt C, Ponsaerts R, De Smedt H, et al. Pannexin channels in ATP release and beyond: An unexpected rendezvous at the endoplasmic reticulum. *Cell Signal.* 2011;23(2):305-316. doi: 10.1016/j.cellsig.2010.07.018 [doi].
43. Penuela S, Lohman AW, Lai W, et al. Diverse post-translational modifications of the pannexin family of channel-forming proteins. *Channels (Austin).* 2014;8(2):124-130. doi: 10.4161/chan.27422 [doi].
44. Lohman AW, Weaver JL, Billaud M, et al. S-nitrosylation inhibits pannexin 1 channel function. *J Biol Chem.* 2012;287(47):39602-39612. doi: 10.1074/jbc.M112.397976 [doi].
45. Negoro H, Lutz SE, Liou LS, et al. Pannexin 1 involvement in bladder dysfunction in a multiple sclerosis model. *Sci Rep.* 2013;3:2152. doi: 10.1038/srep02152 [doi].
46. Dahl G, Qiu F, Wang J. The bizarre pharmacology of the ATP release channel pannexin1. *Neuropharmacology.* 2013;75:583-593. doi: 10.1016/j.neuropharm.2013.02.019 [doi].
47. Wang J, Jackson DG, Dahl G. The food dye FD&C blue no. 1 is a selective inhibitor of the ATP release channel Panx1. *J Gen Physiol.* 2013;141(5):649-656. doi: 10.1085/jgp.201310966 [doi].
48. Poon IKH, Lucas CD, Rossi AG, Ravichandran KS. Apoptotic cell clearance: Basic biology and therapeutic potential. *Nature Reviews Immunology.* 2014;14(3):166-180. <http://dx.doi.org/10.1038/nri3607>. doi: 10.1038/nri3607.
49. Kienitz MC, Bender K, Dermietzel R, Pott L, Zoidl G. Pannexin 1 constitutes the large conductance cation channel of cardiac myocytes. *J Biol Chem.* 2011;286(1):290-298. doi: 10.1074/jbc.M110.163477 [doi].
50. Billaud M, Lohman AW, Straub AC, et al. Pannexin1 regulates alpha1-adrenergic receptor-mediated vasoconstriction. *Circ Res.* 2011;109(1):80-85. doi: 10.1161/CIRCRESAHA.110.237594 [doi].
51. Pinheiro AR, Paramos-de-Carvalho D, Certal M, et al. Histamine induces ATP release from human subcutaneous fibroblasts, via pannexin-1 hemichannels, leading to Ca<sup>2+</sup> mobilization and cell proliferation. *J Biol Chem.* 2013;288(38):27571-27583. doi: 10.1074/jbc.M113.460865 [doi].

52. Sandilos JK, Chiu YH, Chekeni FB, et al. Pannexin 1, an ATP release channel, is activated by caspase cleavage of its pore-associated C-terminal autoinhibitory region. *J Biol Chem*. 2012;287(14):11303-11311. doi: 10.1074/jbc.M111.323378 [doi].
53. Timoteo MA, Carneiro I, Silva I, et al. ATP released via pannexin-1 hemichannels mediates bladder overactivity triggered by urothelial P2Y6 receptors. *Biochem Pharmacol*. 2014;87(2):371-379. doi: 10.1016/j.bcp.2013.11.007 [doi].
54. Mullins GR, Wang L, Raje V, et al. Catecholamine-induced lipolysis causes mTOR complex dissociation and inhibits glucose uptake in adipocytes. *Proc Natl Acad Sci U S A*. 2014;111(49):17450-17455. doi: 10.1073/pnas.1410530111 [doi].
55. Lansley MN, Walker NN, Hargett SR, Stevens JR, Keller SR. Deletion of rab GAP AS160 modifies glucose uptake and GLUT4 translocation in primary skeletal muscles and adipocytes and impairs glucose homeostasis. *Am J Physiol Endocrinol Metab*. 2012;303(10):E1273-86. doi: 10.1152/ajpendo.00316.2012 [doi].
56. Lohman AW, Billaud M, Straub AC, et al. Expression of pannexin isoforms in the systemic murine arterial network. *J Vasc Res*. 2012;49(5):405-416. doi: 10.1159/000338758 [doi].
57. Ramos RR, Swanson AJ, Bass J. Calreticulin and Hsp90 stabilize the human insulin receptor and promote its mobility in the endoplasmic reticulum. *Proc Natl Acad Sci U S A*. 2007;104(25):10470-10475. doi: 0701114104 [pii].
58. Pfaffl MW. Relative quantification. In: Dorak T, ed. *Real-time PCR*. ; 2004:63-63-82.
59. Wang ZV, Deng Y, Wang QA, Sun K, Scherer PE. Identification and characterization of a promoter cassette conferring adipocyte-specific gene expression. *Endocrinology*. 2010;151(6):2933-2939. doi: 10.1210/en.2010-0136 [doi].
60. Ayala JE, Samuel VT, Morton GJ, et al. Standard operating procedures for describing and performing metabolic tests of glucose homeostasis in mice. *Dis Model Mech*. 2010;3(9-10):525-534. doi: 10.1242/dmm.006239 [doi].
61. Chow JD, Lawrence RT, Healy ME, et al. Genetic inhibition of hepatic acetyl-CoA carboxylase activity increases liver fat and alters global protein acetylation. *Mol Metab*. 2014;3(4):419-431. doi: 10.1016/j.molmet.2014.02.004 [doi].
62. Sridharan M, Adderley SP, Bowles EA, et al. Pannexin 1 is the conduit for low oxygen tension-induced ATP release from human erythrocytes. *Am J Physiol Heart Circ Physiol*. 2010;299(4):H1146-52. doi: 10.1152/ajpheart.00301.2010 [doi].
63. Chekeni FB, Elliott MR, Sandilos JK, et al. Pannexin 1 channels mediate 'find-me' signal release and membrane permeability during apoptosis. *Nature*. 2010;467(7317):863-867. doi: 10.1038/nature09413 [doi].

64. Silverman W, Locovei S, Dahl G. Probenecid, a gout remedy, inhibits pannexin 1 channels. *Am J Physiol Cell Physiol*. 2008;295(3):C761-7. doi: 10.1152/ajpcell.00227.2008 [doi].
65. Poon IK, Chiu YH, Armstrong AJ, et al. Unexpected link between an antibiotic, pannexin channels and apoptosis. *Nature*. 2014;507(7492):329-334. doi: 10.1038/nature13147 [doi].
66. Dufresne J, Cyr DG. Regulation of the pannexin-1 promoter in the rat epididymis. *Biol Reprod*. 2014;91(6):143. doi: 10.1095/biolreprod.114.122168 [doi].
67. Qu Y, Misaghi S, Newton K, et al. Pannexin-1 is required for ATP release during apoptosis but not for inflammasome activation. *J Immunol*. 2011;186(11):6553-6561. doi: 10.4049/jimmunol.1100478 [doi].
68. Billaud M, Chiu YH, Lohman AW, et al. A molecular signature in the pannexin1 intracellular loop confers channel activation by the alpha1 adrenoreceptor in smooth muscle cells. *Sci Signal*. 2015;8(364):ra17. doi: 10.1126/scisignal.2005824 [doi].
69. Omatsu-Kanbe M, Inoue K, Fujii Y, et al. Effect of ATP on preadipocyte migration and adipocyte differentiation by activating P2Y receptors in 3T3-L1 cells. *Biochem J*. 2006;393(Pt 1):171-180. doi: BJ20051037 [pii].
70. Wharton J, Meshulam T, Vallega G, Pilch P. Dissociation of insulin receptor expression and signaling from caveolin-1 expression. *J Biol Chem*. 2005;280(14):13483-13486. <http://dx.doi.org/10.1074/jbc.m413891200>. doi: 10.1074/jbc.m413891200.
71. Amoroso F, Falzoni S, Adinolfi E, Ferrari D, Di Virgilio F. The P2X7 receptor is a key modulator of aerobic glycolysis. *Cell Death Dis*. 2012;3(8):e370. <http://dx.doi.org/10.1038/cddis.2012.105>. doi: 10.1038/cddis.2012.105.
72. Zaslavsky A, Li S, Xu Y. Sphingosine-1-phosphate induces a PDGFR-dependent cell detachment via inhibiting  $\beta$ 1 integrin in HEK293 cells. *FEBS Lett*. 2005;579(18):3899-3906. <http://dx.doi.org/10.1016/j.febslet.2005.06.006>. doi: 10.1016/j.febslet.2005.06.006.
73. Ekim B, Magnuson B, Acosta-Jaquez H, Keller JA, Feener EP, Fingar DC. mTOR kinase domain phosphorylation promotes mTORC1 signaling, cell growth, and cell cycle progression. *Mol Cell Biol*. 2011;31(14):2787-2801. <http://dx.doi.org/10.1128/mcb.05437-11>. doi: 10.1128/mcb.05437-11.
74. Ye J. Emerging role of adipose tissue hypoxia in obesity and insulin resistance. *Int J Obes (Lond)*. 2009;33(1):54-66. doi: 10.1038/ijo.2008.229 [doi].
75. Sun S, Xia S, Ji Y, Kersten S, Qi L. The ATP-P2X7 signaling axis is dispensable for obesity-associated inflammasome activation in adipose tissue. *Diabetes*. 2012;61(6):1471-1478. <http://dx.doi.org/10.2337/db11-1389>. doi: 10.2337/db11-1389.
76. Ferrante AW, Jr. The immune cells in adipose tissue. *Diabetes Obes Metab*. 2013;15 Suppl 3:34-38. doi: 10.1111/dom.12154 [doi].

77. Strissel KJ, Stancheva Z, Miyoshi H, et al. Adipocyte death, adipose tissue remodeling, and obesity complications. *Diabetes*. 2007;56(12):2910-2918. <http://dx.doi.org/10.2337/db07-0767>. doi: 10.2337/db07-0767.
78. Kanda H. MCP-1 contributes to macrophage infiltration into adipose tissue, insulin resistance, and hepatic steatosis in obesity. *J Clin Invest*. 2006;116(6):1494-1505. <http://dx.doi.org/10.1172/jci26498>. doi: 10.1172/jci26498.
79. Weisberg SP, Hunter D, Huber R, et al. CCR2 modulates inflammatory and metabolic effects of high-fat feeding. *J Clin Invest*. 2006;116(1):115-124. <http://dx.doi.org/10.1172/jci24335>. doi: 10.1172/jci24335.
80. Shaul ME, Bennett G, Strissel KJ, Greenberg AS, Obin MS. Dynamic, M2-like remodeling phenotypes of CD11c+ adipose tissue macrophages during high-fat diet-induced obesity in mice. *Diabetes*. 2010;59(5):1171-1181. <http://dx.doi.org/10.2337/db09-1402>. doi: 10.2337/db09-1402.
81. Tanaka M, Ikeda K, Suganami T, et al. Macrophage-inducible C-type lectin underlies obesity-induced adipose tissue fibrosis. *Nat Comms*. 2014;5:4982. <http://dx.doi.org/10.1038/ncomms5982>. doi: 10.1038/ncomms5982.
82. Teitelbaum SL. Bone resorption by osteoclasts. *Science*. 2000;289(5484):1504-1508. doi: 8789 [pii].
83. Koeck ES, Iordanskaia T, Sevilla S, et al. Adipocyte exosomes induce transforming growth factor beta pathway dysregulation in hepatocytes: A novel paradigm for obesity-related liver disease. *J Surg Res*. 2014;192(2):268-275. doi: 10.1016/j.jss.2014.06.050 [doi].
84. Ferrante SC, Nadler EP, Pillai DK, et al. Adipocyte-derived exosomal miRNAs: A novel mechanism for obesity-related disease. *Pediatr Res*. 2015;77(3):447-454. doi: 10.1038/pr.2014.202 [doi].
85. Muller G, Schneider M, Biemer-Daub G, Wied S. Microvesicles released from rat adipocytes and harboring glycosylphosphatidylinositol-anchored proteins transfer RNA stimulating lipid synthesis. *Cell Signal*. 2011;23(7):1207-1223. doi: 10.1016/j.cellsig.2011.03.013 [doi].
86. Gombault A, Baron L, Couillin I. ATP release and purinergic signaling in NLRP3 inflammasome activation. *Frontiers in Immunology*. 2013;3. <http://dx.doi.org/10.3389/fimmu.2012.00414>. doi: 10.3389/fimmu.2012.00414.
87. Corriden R, Insel PA. New insights regarding the regulation of chemotaxis by nucleotides, adenosine, and their receptors. *Purinergic Signalling*. 2012;8(3):587-598. <http://dx.doi.org/10.1007/s11302-012-9311-x>. doi: 10.1007/s11302-012-9311-x.
88. Hill LM, Gavala ML, Lenertz LY, Bertics PJ. Extracellular ATP may contribute to tissue repair by rapidly stimulating purinergic receptor X7-dependent vascular endothelial growth factor

- release from primary human monocytes. *The Journal of Immunology*. 2010;185(5):3028-3034. <http://dx.doi.org/10.4049/jimmunol.1001298>. doi: 10.4049/jimmunol.1001298.
89. Isfort K, Ebert F, Bornhorst J, et al. Real-time imaging reveals that P2Y2 and P2Y12 receptor agonists are not chemoattractants and macrophage chemotaxis to complement C5a is phosphatidylinositol 3-kinase (PI3K)- and p38 mitogen-activated protein kinase (MAPK)-independent. *J Biol Chem*. 2011;286(52):44776-44787. <http://dx.doi.org/10.1074/jbc.m111.289793>. doi: 10.1074/jbc.m111.289793.
90. Eun SY, Seo J, Park SW, Lee JH, Chang KC, Kim HJ. LPS potentiates nucleotide-induced inflammatory gene expression in macrophages via the upregulation of P2Y2 receptor. *Int Immunopharmacol*. 2014;18(2):270-276. <http://dx.doi.org/10.1016/j.intimp.2013.11.026>. doi: 10.1016/j.intimp.2013.11.026.
91. Inoue Y, Chen Y, Hirsh MI, Yip L, Junger WG. A3 AND P2Y2 RECEPTORS CONTROL THE RECRUITMENT OF NEUTROPHILS TO THE LUNGS IN A MOUSE MODEL OF SEPSIS. *Shock*. 2007;1. <http://dx.doi.org/10.1097/shk.0b013e318160dad4>. doi: 10.1097/shk.0b013e318160dad4.
92. Walton RG, Zhu B, Unal R, et al. Increasing adipocyte lipoprotein lipase improves glucose metabolism in high fat diet-induced obesity. *J Biol Chem*. 2015;290(18):11547-11556. doi: 10.1074/jbc.M114.628487 [doi].
93. Marangoni RG, Korman BD, Wei J, et al. Myofibroblasts in murine cutaneous fibrosis originate from adiponectin-positive intradermal progenitors. *Arthritis Rheumatol*. 2015;67(4):1062-1073. doi: 10.1002/art.38990 [doi].
94. Chung JJ, Markiewicz MA, Polic B, Shaw AS. Role of NKG2D in obesity-induced adipose tissue inflammation and insulin resistance. *PLoS One*. 2014;9(10):e110108. doi: 10.1371/journal.pone.0110108 [doi].
95. Wernstedt Asterholm I, Tao C, Morley TS, et al. Adipocyte inflammation is essential for healthy adipose tissue expansion and remodeling. *Cell Metab*. 2014;20(1):103-118. doi: 10.1016/j.cmet.2014.05.005 [doi].
96. Sun K, Halberg N, Khan M, Magalang UJ, Scherer PE. Selective inhibition of hypoxia-inducible factor 1alpha ameliorates adipose tissue dysfunction. *Mol Cell Biol*. 2013;33(5):904-917. doi: 10.1128/MCB.00951-12 [doi].
97. Sun K, Park J, Gupta OT, et al. Endotrophin triggers adipose tissue fibrosis and metabolic dysfunction. *Nat Commun*. 2014;5:3485. doi: 10.1038/ncomms4485 [doi].
98. Sun K, Wernstedt Asterholm I, Kusminski CM, et al. Dichotomous effects of VEGF-A on adipose tissue dysfunction. *Proc Natl Acad Sci U S A*. 2012;109(15):5874-5879. doi: 10.1073/pnas.1200447109 [doi].

99. Liu M, Bai J, He S, et al. Grb10 promotes lipolysis and thermogenesis by phosphorylation-dependent feedback inhibition of mTORC1. *Cell Metab.* 2014;19(6):967-980. doi: 10.1016/j.cmet.2014.03.018 [doi].
100. Zhu H, Guariglia S, Li W, et al. Role of extracellular signal-regulated kinase 5 in adipocyte signaling. *J Biol Chem.* 2014;289(9):6311-6322. doi: 10.1074/jbc.M113.506584 [doi].
101. Davis KE, D Neinast M, Sun K, et al. The sexually dimorphic role of adipose and adipocyte estrogen receptors in modulating adipose tissue expansion, inflammation, and fibrosis. *Mol Metab.* 2013;2(3):227-242. doi: 10.1016/j.molmet.2013.05.006 [doi].
102. Mitra MS, Chen Z, Ren H, et al. Mice with an adipocyte-specific lipin 1 separation-of-function allele reveal unexpected roles for phosphatidic acid in metabolic regulation. *Proc Natl Acad Sci U S A.* 2013;110(2):642-647. doi: 10.1073/pnas.1213493110 [doi].
103. Eguchi J, Wang X, Yu S, et al. Transcriptional control of adipose lipid handling by IRF4. *Cell Metab.* 2011;13(3):249-259. doi: 10.1016/j.cmet.2011.02.005 [doi].
104. Banks AS, McAllister FE, Camporez JP, et al. An ERK/Cdk5 axis controls the diabetogenic actions of PPARgamma. *Nature.* 2015;517(7534):391-395. doi: 10.1038/nature13887 [doi].
105. Bi P, Shan T, Liu W, et al. Inhibition of notch signaling promotes browning of white adipose tissue and ameliorates obesity. *Nat Med.* 2014;20(8):911-918. doi: 10.1038/nm.3615 [doi].
106. Cohen P, Levy JD, Zhang Y, et al. Ablation of PRDM16 and beige adipose causes metabolic dysfunction and a subcutaneous to visceral fat switch. *Cell.* 2014;156(1-2):304-316. doi: 10.1016/j.cell.2013.12.021 [doi].
107. Dube JJ, Sitnick MT, Schoiswohl G, et al. Adipose triglyceride lipase deletion from adipocytes, but not skeletal myocytes, impairs acute exercise performance in mice. *Am J Physiol Endocrinol Metab.* 2015;308(10):E879-90. doi: 10.1152/ajpendo.00530.2014 [doi].
108. Gao Z, Zhang J, Henagan TM, et al. P65 inactivation in adipocytes and macrophages attenuates adipose inflammatory response in lean but not in obese mice. *Am J Physiol Endocrinol Metab.* 2015;308(6):E496-505. doi: 10.1152/ajpendo.00532.2014 [doi].
109. Gregor MF, Misch ES, Yang L, et al. The role of adipocyte XBP1 in metabolic regulation during lactation. *Cell Rep.* 2013;3(5):1430-1439. doi: 10.1016/j.celrep.2013.03.042 [doi].
110. He Z, Zhu HH, Bauler TJ, et al. Nonreceptor tyrosine phosphatase Shp2 promotes adipogenesis through inhibition of p38 MAP kinase. *Proc Natl Acad Sci U S A.* 2013;110(1):E79-88. doi: 10.1073/pnas.1213000110 [doi].
111. Herman MA, Peroni OD, Villoria J, et al. A novel ChREBP isoform in adipose tissue regulates systemic glucose metabolism. *Nature.* 2012;484(7394):333-338. doi: 10.1038/nature10986 [doi].

112. Kim HJ, Cho H, Alexander R, et al. MicroRNAs are required for the feature maintenance and differentiation of brown adipocytes. *Diabetes*. 2014;63(12):4045-4056. doi: 10.2337/db14-0466 [doi].
113. Kleiner S, Mepani RJ, Laznik D, et al. Development of insulin resistance in mice lacking PGC-1alpha in adipose tissues. *Proc Natl Acad Sci U S A*. 2012;109(24):9635-9640. doi: 10.1073/pnas.1207287109 [doi].
114. Kwon H, Laurent S, Tang Y, Zong H, Vemulapalli P, Pessin JE. Adipocyte-specific IKKbeta signaling suppresses adipose tissue inflammation through an IL-13-dependent paracrine feedback pathway. *Cell Rep*. 2014;9(5):1574-1583. doi: 10.1016/j.celrep.2014.10.068 [doi].
115. Lee J, Ellis JM, Wolfgang MJ. Adipose fatty acid oxidation is required for thermogenesis and potentiates oxidative stress-induced inflammation. *Cell Rep*. 2015;10(2):266-279. doi: 10.1016/j.celrep.2014.12.023 [doi].
116. Lee SH, Huang H, Choi K, et al. ROCK1 isoform-specific deletion reveals a role for diet-induced insulin resistance. *Am J Physiol Endocrinol Metab*. 2014;306(3):E332-43. doi: 10.1152/ajpendo.00619.2013 [doi].
117. Lodhi IJ, Yin L, Jensen-Urstad AP, et al. Inhibiting adipose tissue lipogenesis reprograms thermogenesis and PPARgamma activation to decrease diet-induced obesity. *Cell Metab*. 2012;16(2):189-201. doi: S1550-4131(12)00278-1 [pii].
118. Lu YH, Dallner OS, Birsoy K, Fayzikhodjaeva G, Friedman JM. Nuclear factor-Y is an adipogenic factor that regulates leptin gene expression. *Mol Metab*. 2015;4(5):392-405. doi: 10.1016/j.molmet.2015.02.002 [doi].
119. Markan KR, Naber MC, Ameka MK, et al. Circulating FGF21 is liver derived and enhances glucose uptake during refeeding and overfeeding. *Diabetes*. 2014;63(12):4057-4063. doi: 10.2337/db14-0595 [doi].
120. McInnes KJ, Smith LB, Hunger NI, Saunders PT, Andrew R, Walker BR. Deletion of the androgen receptor in adipose tissue in male mice elevates retinol binding protein 4 and reveals independent effects on visceral fat mass and on glucose homeostasis. *Diabetes*. 2012;61(5):1072-1081. doi: 10.2337/db11-1136 [doi].
121. Nordstrom SM, Tran JL, Sos BC, Wagner KU, Weiss EJ. Disruption of JAK2 in adipocytes impairs lipolysis and improves fatty liver in mice with elevated GH. *Mol Endocrinol*. 2013;27(8):1333-1342. doi: 10.1210/me.2013-1110 [doi].
122. Odle AK, Haney A, Allensworth-James M, Akhter N, Childs GV. Adipocyte versus pituitary leptin in the regulation of pituitary hormones: Somatotropes develop normally in the absence of circulating leptin. *Endocrinology*. 2014;155(11):4316-4328. doi: 10.1210/en.2014-1172 [doi].
123. Oh CM, Namkung J, Go Y, et al. Regulation of systemic energy homeostasis by serotonin in adipose tissues. *Nat Commun*. 2015;6:6794. doi: 10.1038/ncomms7794 [doi].

124. O'Hara L, McInnes K, Simitsidellis I, et al. Autocrine androgen action is essential for leydig cell maturation and function, and protects against late-onset leydig cell apoptosis in both mice and men. *FASEB J.* 2015;29(3):894-910. doi: 10.1096/fj.14-255729 [doi].
125. Ohno H, Shinoda K, Ohyama K, Sharp LZ, Kajimura S. EHMT1 controls brown adipose cell fate and thermogenesis through the PRDM16 complex. *Nature.* 2013;504(7478):163-167. doi: 10.1038/nature12652 [doi].
126. Owen C, Czopek A, Agouni A, et al. Adipocyte-specific protein tyrosine phosphatase 1B deletion increases lipogenesis, adipocyte cell size and is a minor regulator of glucose homeostasis. *PLoS One.* 2012;7(2):e32700. doi: 10.1371/journal.pone.0032700 [doi].
127. Paschos GK, Ibrahim S, Song WL, et al. Obesity in mice with adipocyte-specific deletion of clock component arntl. *Nat Med.* 2012;18(12):1768-1777. doi: 10.1038/nm.2979 [doi].
128. Ryu MJ, Kim SJ, Kim YK, et al. Crif1 deficiency reduces adipose OXPHOS capacity and triggers inflammation and insulin resistance in mice. *PLoS Genet.* 2013;9(3):e1003356. doi: 10.1371/journal.pgen.1003356 [doi].
129. Sha H, Sun S, Francisco AB, et al. The ER-associated degradation adaptor protein Sel1L regulates LPL secretion and lipid metabolism. *Cell Metab.* 2014;20(3):458-470. doi: 10.1016/j.cmet.2014.06.015 [doi].
130. Sumara G, Sumara O, Kim JK, Karsenty G. Gut-derived serotonin is a multifunctional determinant to fasting adaptation. *Cell Metab.* 2012;16(5):588-600. doi: 10.1016/j.cmet.2012.09.014 [doi].
131. Villanueva CJ, Vergnes L, Wang J, et al. Adipose subtype-selective recruitment of TLE3 or Prdm16 by PPARgamma specifies lipid storage versus thermogenic gene programs. *Cell Metab.* 2013;17(3):423-435. doi: 10.1016/j.cmet.2013.01.016 [doi].
132. Wang F, Mullican SE, DiSpirito JR, Peed LC, Lazar MA. Lipoatrophy and severe metabolic disturbance in mice with fat-specific deletion of PPARgamma. *Proc Natl Acad Sci U S A.* 2013;110(46):18656-18661. doi: 10.1073/pnas.1314863110 [doi].
133. Yoon MJ, Yoshida M, Johnson S, et al. SIRT1-mediated eNAMPT secretion from adipose tissue regulates hypothalamic NAD<sup>+</sup> and function in mice. *Cell Metab.* 2015;21(5):706-717. doi: 10.1016/j.cmet.2015.04.002 [doi].
134. Zemaný L, Kraus BJ, Norseen J, et al. Downregulation of STRA6 in adipocytes and adipose stromovascular fraction in obesity and effects of adipocyte-specific STRA6 knockdown in vivo. *Mol Cell Biol.* 2014;34(6):1170-1186. doi: 10.1128/MCB.01106-13 [doi].
135. Abel ED, Peroni O, Kim JK, et al. Adipose-selective targeting of the GLUT4 gene impairs insulin action in muscle and liver. *Nature.* 2001;409(6821):729-733. doi: 10.1038/35055575 [doi].

136. Bettaieb A, Matsuo K, Matsuo I, et al. Adipose-specific deletion of src homology phosphatase 2 does not significantly alter systemic glucose homeostasis. *Metabolism*. 2011;60(8):1193-1201. doi: 10.1016/j.metabol.2011.01.004 [doi].
137. Lackey DE, Lynch CJ, Olson KC, et al. Regulation of adipose branched-chain amino acid catabolism enzyme expression and cross-adipose amino acid flux in human obesity. *Am J Physiol Endocrinol Metab*. 2013;304(11):E1175-87. doi: 10.1152/ajpendo.00630.2012 [doi].
138. Mottillo EP, Balasubramanian P, Lee YH, Weng C, Kershaw EE, Granneman JG. Coupling of lipolysis and de novo lipogenesis in brown, beige, and white adipose tissues during chronic beta3-adrenergic receptor activation. *J Lipid Res*. 2014;55(11):2276-2286. doi: 10.1194/jlr.M050005 [doi].
139. Mullican SE, Tomaru T, Gaddis CA, Peed LC, Sundaram A, Lazar MA. A novel adipose-specific gene deletion model demonstrates potential pitfalls of existing methods. *Mol Endocrinol*. 2013;27(1):127-134. doi: 10.1210/me.2012-1267 [doi].
140. Vernochet C, Damilano F, Mourier A, et al. Adipose tissue mitochondrial dysfunction triggers a lipodystrophic syndrome with insulin resistance, hepatosteatosis, and cardiovascular complications. *FASEB J*. 2014;28(10):4408-4419. doi: 10.1096/fj.14-253971 [doi].
141. Chartoumpakis DV, Palliyaguru DL, Wakabayashi N, et al. Notch intracellular domain overexpression in adipocytes confers lipodystrophy in mice. *Mol Metab*. 2015;4(7):543-550. doi: 10.1016/j.molmet.2015.04.004 [doi].
142. Ellis JM, Bowman CE, Wolfgang MJ. Metabolic and tissue-specific regulation of acyl-CoA metabolism. *PLoS One*. 2015;10(3):e0116587. doi: 10.1371/journal.pone.0116587 [doi].
143. Zhang LJ, Guerrero-Juarez CF, Hata T, et al. Innate immunity. dermal adipocytes protect against invasive staphylococcus aureus skin infection. *Science*. 2015;347(6217):67-71. doi: 10.1126/science.1260972 [doi].
144. Long JZ, Svensson KJ, Tsai L, et al. A smooth muscle-like origin for beige adipocytes. *Cell Metab*. 2014;19(5):810-820. doi: 10.1016/j.cmet.2014.03.025 [doi].
145. Schmidt BA, Horsley V. Intradermal adipocytes mediate fibroblast recruitment during skin wound healing. *Development*. 2013;140(7):1517-1527. doi: 10.1242/dev.087593 [doi].
146. Berry R, Rodeheffer MS. Characterization of the adipocyte cellular lineage in vivo. *Nat Cell Biol*. 2013;15(3):302-308. doi: 10.1038/ncb2696 [doi].
147. Bozec A, Bakiri L, Jimenez M, et al. Osteoblast-specific expression of fra-2/AP-1 controls adiponectin and osteocalcin expression and affects metabolism. *J Cell Sci*. 2013;126(Pt 23):5432-5440. doi: 10.1242/jcs.134510 [doi].
148. Jeffery E, Berry R, Church CD, et al. Characterization of cre recombinase models for the study of adipose tissue. *Adipocyte*. 2014;3(3):206-211. doi: 10.4161/adip.29674 [doi].

149. Lee KY, Russell SJ, Ussar S, et al. Lessons on conditional gene targeting in mouse adipose tissue. *Diabetes*. 2013;62(3):864-874. doi: 10.2337/db12-1089 [doi].
150. Sassmann A, Offermanns S, Wettschureck N. Tamoxifen-inducible cre-mediated recombination in adipocytes. *Genesis*. 2010;48(10):618-625. doi: 10.1002/dvg.20665 [doi].
151. Lee YH, Petkova AP, Konkar AA, Granneman JG. Cellular origins of cold-induced brown adipocytes in adult mice. *FASEB J*. 2015;29(1):286-299. doi: 10.1096/fj.14-263038 [doi].
152. Mitschke MM, Hoffmann LS, Gnad T, et al. Increased cGMP promotes healthy expansion and browning of white adipose tissue. *FASEB J*. 2013;27(4):1621-1630. doi: 10.1096/fj.12-221580 [doi].
153. Contreras GA, Lee YH, Mottillo EP, Granneman JG. Inducible brown adipocytes in subcutaneous inguinal white fat: The role of continuous sympathetic stimulation. *Am J Physiol Endocrinol Metab*. 2014;307(9):E793-9. doi: 10.1152/ajpendo.00033.2014 [doi].
154. Xu J, Morinaga H, Oh D, et al. GPR105 ablation prevents inflammation and improves insulin sensitivity in mice with diet-induced obesity. *J Immunol*. 2012;189(4):1992-1999. doi: 10.4049/jimmunol.1103207 [doi].
155. Kiss Z, Crilly KS. Adenosine triphosphate (ATP) and other nucleotides stimulate the hydrolysis of phosphatidylethanolamine in intact fibroblasts. *Lipids*. 1991;26(10):777-780.
156. Pfeilschifter J, Merriweather C. Extracellular ATP and UTP activation of phospholipase D is mediated by protein kinase C-epsilon in rat renal mesangial cells. *Br J Pharmacol*. 1993;110(2):847-853.
157. Horl G, Wagner A, Cole LK, et al. Sequential synthesis and methylation of phosphatidylethanolamine promote lipid droplet biosynthesis and stability in tissue culture and in vivo. *J Biol Chem*. 2011;286(19):17338-17350. doi: 10.1074/jbc.M111.234534 [doi].
158. Muller G, Wied S, Walz N, Jung C. Translocation of glycosylphosphatidylinositol-anchored proteins from plasma membrane microdomains to lipid droplets in rat adipocytes is induced by palmitate, H<sub>2</sub>O<sub>2</sub>, and the sulfonylurea drug glimepiride. *Mol Pharmacol*. 2008;73(5):1513-1529. doi: 10.1124/mol.107.043935 [doi].
159. Van Epps-Fung M, Gupta K, Hardy RW, Wells A. A role for phospholipase C activity in GLUT4-mediated glucose transport. *Endocrinology*. 1997;138(12):5170-5175. doi: 10.1210/endo.138.12.5596 [doi].
160. Whitehead JP, Molero JC, Clark S, Martin S, Meneilly G, James DE. The role of Ca<sup>2+</sup> in insulin-stimulated glucose transport in 3T3-L1 cells. *J Biol Chem*. 2001;276(30):27816-27824. doi: 10.1074/jbc.M011590200 [doi].
161. Worrall DS, Olefsky JM. The effects of intracellular calcium depletion on insulin signaling in 3T3-L1 adipocytes. *Mol Endocrinol*. 2002;16(2):378-389. doi: 10.1210/mend.16.2.0776 [doi].

162. Leto D, Saltiel AR. Regulation of glucose transport by insulin: Traffic control of GLUT4. *Nat Rev Mol Cell Biol.* 2012;13(6):383-396. doi: 10.1038/nrm3351 [doi].
163. Bose A, Guilherme A, Robida SI, et al. Glucose transporter recycling in response to insulin is facilitated by myosin Myo1c. *Nature.* 2002;420(6917):821-824. doi: 10.1038/nature01246 [doi].
164. Chen XW, Leto D, Chiang SH, Wang Q, Saltiel AR. Activation of RalA is required for insulin-stimulated Glut4 trafficking to the plasma membrane via the exocyst and the motor protein Myo1c. *Dev Cell.* 2007;13(3):391-404. doi: S1534-5807(07)00268-7 [pii].
165. Xie X, Gong Z, Mansuy-Aubert V, et al. C2 domain-containing phosphoprotein CDP138 regulates GLUT4 insertion into the plasma membrane. *Cell Metab.* 2011;14(3):378-389. doi: 10.1016/j.cmet.2011.06.015 [doi].
166. Martens S, Kozlov MM, McMahon HT. How synaptotagmin promotes membrane fusion. *Science.* 2007;316(5828):1205-1208. doi: 1142614 [pii].
167. Koupenova M, Ravid K. Adenosine, adenosine receptors and their role in glucose homeostasis and lipid metabolism. *J Cell Physiol.* 2013. doi: 10.1002/jcp.24352 [doi].
168. Vannucci SJ, Nishimura H, Satoh S, Cushman SW, Holman GD, Simpson IA. Cell surface accessibility of GLUT4 glucose transporters in insulin-stimulated rat adipose cells. modulation by isoprenaline and adenosine. *Biochem J.* 1992;288 ( Pt 1)(Pt 1):325-330.
169. Tanowitz HB, Jelicks LA, Machado FS, et al. Adipose tissue, diabetes and chagas disease. *Adv Parasitol.* 2011;76:235-250. doi: 10.1016/B978-0-12-385895-5.00010-4 [doi].
170. Combs TP, Nagajyothi, Mukherjee S, et al. The adipocyte as an important target cell for trypanosoma cruzi infection. *J Biol Chem.* 2005;280(25):24085-24094. doi: M412802200 [pii].
171. Suga H, Eto H, Aoi N, et al. Adipose tissue remodeling under ischemia: Death of adipocytes and activation of stem/progenitor cells. *Plast Reconstr Surg.* 2010;126(6):1911-1923. doi: 10.1097/PRS.0b013e3181f4468b [doi].
172. Gnad T, Scheibler S, von Kugelgen I, et al. Adenosine activates brown adipose tissue and recruits beige adipocytes via A2A receptors. *Nature.* 2014;516(7531):395-399. doi: 10.1038/nature13816 [doi].

## PUBLICATIONS RESULTING FROM THIS WORK

Adamson SE, Leitinger N. The role of pannexin1 in the induction and resolution of inflammation.

*FEBS Lett.* 2014 Apr 17;588(8):1416-22. (Review)

Adamson SE, Meher AK, Chiu Y, Sandilos JK, Oberholtzer NP, Walker NN, Hargett SR, Seaman SA, Peirce-Cottler SM, Isakson BE, McNamara CA, Keller SR, Harris TE, Bayliss DA, Leitinger N.

Pannexin 1 is required for full activation of insulin-stimulated glucose uptake in adipocytes.

*Molecular Metabolism*, 2015. DOI: <http://dx.doi.org/10.1016/j.molmet.2015.06.009> (In Press)

Adamson SE, Seaman SA, Montgomery G, Peirce-Cottler SM, Leitinger N. Myeloid P2Y2 receptor controls assembly of macrophages into crown-like structures but is dispensable for whole body insulin resistance in diet-induced obese mice. (Manuscript in Preparation)